CHEMICAL REVIEWS

Review

Metal Halide Perovskite Nanocrystals: Synthesis, Post-Synthesis Modifications, and Their Optical Properties

Javad Shamsi,[†,⊥] Alexander S. Urban,[φ] Muhammad Imran,[‡,†] Luca De Trizio,*[,†] and Liberato Manna*[,†,∥]
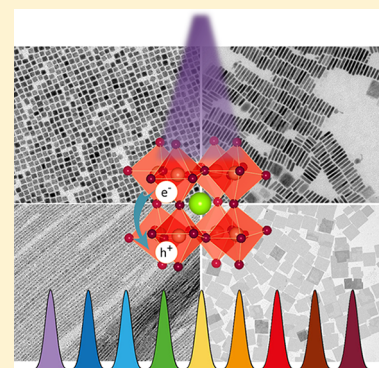
[†]Nanochemistry Department, Istituto Italiano di Tecnologia, Via Morego 30, 16163 Genova, Italy

[‡]Dipartimento di Chimica e Chimica Industriale, Università degli Studi di Genova, Via Dodecaneso 31, 16146 Genova, Italy

[φ]Nanospectroscopy Group, Department of Physics and Center for Nanoscience (CeNS), Ludwig-Maximilians-Universität (LMU), Amalienstaße 54, 80799 Munich, Germany

[∥]Kavli Institute of Nanoscience and Department of Chemical Engineering, Delft University of Technology, PO Box 5, 2600AA Delft, The Netherlands

ABSTRACT: Metal halide perovskites represent a flourishing area of research, which is driven by both their potential application in photovoltaics and optoelectronics and by the fundamental science behind their unique optoelectronic properties. The emergence of new colloidal methods for the synthesis of halide perovskite nanocrystals, as well as the interesting characteristics of this new type of material, has attracted the attention of many researchers. This review aims to provide an up-to-date survey of this fast-moving field and will mainly focus on the different colloidal synthesis approaches that have been developed. We will examine the chemistry and the capability of different colloidal synthetic routes with regard to controlling the shape, size, and optical properties of the resulting nanocrystals. We will also provide an up-to-date overview of their postsynthesis transformations, and summarize the various solution processes that are aimed at fabricating halide perovskite-based nanocomposites. Furthermore, we will review the fundamental optical properties of halide perovskite nanocrystals by focusing on their linear optical properties, on the effects of quantum confinement, and on the current knowledge of their exciton binding energies. We will also discuss the emergence of nonlinear phenomena such as multiphoton absorption, biexcitons, and carrier multiplication. Finally, we will discuss open questions and possible future directions.

CONTENTS

1. INTRODUCTION

Metal halide perovskites (MHPs) were first reported in 1893,[1] but it was not until the 1990s that they began to attract the attention of the scientific and engineering communities. Initially, there was a focus on light-emitting devices and transistors due to their intriguing optical and electronic properties. However, it took until 2012 for the real potential of these materials to be discovered. MHPs were originally used as sensitizing materials in dye-sensitized solar cells, but it was rapidly determined that, in addition to boosting the absorption cross section of the resulting device, they also exhibit impressive charge transport properties.[2−5] These findings have generated much interest in halide perovskites, and the efficiency of single cell perovskite-based photovoltaic devices has exceeded 23% over a relatively short period.[6−8]

Interestingly, despite being counterintuitive, perovskites were proved to be good not only for separating charges and creating electricity but also for bringing charges together to create light.[9−11] In addition to their relatively low nonradiative recombination rates, their high color purity makes them interesting candidates for light-emitting diodes (LEDs) and lasers.[12] Unfortunately, bulk perovskite structures seem limited with regard to their photoluminescence quantum yield (PLQY) and this is mainly due to two key limiting factors: (i) the presence of mobile ionic defects, which are characterized by a low formation energy and (ii) a small exciton binding energy in MHPs, which results in low electron−hole capture rates for radiative recombination. Moreover, in MHP films that are prepared from precursor solutions, dominant intrinsic defects are not as benign as was initially thought.[13] This was demonstrated by a grain-to-grain variation in the PL intensity; it was discovered that the grain boundaries were normally weakly emissive and exhibited faster nonradiative decay.[14] Consequently, researchers turned their attention to perovskite nanocrystals (NCs), with the intention of not only boosting the PLQY of conventional semiconducting materials, but also accessing the quantum-confinement size regime, which could be used as an additional method for tuning the emission of such materials. The first perovskite

NCs were synthesized in 2014,[15] and since then, research on these compounds has virtually exploded. In the preparation of MHP NCs, organic capping ligands enable the growth of crystals in the nanometer size range, and they actively passivate surface defects in a similar way to the synthesis of more traditional NCs. It is also possible to finely tune the size and shape of the NCs, so that one can prepare either bulklike NCs (i.e., particles that are large enough to exhibit optical properties similar to those of bulk crystals or films) or nanostructures like nanoplatelets (NPLs), nanosheets (NSs), nanowires (NWs), and quantum dots (QDs). The sizes of these nanostructures can be controlled down to a single perovskite layer, and, consequently, significantly below the exciton Bohr radius (hence in the strong quantum confinement regime).[16−19] The composition, structure, and size of the NCs can be tuned not only during the synthesis, but also via postsynthesis transformations, for example through ion exchange or exfoliation.[20−23]

The peculiar nature of the band structure of MHPs is such that defect states tend to be either localized within the valence and conduction bands or to be essentially "inert", resulting in perovskite NCs with a high PL efficiency. Consequently, perovskite NCs are often referred to as being "defect-tolerant". This does not mean that they do not have any defects which induce nonradiative recombination, but rather that the need for extensive passivation (as in metal chalcogenide NCs, for example) is less demanding. Over the past few years, MHP NCs have been optimized toward having emission wavelengths that are tunable throughout the entire visible spectral range (and beyond), and their quantum yields (QYs) have approached 100%.[24,25] Nearly five years have passed since the pioneering colloidal syntheses of MHP NCs.[15,26] Since then, countless innovations in their synthesis and processing have delivered materials that have been tested in solar cells (both as active materials[27−29] and as downconverters[30]), solar concentrators,[31] visible light communications,[32] electroluminescent diodes,[33,34] photodetectors,[35] and photocatalysis.[36] Among the different members of the vast perovskite family, lead-based halide perovskite (LHP) NCs have been found to be great alternatives to well-established II−VI, III−V, and IV−VI QDs. Here, we direct the readers to recent reviews for a comprehensive comparison of LHP NCs with more traditional QDs.[37−39]

Despite such rapid advancements in material syntheses and device applications, studies on the optical properties of perovskite NCs have significantly lagged behind. Many questions pertaining to halide perovskites in general remain unanswered,[40−42] and this is also the case of perovskite NCs. For example, it is has now been well-established that the PLQY of LHP NCs varies depending on the synthetic approach, and that even small modifications to a given synthetic protocol can strongly influence their optical properties. The reasons behind such a wide variability in their optical properties is that these properties strongly depend on the stoichiometric ratios of the ions in the perovskite structure,[43] as well as on the types of coating ligands and on how the surface is terminated in general.[44,45] However, the investigation into these aspects is still in its infancy.

Several review articles on the chemistry and optical properties of MHP NCs have been published in the last couple of years.[46−54] This review article seeks to summarize the recent developments in colloidal synthetic methods for the preparation of MHP NCs and their postsynthesis treatments,

in order to analyze the strengths and weaknesses of each method. It then gives a snapshot of the current knowledge on their optical properties. Our review is structured into four main sections: (i) a brief introduction to MHP NCs will be given in order to provide an understanding of their nature, crystal structures, and optical properties. (ii) We will then present a detailed explanation and analysis of the most recent trends in the colloidal synthesis of MHP NCs. Our intention is to provide a comprehensive overview of the different synthetic routes for MHP NCs, highlighting how size and shape control can be achieved. (iii) We will give a broad summary of postsynthesis modifications of MHP NCs, which are applied to either manipulate their optical properties or to increase their stability. (iv) The last section will deal with recent progress in understanding the optical properties of MHP NCs, such as their linear and nonlinear optical features, quantum confinement effects, and exciton binding energies. We will end the review with our vision for the future of this field.

2. BRIEF INTRODUCTION TO MHP NCS

2.1. History of Colloidal Synthesis of MHP NCs

Interest in semiconductor NCs was generated by the discovery of quantum-size effects in the optical spectra of nanometer-sized semiconductors in the early 1980s.[55,56] Notably, the quantum confinement effect in MHPs (i.e., $CsPbX_3$) was reported long before widespread attention was paid to bulk crystals and thin films of these materials.[57−59] We direct the readers to recent reviews for a more detailed historical background of MHPs NCs.[37,38] Parallel to the work on classic colloidal semiconductor NCs, a seminal paper was published in 2011 on methylammonium (MA) lead iodide ($MAPbI_3$) in the form of nanometer-sized crystals as a promising PV material.[60] That work captured the attention of the colloidal chemistry community, which started to conduct research on this interesting class of medium-bandgap semiconductors. The first solution-based colloidal approach to produce MHPs NCs was published some years later, when Schmidt et al. were able to prepare $MAPbBr_3$ NCs (for more information, see section 3.2.11) with a PLQY of 20%[15] at the end of 2013. Soon after (in 2015), Protesescu et al. reported a colloidal synthesis of monodisperse $CsPbX_3$ NCs; they adopted the standard hot-injection method[90] that is typically employed for classic colloidal QDs (such as CdSe and PbSe) to fit the requirements of the new chemicals and solvents needed to prepare perovskite NCs.[26] The prominent work of Protesescu et al. evidences that LHP NCs have three remarkable properties: (i) a high PLQY (up to 90%), which can be reached without having to conduct any specific postsynthesis treatment; (ii) a PL with a narrow full width at half-maximum (fwhm), namely below 100 meV; (iii) and a PL that is tunable across the entire visible spectral range by simply varying the nature and ratio of the halide ions in the structure.[26] The ease by which these NCs could be synthesized, their interesting properties, as well as the many questions that have arisen in light of these initial reports have been the main attractions for researchers from various fields.

2.2. Crystal Structure, Ionic Nature, and Defect Tolerance

"Three-dimensional" (3D) perovskite structures are formed by three primary ions, and they have an ABX_3 stoichiometry (Figure 1, panels a and b). For all-inorganic halide counterparts, the monovalent A-cation is cesium or rubidium, the divalent B-cation is lead, tin, or germanium, and X is a halide
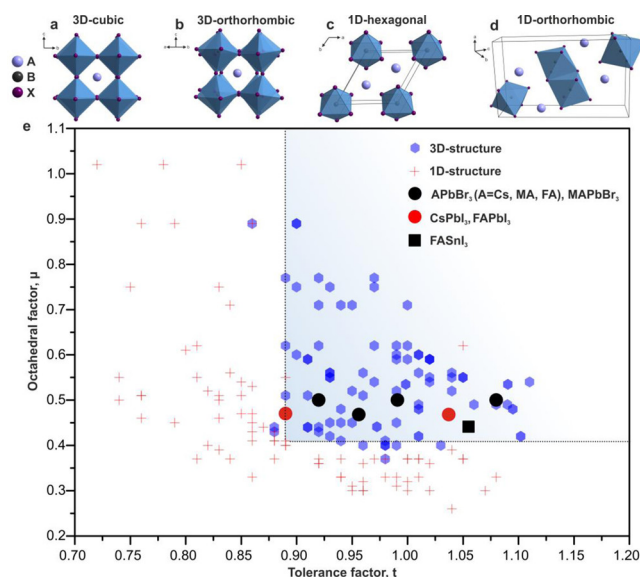

Figure 1. Schematic representations of (a) an ideal 3D cubic structure, as observed in α-$FAPbI_3$; (b) an orthorhombically distorted 3D structure, typically reported for $CsPbBr_3$; (c) a one-dimensional (1D) hexagonal lattice, found in the yellow phase of $FAPbI_3$; and (d) a 1D orthorhombic structure, found in the yellow phase of $CsPbI_3$. (e) Reported 3D and 1D structures of different all-inorganic and hybrid organic−inorganic ABX_3 MHP compounds. The light blue squared area represents the region in which stable compounds are located. The tolerance and octahedral factors were mainly taken from the report of Travis et al.[66] All panels are reproduced from ref 67. Copyright 2017 American Chemical Society.

ion, namely chlorine, bromine, iodine, or a combination of them.[61] Organic−inorganic perovskite compounds, however, have either methylammonium (MA) or formamidinium (FA) as the A cation.[62] The A and B cations coordinate with 12 and 6 X anions, respectively, forming cuboctahedral and octahedral structures. Notably, the Goldschmidt tolerance factor, t, has been used extensively to predict the stability of perovskite structures based only on the chemical formula ABX_3 and the ionic radii, r_i, of the ions (A, B, X): $(t = r_A + r_X/\sqrt{2(r_B + r_X)})$.[63] In general, stable 3D perovskite structures are formed when the tolerance factor is within the range of 0.76−1.13, while other perovskite-related structures are stable outside this range.[64] For this reason, only a limited number of A-cations (Cs, MA, and FA) can give rise to stable structures in the case of LHP perovskites. Other possible candidates are either too small (Na, K, and Rb) or too large (imidazolium, ethylamonium, and guanidinium).[65] Perovskites at the edge of the tolerance factor requirement, such as $FAPbI_3$ ($t \sim 1$) and $CsPbI_3$ ($t \sim 0.8$), easily undergo a phase transition at room temperature (RT) to more stable hexagonal and orthorhombic phases (Figure 1, panels c and d), respectively. These are also referred to as "yellow phases".[65] Perovskite structures are further constrained by the octahedral factor, μ, which is defined as $\mu = r_B/r_X$. The μ describes the stability of the BX_6^{2-} octahedra, and it depends on the radii of both the B and X ions. The stability range for μ is between 0.442 and 0.895.[66] The tolerance and octahedral factors are currently used to predict the stability of novel possible perovskite combinations (see Figure 1e).[67,68]

Perovskite compounds are mostly held together by ionic bonding, and this is one of the reasons for the ease by which

highly crystalline NCs can be fabricated even at low temperatures.[69] One of the key features of MHPs that has been ascribed to their success as high-performance semiconductors is their defect tolerance, which is an ability to retain the electronic structure of the pristine material even in the presence of a large concentration of defects. The reported defect-tolerance of MHPs is corroborated by first-principles density-functional theory (DFT) calculations of the formation energy of point defects and their effect on the electronic structure.[13] For perovskites, the defect chemistry and physics is still not well-understood, but vacancy-related defects are considered to have energies close to, or within, the energy bands (see the section "optical properties" for further details).[38,69]

2.3. Different Phases (3D, Two-Dimensional (2D), Zero-Dimensional (0D), and Double Perovskites)

So far, most research on lead halide perovskite NCs has focused on NCs with a 3D $APbX_3$ crystal structure and composition, but the general reactivity of this class of halide perovskites and their intrinsic toxicity has also stimulated research in various directions. First, the high ionicity and structural instability of LHP NCs, which limits their ability to be used in a range of applications, can actually be considered a positive feature, since the $APbX_3$ lattice can be easily reorganized into other phases. This has triggered an extensive investigation into NCs with other structures and compositions, also defined as "perovskite-related structures", such as Cs_4PbX_6 and $CsPb_2X_5$ (so-called 0D and 2D structures, respectively). While a 3D $APbX_3$ structure is characterized by corner sharing $[PbX_6]^{4-}$ octahedra with the A^+ cations filling the voids created by four neighboring PbX_4^{4-} octahedra (resulting in a cubic or pseudocubic structure, see Figure 2a,b), the PbX_6^{4-} octahedra in A_4PbX_6 structures are completely decoupled in all dimensions and the halide ions are no longer shared between them (Figure 2, panels c).[70] Recently, layered perovskites have come under immense scrutiny. $CsPb_2X_5$ have emerged as a 2D version of lead halide perovskite materials with a tetragonal phase which consists of alternating Cs^+ and $[Pb_2X_5]^-$

polyhedron layers, similar to that of layered double hydroxides (Figure 2d).[71] Another type of 2D perovskites is the A_2PbX_4 phase, which is made of alternating layers of corner-sharing $[PbX_6]^{4-}$ octahedra and bulky cations (Figure 2e).[72]

The toxicity of lead (and its bioaccumulation in the ecosystem) is the major limitation of $APbX_3$ NC systems, and this has urged researchers to look into alternative materials with comparable optoelectronic properties, such as Cs_2SnI_6 NCs.[73−77] However, there has been very limited success to date. Cs_2SnI_6 crystallizes in the face-centered cubic (*fcc*) structure. The unit cell is composed of four $[SnI_6]^{2-}$ octahedra at the corners and at the face centers and eight Cs^+ cations at the tetragonal interstitials (Figure 2f). A Cs_2SnI_6 structure is a perovskite derivative, and it is obtained by removing half of the Sn atoms at each center of the $[SnI^6]$ octahedron at regular intervals.[73] For this reason, the structure is also referred to as a "vacancy ordered double perovskite". In the search for lead-free metal halide compounds, two main strategies are currently being pursued: a "simple" substitution of Pb^{2+} cations with other less toxic divalent metal ions from the same group IV, such as Sn or Ge,[78] or a replacement of every two divalent Pb^{2+} ions with one monovalent M^+ and one trivalent M^{3+} cations (i.e., $2Pb^{2+} \rightarrow B^+ + B^{3+}$), generating quaternary $A_2B^+B^{3+}X_6$ systems (also named "double perovskites", Figure 2g).[79] The diversity of halide materials related to LHPs is explored by introducing other transition or post-transition metals, such as Fe^{3+} and Bi^{3+}.[80−84] $Cs_3M_2X_9$ ($M = Fe^{3+}$, Bi^{3+}) crystallizes in the hexagonal space group $P6_3/mmc$. This consists of isolated clusters, each made of two face-sharing octahedra, and having $M_2Br_9^{3-}$ formula, with Cs^+ serving as bridging ions between the clusters (Figure 2h). Conversely, antimony-based halide compounds crystallize in a layered structure in which each $Sb_2Br_9^{3-}$ cluster shares corners with 3 octahedra (Figure 2i).[76]

3. COLLOIDAL SYNTHESIS METHODS

To prepare high quality MHP NCs in terms of having control over the size, shape and quality of their optical properties, much effort has been devoted to developing reliable and straightforward synthetic strategies. These approaches can be classified either as "top-down" or "bottom-up". Top-down strategies comprise a fragmentation and structuring of macroscopic solids, either mechanically (e.g., ball-milling in the presence of surfactants[85]) or chemically (e.g., chemical exfoliation,[22] etc.), whereas the bottom-up routes start with molecules and ions and proceed via gas- or liquid-phase chemical reactions. It has been proven that, among all bottom-up approaches, the liquid-phase one is the best for the fabrication of well-defined colloidal MHP NCs (Scheme 1).[48,86] In this review, we will focus on the two most developed liquid-phase methods for the synthesis of colloidal MHP NCs: the hot injection (HI) method and the ligand-assisted reprecipitation (LARP) method.[47,87] In short, the HI route requires high temperatures and an inert atmosphere, which inevitably increases the cost and could limit the output in mass production.[88] To overcome these two potential limitations, the LARP method can be employed as a more cost-effective alternative, as it delivers high quality perovskite NCs in an ambient atmosphere at RT (see section 3.2).[89]

3.1. Hot Injection Strategy

The first HI method was developed two and half decades ago for the synthesis of cadmium chalcogenide NCs.[90] This approach is based on the rapid injection of a precursor into a
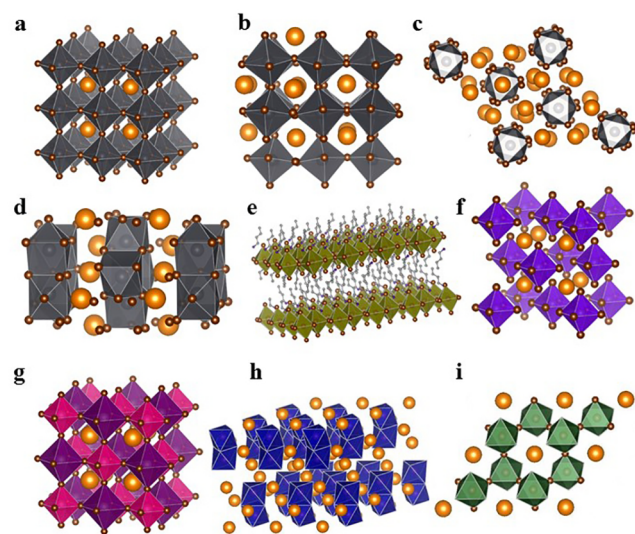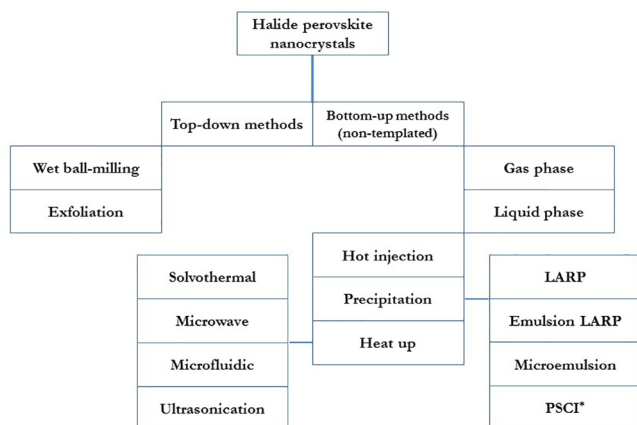

Figure 2. Schematic representation of different metal halide structures: (a) cubic-phase ABX_3 (3D); (b) pseudocubic ABX_3 (3D); (c) A_4BX_6 (0D); (d) AB_2X_5 (2D); (e) A_2BX_4 (2D); (f) A_2BX_6 (0D); (g) $A_2B^+B^{3+}X_6$ (3D); and (h and i) $A_3B_2X_9$ (2D).

Scheme 1. Outline of the Various Methods Employed in the Synthesis of MHP Nanocrystals

*Polar solvent controlled ionization.

hot solution of the remaining precursors, ligands, and a high boiling solvent.[91−93] The HI method generally enables the synthesis of small NCs with a narrow size distribution by attaining a separation between the nucleation and growth stages.[94] Immediately after the injection, a rapid nucleation burst occurs with a simultaneous formation of small nuclei. A rapid depletion of monomers terminates the nucleation stage, after which the nuclei continue growing (with ideally no new nuclei forming). Over time, this leads to the evolution of a NCs' population, which is characterized by a narrow size distribution. This happens if the reaction is stopped when it is still in the size-focusing regime (i.e., when there are still plenty of monomers in the growth environment).[95] The key parameters that enables to control the size, size-distribution, and shape of colloidal NCs synthesized by the HI method are (i) the ratio of the surfactants to the precursors; (ii) the injection temperature of the cation or anion precursor; (iii) the reaction time; and (iv) the concentration of the precursors. In 2015, Protesescu et al. extended the HI approach so that it could be used for the colloidal synthesis of cesium LHP NCs (CsPbX$_3$, X = Cl, Br, and I).[26] CsPbX$_3$ NCs were obtained by injecting Cs-oleate into a hot solution (140−200 °C) of PbX$_2$ (X= Cl, Br, I) salts, which served both as the Pb^{2+} and X$^−$ source, dissolved in octadecene (ODE), carboxylic acids, and primary amines (see Figure 3). They observed that equal ratios of amines and acids resulted in the formation of monodisperse NCs whose size could be adjusted by varying the reaction temperature. Mixed-halide perovskite NCs could also be conveniently synthesized by simply adjusting the ratios of lead halide salts (PbCl$_2$/PbBr$_2$ or PbBr$_2$/PbI$_2$). The PL emission of the resulting NCs could be finely modulated across the entire visible spectrum (410−700 nm) by varying the halide composition or by tuning the size of NCs. Subsequently, the HI method was further extended to MAPbX$_3$ (X = Br, I) NC systems by replacing Cs-oleate with a methylamine solution.[96] MAPbBr$_3$ and MAPbI$_3$ NCs were successfully obtained by varying the relative amount of oleylamine (OLA) and oleic acid (OA) capping ligands.

The HI protocol was further developed for the synthesis of perovskite-related lead halide based materials. For instance, Cs$_4$PbX$_6$ (X = Cl, Br, I) NCs were successfully prepared by working under Cs$^+$ and OLA-rich conditions compared to those used in the conventional CsPbBr$_3$ NCs synthesis.[97] The
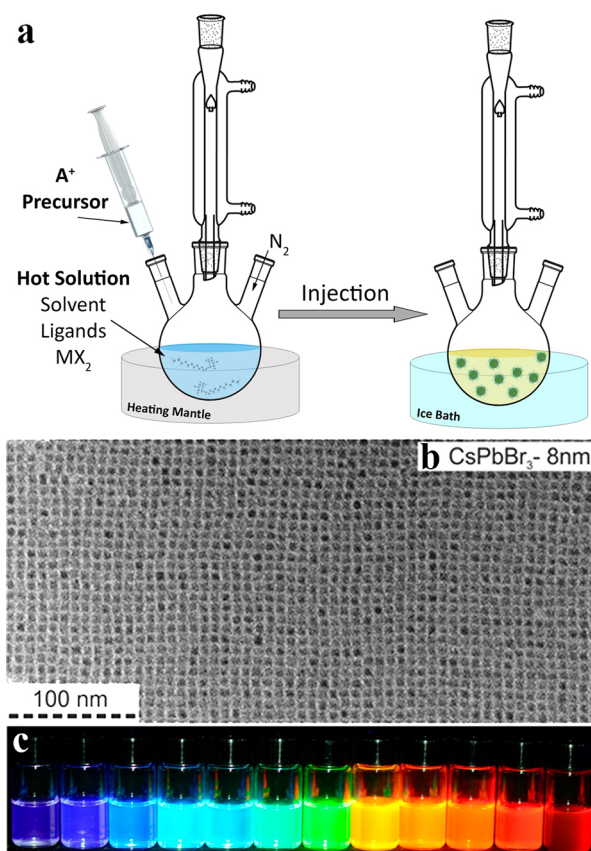

Figure 3. (a) Sketch of the HI method used for the synthesis of colloidal MHP NCs. (b) A typical TEM image of CsPbBr$_3$ NCs obtained using the hot injection (HI) strategy. (c) Colloidal perovskite CsPbX$_3$ (X = Cl, Br, I) NC dispersions (in each vial, the NCs have a different halide composition) in toluene under an ultraviolet (UV) lamp (λ = 365 nm). Panels (b) and (c) are adapted from ref 26. Copyright 2015 American Chemical Society.

resulting NCs were nearly monodisperse, and their size could be further tuned from 9 to 37 nm.[97] Various other groups have reported the synthesis of CsPb$_2$Br$_5$ NCs using octylamine and OA as surfactants in an excess of the PbBr$_2$ precursor.[98]

In order to gain insight into the growth kinetics of CsPbX$_3$ NCs that are produced via the HI approach, Lignos et al. employed a droplet-based microfluidic platform.[99,100] Following the in situ absorption and photoluminescence of CsPbX$_3$ NCs, they revealed that the entire nucleation and growth took place in the first 1−5 s of the reaction, highlighting the fact that these NCs have extremely fast reaction kinetics. Slightly different results were reported by Koolyk et al., who investigated the growth kinetics of CsPbBr$_3$ and CsPbI$_3$ NCs by taking aliquots at different stages of the reaction and analyzing them by transmission electron microscopy (TEM).[101] They observed that the size focusing regime in CsPbI$_3$ NCs lasted for the first 20 s, and that it was followed by a subsequent size defocusing regime. However, they found that the growth of CsPbBr$_3$ NCs was not characterized by any size focusing regime; instead, it was characterized by a broadening of the size distribution from the very beginning, and this persisted during the whole reaction time of 40 s.[101] Later, Udayabhaskararao et al. monitored the growth of CsPbX$_3$ NCs at different stages using electron microscopy, and they eventually proposed a two-step growth mechanism.[102] During the first step of this mechanism, Pb° NCs form, and these act

as seeds onto which CsPbX$_3$ NCs nucleate. In the second stage, the NCs grow through self-assembly and oriented attachment. However, these authors did not provide any evidence of the initial formation of Pb^o NCs. Furthermore, it has now been well-established that Pb^o clusters on the surface of NCs are formed by the electron beam irradiation when they are observed under an electron microscope.[103,104] Therefore, this mechanism can be dismissed.

Overall, the large variability in the quality of the manufactured MHP NCs reported in literature reveals that, in contrast to classic colloidal heat-up or hot-injection techniques that are used to produce II−VI (e.g., CdTe, CdSe, CdS, and HgS), IV−VI (e.g., PbSe), III−V (e.g., InP and InAs), or ternary I−III−VI (e.g., CuInS$_2$) QDs, the research community still does not fully understand the MHP NCs nucleation and growth processes. The fact that the nucleation and growth steps of MHPs NCs are fast and hardly separable in time is likely due to the extreme ease by which these ionic crystals are formed in solution. The challenge in controlling the nucleation and the growth with a high ensemble uniformity has been one of the major obstacles impeding the exploration and the utilization of the properties of CsPbX$_3$ NCs.[105] However, a recent study has demonstrated that this challenge can be overcome by working under thermodynamic equilibrium instead of kinetic control.[106]

An important weakness of colloidal MHP NCs (and of halide perovskites in general) is their high solubility in polar solvents. This means that they have a poor stability under ambient atmospheric conditions (with variable humidity, heat, and/or light), and this causes a drop in their PLQY.[89] An example of this can be seen in Yuan et al.'s work,[107] in which they demonstrated that perovskite NCs are particularly sensitive to the antisolvents that are used in their cleaning. Starting from CsPbBr$_{1−x}$I$_x$ NCs, they found that different antisolvents, like isopropanol, n-butanol, or acetone, can change the halide composition of the NCs and, thus, their overall optical properties.[107] The Surface, Shape, and Phase Postmodifications section of this review will focus on this aspect of postsynthesis treatment. For now, we will discuss the works that have taken the instability issue into account at the synthesis stage and that have attempted to adapt countermeasures. In order to counterbalance the stripping of halide ions, which accompanies the use of polar antisolvents, Woo et al. found that the stability of CsPbX$_3$ NCs can be considerably enhanced, without a drastic drop in the PLQY, by working under halide-rich conditions.[108] In that work, ZnBr$_2$ was used as an extra source of Br ions in addition to the PbBr$_2$ precursor. The resulting NCs had more halide-rich compositions (Cs:Pb:Br = 1.0:1.2:3.4) than those synthesized in the absence of metal bromide (Cs:Pb:Br = 1.0:1.0:2.8). This approach was defined by the authors as the first successful attempt to stabilize CsPbX$_3$ NCs (where X is Br or I) in situ by inorganic passivation.[108] The term "inorganic passivation" is, however, not entirely accurate, as the NCs were still passivated with organic molecules.

One major drawback of the HI methods described so far is that they rely on the use of metal halide salts as both a cation and an anion precursor, and this limits the possibility of working with the desired ion stoichiometry.[26,109] In order to overcome such restrictions, Liu et al. developed the so-called "three-precursor" HI approach for the synthesis of CsPbX$_3$ (X = Cl, Br, or I) NCs.[110] Their novelty consisted of using NH$_4$X (X = Cl, Br, or I) and PbO as sources of halide and lead ions

separately, instead of conventional PbX$_2$ (X = Cl, Br, or I) salts.[110] As had already been stated by Woo et al.,[108] the CsPbBr$_3$ NCs that had been synthesized under Br-rich conditions (that is, by employing an excess of NH$_4$Br) had better optical properties and a remarkably better stability than the standard NCs, as they endured the purification step.[110]

Yassitepe et al. further developed the three precursor HI approach in order to synthesize OA-capped CsPbX$_3$ NCs by eliminating alkylamines from the synthesis.[111] In their approach, Cs-acetate and Pb-acetate were reacted with quaternary alkylammonium halides, such as tetraoctylammonium halides (TOA-X), which cannot form protonated ammonium species even when protons are present. It was observed that the absence of oleylamine considerably speeded up the growth kinetics, enabling the synthesis of CsPbX$_3$ NCs at a lower temperature (i.e., 75 °C). The CsPbBr$_3$ NCs that were obtained by this approach exhibited PLQYs up to 70%, as well as an enhanced colloidal stability. This method, however, failed to produce CsPbI$_3$ NCs of a similar quality and stability.[111] The three-precursor HI approach was later adopted and modified by Protesescu et al. for the colloidal synthesis of FAPbX$_3$ NCs.[67,112,113] In short, FAPbBr$_3$ NCs were prepared by reacting FA and Pb acetates with oleic acid in ODE and, subsequently, injecting oleylammonium bromide. The final product contained also a 5−10% of NH$_4$Pb$_2$Br$_5$ byproduct that might have formed upon the thermal decomposition of FA$^+$ to NH$_4^+$ during the synthesis.[112] Phase pure FAPbI$_3$ NCs with a better optical quality were successfully synthesized in 2017 by the two precursor HI method by reacting FA-oleate with a PbI$_2$ complex in the presence of oleic acid and oleylamine in ODE with an excess of FA (FA:Pb = 2.7) at 80 °C.[67]

Although the three-precursor HI approach allows one to work with the desired stoichiometry of ions (since the halide and the metal cations sources are no longer linked), its potential versatility is limited by a series of disadvantages. First, the fact that a synthesis of CsPbI$_3$, CsPbCl$_3$, and MAPbX$_3$ (X = Br, I) NCs has not yet been reported using this strategy suggests that the halide precursors react poorly under the reaction conditions of this approach.[67,112,114] Moreover, a considerable amount of undesired secondary phases, which are ascribed to the decomposition of the alkylammonium halide precursor, were found in the synthesis of FAPbX$_3$ NCs.[112] In order to compensate for the limitations of the three precursor HI approach, new methods have recently been reported by Imran et al.[43] and by Creutz et al.[115] Both these strategies are based on the use of highly reactive halides as anion precursors, which can be conveniently injected into a solution of metal carboxylates. Upon injection, the NCs immediately begin to nucleate and grow. Imran et al. demonstrated how benzoyl halides, which are employed as a halide source, can be used to prepare an entire family of all-inorganic and hybrid lead halide perovskite NCs (CsPbX$_3$, MAPbX$_3$, FAPbX$_3$; X = Cl$^−$, Br$^−$, I$^−$) with good control over the size distribution and phase purity.[43] Similarly, Creutz et al. used silyl halides to synthesize Cs$_2$AgBiX$_6$ NCs (these materials will be covered in the Pb-Free Metal Halide Perovskite NCs section).[115] Of particular relevance is that these strategies enable one to work with desired cation/anion ratios, and, more specifically, in a halide-rich environment. In some systems, this was observed to strongly increase the PLQY of the resulting NCs: for instance, CsPbCl$_3$ NCs synthesized with either the LARP or the two-precursor HI approach were characterized by significant

Scheme 2. Shape and Size Control of CsPbBr₃ NCs in the HI Approach[a]
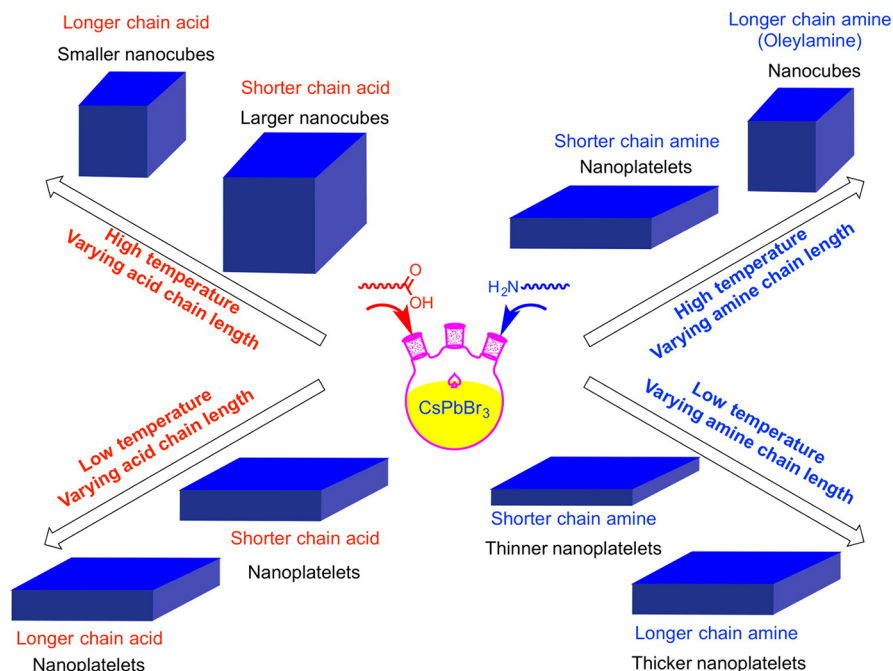
[a]Reproduced from ref 120. Copyright 2016 American Chemical Society.

nonradiative carrier recombinations,[116,117] while the use of an excess of benzoyl chloride (halide-rich conditions) boosted their PLQY up to a record value of 65%.[43]

3.1.1. Size and Shape Control of Lead Halide Perovskite NCs by the HI Approach. Size and shape control is made possible in the HI strategy mainly by varying the ligand combinations and ratios as well as the reaction temperature. As a general trend, the use of OLA and OA at low reaction temperatures (in the range of 90−130 °C) tends to encourage the NCs to grow anisotropically, producing quasi 2D geometries, which are usually referred to as "nanoplatelets" (NPLs).[118] On the other hand, high reaction temperatures (i.e., 170−200 °C) and long reaction times lead to nanowires (NWs).[119] In order to investigate the effect of ligands on the morphology of CsPbBr₃ NCs, Pan et al. carried out a comprehensive study by systematically varying the chain length of the alkyl amines and carboxylic acids used in the reaction.[120] In one series of experiments, while keeping the amount of OLA fixed, they added different carboxylic acids (at 170 °C). An increase in the average edge length of CsPbBr₃ nanocubes, from 9.5 to 13 nm, occurred when the chain length of the carboxylic acids was shortened. Furthermore, working with OA and lowering the reaction temperature to 140 °C, NPLs with a thickness of 2.5 nm and a width of 20 nm were formed (see Scheme 2). In a second series of experiments, the amount of oleic acid was fixed, and different alkylamines were tested at 170 °C. In every experiment, the authors observed the formation of NPLs, except when OLA was used, which could still lead to the formation of NPLs at lower reaction temperatures (140 °C).

While many work attempts have been made to control the lateral size of lead halide based nanocubes, some efforts have also been dedicated to synthesizing anisotropic nanostructures, such as NPLs and NWs, with control over their dimensions. Song et al. reported a HI synthesis of atomically thin CsPbBr₃ nanosheets (NSs) with a thickness of 3.3 nm and an edge

length of about 1 μm using dodecylamine and oleic acid and prolonging the reaction time up to 3 h (see Figure 4a).[121] The same year (2016), Shamsi et al. reported the synthesis of CsPbBr₃ NSs with tunable lateral dimensions from 200 nm up to a few micrometers while keeping their thickness to few unit cells (see Figure 4b).[122] This was achieved by employing short chain ligands, namely octylamine and octanoic acid, in addition to the conventional OA and OLA. In parallel, another work by
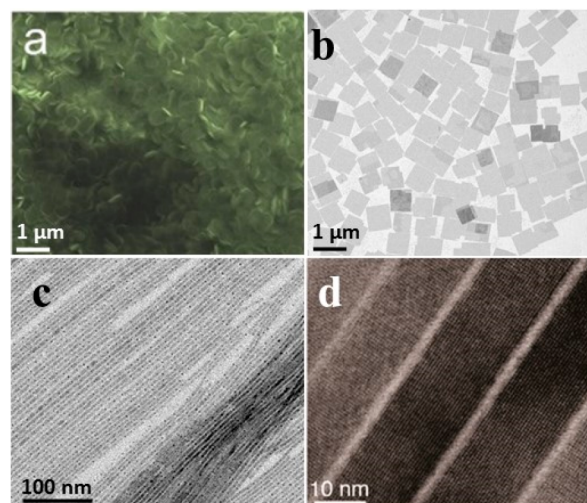
Figure 4. (a) Scanning electron microscopy (SEM) and (b) low-magnification transmission electron microscopy (TEM) images of CsPbBr₃ NSs. (c) Low- and (d) high-resolution TEM micrographs of CsPbBr₃ NWs. (a) is reproduced with permission from ref 121. Copyright 2016 Wiley-VCH. Panel b is reproduced from ref 122. Copyright 2016 American Chemical Society. (c) is reproduced from ref 123. Copyright 2016 American Chemical Society. (d) is reproduced from ref 124. Copyright 2016 American Chemical Society.
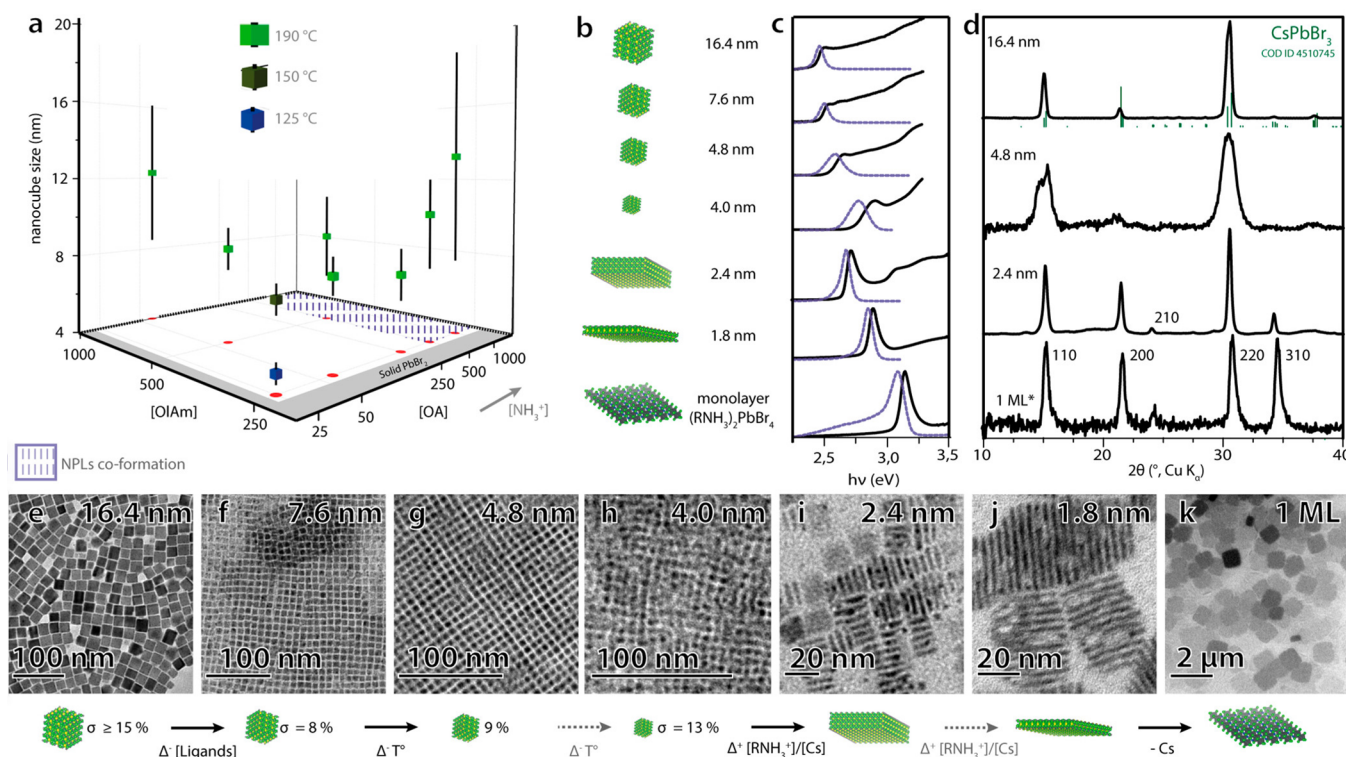
Figure 5. (a) Variation in the size of CsPbBr$_3$ nanocubes, depending on the concentration of oleylamine (OLA), OA, and the reaction temperature (vertical bars represent the size distributions). (b) Illustration of the different CsPbBr$_3$ nanostructures that were obtained using OLA and OA as ligands, together with their corresponding: (c) absorbance (black lines) and photoluminescence (blue dashed line) spectra; (d) X-ray diffraction (XRD) patterns; and (e−k) TEM images. All panels are reproduced from ref 105. Copyright 2016 American Chemical society.

Imran et al. demonstrated the synthesis of CsPbBr$_3$ NWs with a tunable width down to a few unit cells (see Figure 4c) via the HI approach.[123] Green-emitting CsPbBr$_3$ NWs with a width of 10−20 nm (hence they are nonconfined) were prepared by employing octylamine and OLA only (no carboxylic acid was used).[124] The diameter of the NWs could be decreased from 10 to 3.4 nm by introducing a short chain carboxylic acid (octanoic acid or hexanoic acid).[123] Zhang et al. later reported a synthesis strategy to prepare thin[124] and ultrathin[16] CsPbBr$_3$ nanowires (with a width of 2.2 ± 0.2 nm and length of up to several microns Figure 4d). The NWs were prepared by using OLA, OA, and dodecyl amine as a ligand via the HI approach, and a stepwise purification was carried out to enhance the yield.[16]

To better elucidate the way alkylamines and carboxylic acids interact with each other before and during the HI synthesis, Almeida et al. conducted an in depth investigation into the interplay between oleylamine and oleic acid, and they studied the effects of the relative concentration on the size, size distribution, and shape of CsPbBr$_3$ NCs.[105] They found that, by increasing the concentration of ligands, the precipitation temperature of PbBr$_2$ could be significantly enhanced from 195 to 290 °C, allowing syntheses of CsPbBr$_3$ NCs to be conducted at higher temperatures. It was revealed, by Nuclear Magnetic Resonance (NMR) analysis, that the concentration of oleylammonium species could be increased not only by increasing the concentration of oleic acid, but also by lowering the reaction temperature. The concentration of oleylammonium species was found to determine the shape of the final NCs: a high concentration of oleylammonium species (which is achievable in a highly acidic environment) causes the NCs to grow anisotropically, whereas a low concentration leads to the

formation of nanocubes (Figure 5). This proves that oleylammonium species, and primary alkyl ammonium species in general, are able to compete with Cs$^+$ ions for the surface passivation of the NCs, generating platelet-shaped particles or even layered structures. The same study reported that the Ostwald ripening could be suppressed by reducing the concentration of ligands (to the minimum amount needed to solubilize PbBr$_2$ at a given temperature). As a result, CsPbBr$_3$ nanocubes from 4.0 to 16.4 nm with narrow size distribution (8 to 15%) could be prepared (Figure 5). In addition to varying the length of the ligands and the ratio of amine to acid, control over the size of CsPbBr$_3$ NCs can also be achieved by employing extra halide sources such as alkylammonium bromide or ZnBr$_2$ salts.[106,125] In the first case, the size of the CsPbBr$_3$ nanocubes could be finely tuned from 17.5 to 3.8 nm by varying the amount of OLA-HBr but keeping the reaction temperature and the ligand concentration fixed.[125] In the second case, Dong et al. demonstrated excellent control over the size and size distribution of CsPbX$_3$ NCs by adjusting the reaction temperature and the ZnX$_2$/PbX$_2$ ratio in the reaction mixture.[106] It is particularly interesting that, in this latter case, an excess of ZnX$_2$ was found to strongly influence the surface passivation of the resulting NCs, eventually leading to a high PLQY.

A disadvantage of the HI method is that Cs/FA-oleate precursors, which have to be prepared in a separate flask before the actual reaction, are solid at RT, therefore they often require a preheating step (up to 100 °C) prior to their injection. It is also known that it is not easy to up-scale this strategy since the injection of large quantities of a precursor at a high temperature results in a remarkable drop in the temperature as well as an inhomogeneous nucleation. Consequently, this

method cannot be used for large scale production.[26] To overcome these limitations, different groups have developed alternative routes which rely on the same precursors, ligands, and solvents that are used for the HI route, but they mix all the chemicals together in one-pot and react them either by using a heating mantle (heat-up or solvothermal approaches) or by ultrasonication or microwave irradiation.[99,117,129,130,133,134]

Chen et al. reported a solvothermal synthesis of both $CsPbX_3$ nanocubes and NWs.[126] In short, $CsPbX_3$ nanocubes were synthesized by directly mixing precursors (such as cesium carbonate and lead halide salts) together with ligands, and the resulting mixture was heated up in an autoclave at the desired temperature for a certain amount of time. Ultrathin $CsPbBr_3$ NWs were obtained when predissolved precursors (such as Cs-oleate and lead halide dissolved in ODE by using OA and OLA) were used. In 2016, Tong et al. first reported a single step ultrasonication-assisted synthesis to produce $CsPbX_3$ NCs with a tunable halide composition, thickness, and morphology (Figure 6).[117] The same authors later extended the procedure,
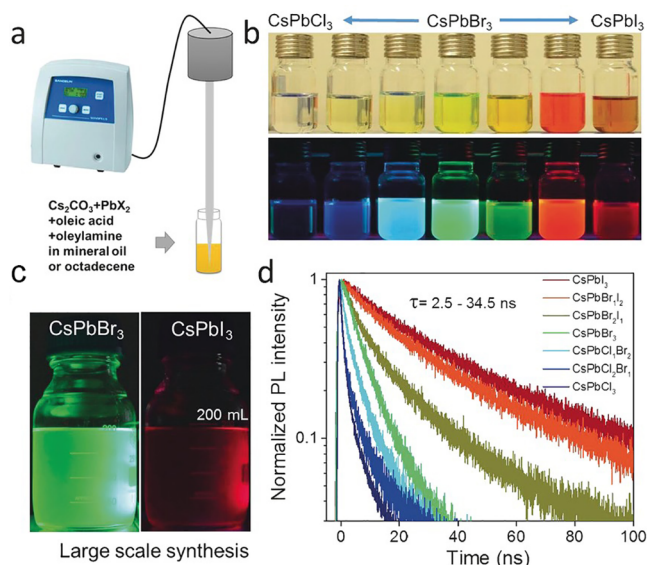

Figure 6. Single step ultrasonication method: (a) schematic illustration of a $CsPbX_3$ NC synthesis; (b) colloidal dispersions of $CsPbX_3$ NCs with different halide compositions in hexane under room light (top) and UV light (bottom, λ_{ex} = 367 nm); (c) photograph (under UV light) of $CsPbBr_3$ and $CsPbI_3$ NCs solutions obtained by scaling up the reaction; and (d) PL decay curves of the samples shown in panel (b). All panels are reproduced with permission from ref 117. Copyright 2016 Wiley-VCH.

prolonging the reaction time in order to produce $CsPbX_3$ NWs.[127] Similarly, $CsPb(Br/I)_3$ nanorods (NRs) were also prepared by adjusting the ratios of ligands (OLA/OA) and the reaction temperature.[128]

In 2017, Pan et al. introduced the microwave irradiation strategy for the synthesis of $CsPbX_3$ NCs with tunable morphologies.[129] In the same year, Shamsi et al. modified this approach to produce quantum-confined blue-emitting $CsPbBr_3$ NPLs with a unimodal thickness distribution.[130] In this method, a certain amount of isopropanol can trigger the nucleation of otherwise unreactive precursors at RT. The NPLs were then grown by simply heating the solution in a microwave oven.[130] Recently, Liu et al. further optimized the microwave-based strategy by introducing diethylene glycol

butyl ether along with ODE in order to enhance the absorption capacity of the microwave irradiation. In this approach, the dimensionality of $CsPbBr_3$ NCs could be tuned from cubes to NRs or NSs by adjusting the relative amounts of ligands, solvents, and $PbBr_2$ salt.[131] Liu et al. and Long et al. later adopted the same strategy to prepare $CsPbX_3$ NCs.[132,133] Ye et al. proposed alternative one-step approaches for the synthesis of inorganic $CsPbX_3$ NCs:[117,134] in short, PbX_2 and $CsCO_3$ precursors were added to the mixture containing ODE, OA, and OLA, and the reaction mixture was heated up to 100 °C for 15–30 min. In the same year, Yang et al.reported a heat-up approach for a large scale synthesis of ultrathin $CsPbBr_3$ NPLs with tunable dimensions by varying the reaction kinetics.[135] The thickness of the $CsPbBr_3$ NPLs was increased from 1.3 to 3.1 nm by increasing the temperature from 100 to 180 °C. In 2017, Zhai et al. adopted the solvothermal approach,[126] and they were able to transform $CsPbBr_3$ NPLs into Cs_4PbBr_6 NCs.[136]

All approaches discussed so far mainly rely on a binary ligands system that is composed of carboxylic acids (mainly OA) and alkyl amines. It is has now been well-established that the surface of LHPs NCs is dynamically stabilized with either oleylammonium halide or Cs oleate.[103,289] However, the final ligand's composition strongly depends on the processing conditions. For instance, upon the use of polar solvents during washing cycles, the ammonium ligands are more prone to be detached from the surface than carboxylate groups are, and this eventually modifies the final PLQY.[120] To address this issue, Krieg et al. proposed a new capping strategy based on long chain zwitterionic molecules (i.e., 3-(N,N-dimethyloctadecylammonio)propanesulfonate).[137] These molecules bind strongly to the NC surface, and this improves the chemical durability of the material. In particular, this class of ligands allows for the isolation of clean NCs with high PLQYs (above 90%) after four rounds of precipitation/redispersion, along with much higher overall reaction yields of uniform and colloidal dispersible NCs.[137]

3.1.2. Mixed A/B Cations Engineering of ABX_3 NCs by HI.

Inspired by the opportunity to produce LHP NCs with a mixed halide composition, which allows for the tunability of their resulting band gap, various groups started to explore the possibility of preparing ABX_3 NCs using mixed A and B cations. For instance, in 2017, Amgar et al. and Wu et al. reported the synthesis of $Cs_xRb_{1-x}BX_3$ by adjusting the Cs^+ and Rb^+ precursor ratios in the HI synthesis.[138,139] Interestingly, NC samples with a higher fraction of small Rb^+ ions had a higher band gap. In the same year, Wang et al. reported that a partial substitution of Pb^{2+} with Sn^{4+} ions not only enhanced the stability of the NCs, but also their optical properties.[140] Protesescu et al. and Wang et al. reported an HI-based synthesis of mixed organic inorganic $FA_xCs_{1-x}PbBr_{3-x}I_x$ and $FA_xCs_{x-1}PbI_3$ (0 ≤ x ≤ 3) perovskite NCs, NSs, and NWs.[67,141] Both reports concluded that the introduction of FA cations along with Cs ions in the A sites considerably enhances the stability of these compounds. Vashishtha et al. demonstrated that conventional monovalent A cations, such as Cs, Rb, MA, and FA, could be replaced by Tl^{3+} ions. Tl_3PbX_5 NCs (X= Cl, Br, I) and $TlPbI_3$ NCs were prepared using the standard HI approach by replacing Cs-oleate with Tl-oleate.[142] The HI of Tl-oleate into the PbX_2 solution (130–175 °C) resulted in faceted spheroidal Tl_3PbX_5 (X= Br, I) NCs with an orthorhombic crystal structure, whereas Tl_3PbCl_5 NCs crystallize in the tetragonal phase.[142]

By making simple modifications to the standard HI approach, lead halide based NC systems were successfully doped with either Mn^{2+}, Bi^{3+}, or rare earth (RE) ions in order to alter their optical properties.[143−148] Liu et al. and Parobek et al. almost simultaneously reported an HI synthesis of Mn^{2+} doped $CsPbCl_3$ NCs with fine control over the doping content. In both cases, the incorporation of Mn^{2+} ions was achieved by simply employing $MnCl_2$, in addition to $PbCl_2$, in the conventional HI method that had previously been reported for the synthesis of $CsPbX_3$ NCs (Figure 7, panels a and
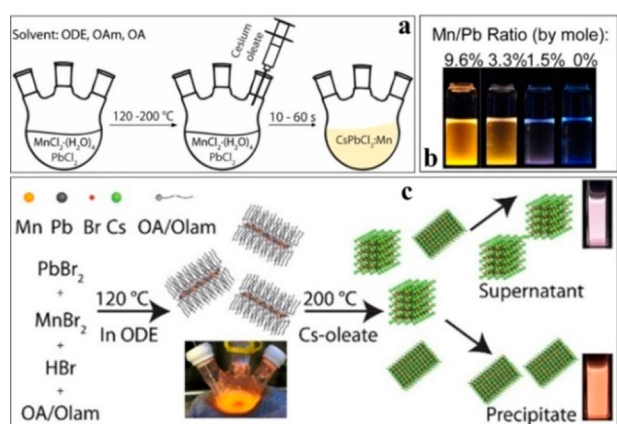

Figure 7. Illustrations of the HI approaches used for the preparation of (a) Mn-doped $CsPbCl_3$ and (c) Mn-doped $CsPbBr_3$ NCs. (b) Photograph of Mn doped $CsPbCl_3$ NCs with different Mn-contents, illuminated by a UV lamp (365 nm). (a) is reproduced from ref 150. Copyright 2016 American Chemical Society. (b) is reproduced from ref 149. Copyright 2016 American Chemical Society. (c) is reproduced from ref 152. Copyright 2018 American Chemical Society.

b).[149,150] Later, Das Adhikari et al. further optimized the inclusion of Mn^{2+} ions in $CsPbCl_3$ NCs by using RNH_3Cl in addition to the $MnCl_2$ salt.[148,151] The authors claimed that the alkyl ammonium chloride precursor could allow the morphology to be precisely controlled and could enable Mn to be incorporated into $CsPbCl_3$ NCs. The following year, a similar strategy was adopted and slightly modified by Parobek et al. for the synthesis of Mn-doped $CsPbBr_3$ NCs.[152] Instead of using an alkyl ammonium halide precursor, the authors employed HBr, which was initially mixed with $PbBr_2$, $MnBr_2$, OA, and OLA to form $L_2[Pb_{1−x}Mn_x]Br_4$ (L = ligand) organometallic complexes. Such compounds, which exhibit a strong Mn fluorescence, were subsequently transformed into Mn-doped $CsPbBr_3$ NCs by injecting the Cs precursor at a high temperature (Figure 7c).[152] It is particularly interesting that doping $CsPbX_3$ NCs with Mn^{2+} ions increased their stability under ambient conditions and against thermal annealing.[153,154] Similarly, heterovalent dopants, such as Ce^{3+} and Bi^{3+} ions, were introduced into $CsPbBr_3$ NCs.[155,156] Milstein et al. recently reported ytterbium-doped $CsPbCl_3$ NCs by means of an HI synthesis following their previous three-precursor approach for double perovskites.[157]

3.1.3. Pb-Free Metal Halide Perovskite NCs. The first colloidal syntheses of lead-free perovskite NCs via the HI approach were reported in 2016 by Jellicoe et al.[78] and Wang et al.[158] The former group was able to prepare $CsSnX_3$ NCs by reacting SnX_2 salts, which were dissolved in tri-n-octylphosphine (TOP) and injecting the resulting solution into a

mixture of $CsCO_3$, OA, and OLA at 170 °C.[78] Wang at al. fabricated Sn^{4+}-based perovskite NCs, with a Cs_2SnI_6 composition, which exhibited a PL peak around 620 nm (2.0 eV) and a full width at half-maximum of 49 nm (0.16 eV).[158] The variation in the reaction time enabled the size and shape of Cs_2SnI_6 NCs to be tuned so that spherical quantum dots, NRs, NWs, nanobelts, and NPLs could be selectively prepared (Figure 8).[158] The HI synthesis of Sn-based compounds was
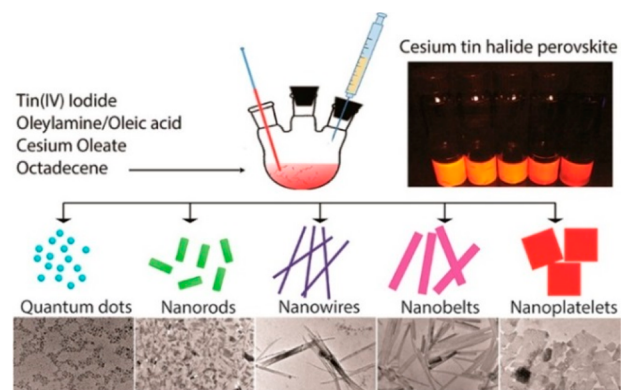

Figure 8. Scheme showing the synthesis of perovskite Cs_2SnI_6 NCs, with corresponding photographs of the as-prepared Cs_2SnI_6 samples under UV light and TEM images of Cs_2SnI_6 NCs with different shapes. Reproduced from ref 158. Copyright 2017 American Chemical Society.

later modified slightly to access different shapes.[18,75,158] For example, Wong et al. synthesized 2D $CsSnI_3$ NPLs, with a thickness of less than 4 nm,[18] by using a combination of long and short chain amines (OLA and octylamine) and a short chain carboxylic acid (octanoic acid). In 2018, Wu et al. reported a synthesis of ternary $CsGeI_3$ NCs by means of an HI approach.[159] The NCs were synthesized by simply injecting Cs-oleate into a solution of GeI_2 which had been dissolved in ODE, OA, and OLA.[159]

Many attempts have been made to prepare Pb-free perovskite NCs by simply substituting Pb^{2+} ions with ternary cations, such as Bi^{3+} or Sb^{3+}, forming $Cs_3M_2X_9$ compounds, or by the so-called "cation transmutation" strategy, namely, the replacement of two Pb^{2+} ions with one monovalent M^+ ion and one trivalent M^{3+} ion, forming a $A_2M^{+}M^{3+}X_6$ double-perovskite structure (see section 2.3). Examples are $Cs_3Sb_2I_9$ and $Rb_3Sb_2I_9$, NCs that have been prepared with different morphologies using the HI synthesis route.[160−162] Also, in 2018, "double-perovskite" Cs_2AgBiX_6 (X = Cl or Br) NCs were synthesized by means of HI approaches.[159,115,163,164] Double perovskites in the form of NCs were reported by two groups using two different HI synthetic routes. Creutz et al.[115] employed, for the first time, trimethylsilyl halides which were injected at 140 °C into a solution of metal acetate precursors (i.e., silver acetate, cesium acetate, and bismuth acetate). The solution was then dissolved in ODE, OA, and OLA, which immediately triggered the nucleation and growth of the NCs (Figure 9). Around the same time, Zhou et al. were the first to prepare a solution of $AgNO_3$, $BiBr_3$, ODE, OA, OLA, and HBr, followed by an injection of Cs-oleate at 200 °C to synthesize lead-free $Cs_2AgBiBr_6$ NCs.[163]

3.2. LARP Approach

The supersaturated recrystallization process dates back more than 5000 years, when salt was recrystallized in clay pots in
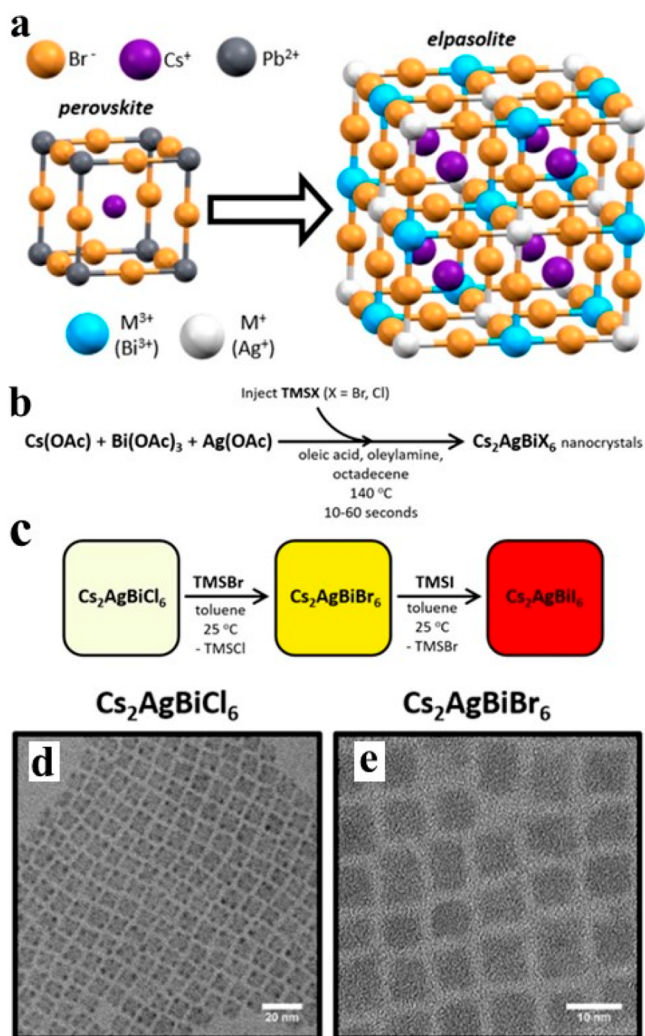
Figure 9. (a) The structure of a double perovskite crystal (e.g., Cs$_2$AgBiBr$_6$). (b) Scheme of the HI synthesis of Cs$_2$AgBiX$_6$ NCs and (c) their postsynthesis anion-exchange reactions using trimethylsilyl halide reagents. TEM images of (d) Cs$_2$AgBiCl$_6$ and (e) Cs$_2$AgBiBr$_6$ NCs. All panels are reproduced from ref 115. Copyright 2018 American Chemical Society.

South Poland in 3500 BC.[165] This simple process consists of dissolving the desired ions in a solvent, reaching an equilibrium concentration, and subsequently moving the solution into a nonequilibrium state of supersaturation. The supersaturated state can be reached, for example, by varying the temperature (cooling down the solution), by evaporating the solvent, or by adding a miscible cosolvent in which the solubility of the ions is low. Under such conditions, spontaneous precipitation and crystallization reactions occur until the system reaches an equilibrium state again. This technique was also successfully extended, in the nineties, to prepare organic nanoparticles and polymer dots.[166,167] If this process is carried out in the presence of ligands, hence the name "ligand-assisted reprecipitation" (LARP), the formation and growth of crystals can be controlled down to the nanoscale, allowing for the fabrication of colloidal NCs (Scheme 3).

The LARP technique, when applied to perovskite systems, simply consists of dropping the desired precursor salts, dissolved in a good polar solvent, such as dimethylformamide (DMF), dimethylsulfoxide (DMSO), etc., into a poor solvent

Scheme 3. LARP Synthesis Approach
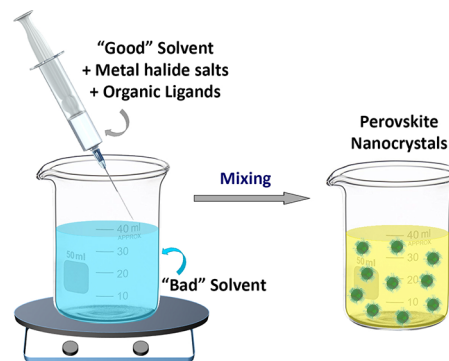
(such as toluene or hexane) in the presence of ligands. The salts that are typically used in the LARP approach are MX$_2$ (M = Pb, Sn, etc.), CsX, MAX, and FAX, where X = Cl, Br, and I. The mixture of the two solvents induces an instantaneous supersaturation, which triggers the nucleation and the growth of perovskite NCs. It is straightforward to understand that, being the LARP synthesis carried out in air using a quite simple chemical apparatus, differently from the HI techniques, it can be easily scaled up, allowing for the large-scale production of MHP NCs, up to the gram scale.[130,168,169] As in the case in the hot-injection or heat-up methods, that are described in the previous sections, nucleation and growth stages in the LARP approach cannot be separated in time.[99] The first reports on LARP syntheses of hybrid organic−inorganic lead halide based perovskite NCs date back to 2012 when Papavassiliou et al. solubilized MAPbX$_3$, (MA)-(CH$_3$C$_6$H$_4$CH$_2$NH$_3$)$_2$Pb$_2$X$_7$, or (MA)(C$_4$H$_9$NH$_3$)$_2$Pb$_2$X$_7$ (X = Br, Cl or I) salts in DMF (or acetonitrile) and dropped the corresponding solutions in toluene (or in a mixture of toluene and PMMA).[170] They observed the formation of luminescent NCs, with sizes on the order of 30−160 nm, and PL intensities much higher than those expected for the bulk MAPbX$_3$ counterparts. It took a few more years before the LARP procedure was finally developed to synthesize organic−inorganic MAPbX$_3$ NCs, and then it was extended to ABX$_3$ NC systems (A = MA, FA, or Cs; B = Pb, Sn, Bi, or Sb; X = Cl, Br, or I). In the following sections, we will briefly describe the LARP approaches that have been proposed so far for each system, illustrating how composition, size, shape, and phase control have been achieved in MHP NCs.

3.2.1. MAPbX$_3$ NCs. The first LARP approach to organic−inorganic MAPbBr$_3$ NCs was demonstrated and systematically studied in 2015 by Zhang et al.,[171] who prepared a clear precursor solution by dissolving PbBr$_2$ and MABr salts in alkyl amines, carboxylic acids, and DMF. A fixed amount of this solution was then dropped into toluene at RT under vigorous stirring to form colloidal NCs. In order to understand the specific role of alkyl amines and carboxylic acids, different amines (hexylamine, octylamine, dodecylamine, hexadecylamine) and acids (OA, octanoic acid, or butyric acid) were tested. Interestingly, the formation of MAPbBr$_3$ NCs could be achieved even without the use of amines, but there was no control over the size of the crystals. On the other hand, the exclusion of carboxylic acids from the synthesis resulted in aggregated NCs. On the basis of these control experiments, the authors concluded that the role of amines was to regulate the kinetics of the crystallization, and thus the NCs' size, while the organic acids were thought to suppress NC aggregation. In the

years that followed, this same approach was exploited and further optimized by different groups.[172−174] Huang et al., for example, demonstrated that the size and size distribution of MAPbBr$_3$ NCs could be better controlled by introducing OLA together with OA and varying the reaction temperature (by heating toluene up to 60 °C).[172] Arunkumar et al. demonstrated that it is possible to dope MAPbX$_3$ NCs with Mn^{2+} simply by adding MnCl$_2$ to the precursor solution.[173]

Other ligands were subsequently proved to work efficiently in the LARP synthesis of MAPbBr$_3$ NCs. Gonzalez-Carrero et al. showed that OLA and OA could be replaced by 2-adamantylammonium bromide as the only capping ligand to improve the optical properties of the final NCs. Luo et al. produced size tunable MAPbX$_3$ (X = Cl, Br, or I) NCs by employing two branched capping ligands, (3-aminopropyl)-triethoxysilane (APTES) and polyhedral oligomeric silsesquioxane (POSS) PSS-[3-(2-aminoethyl)amino]-propylheptaisobutyl-substituted (NH$_2$-POSS).[175] The authors proposed that, compared to straight-chain ligands, APTES and NH$_2$−POSS offer greater control over the NCs' size, as they are able to protect the formed NCs from being dissolved by DMF.[24] Veldhuis et al. introduced the use of benzoyl alcohol as an auxiliary ligand (together with octylamine and OA), which was found to accelerate the reaction kinetics and to improve the optical properties of the resulting NCs.[176] Luo et al. employed peptides, namely 12-aminododecanoic acid, as the only ligand in the synthesis of MAPbBr$_3$ NCs. Peptides, which have both −NH$_2$ and −COOH groups, enabled a good control over the size of the resulting NCs.[177] Minor modifications to the LARP process were also proposed in order to further optimize the process. Shamsi et al., for example, devised an alternative LARP approach in which PbX$_2$ salts are dissolved in N-methylformamide (NMF), rather than in the typical DMF, together with OLA and OA. The solution is heated up to 100 °C for 10 min and eventually added dropwise at RT to a poor solvent (such as dichlorobenzene or chloroform).[178] The advantage of this approach is that MA$^+$ ions are formed in situ during the heating step (by a transamidation reaction), therefore there is no need to previously synthesize MAX salts.[178] It is worth mentioning that the same approach could also yield bulk crystals at RT with no need for an antisolvent (Scheme 4).[178]

Dai et al. mixed both good solvents and poor solvents by means of a spray, producing MAPbBr$_3$ NCs with a good size distribution.[179] In this particular approach, the precursor's solution (MABr, PbBr$_2$, OA, octylamine in DMF) was sprayed onto a poor solvent (toluene). The micrometer-sized droplets of the sprayed solution are believed to provide a large contact surface area between the two solutions, allowing for a more homogeneous mixing.
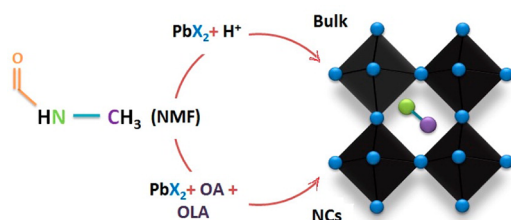
3.2.2. Size and Shape Control over MAPbX$_3$ NCs.
Soon after the development of the LARP synthesis of MAPbX$_3$ NCs, efforts were made to optimize the PL of the materials and to control their size and shape. In 2015, Sichert et al. were the first group to report a LARP synthesis of MAPbBr$_3$ NPLs in which no carboxylic acid was employed; only octylammonium and MA$^+$ ions were used as ligands.[17] The systematic increase in the octylammonium/MA$^+$ ratio caused a reduction in the thickness of the resulting NPLs. The exception to this was the use of octylammonium only (octylammonium/MA$^+$ → ∞), when "single layered" NPLs were observed, similar to what was reported in the studies on layered perovskite macrocrystals.[180] Analogous results were achieved in 2016 by different groups. Kumar et al., for example, demonstrated that they could control the thickness of MAPbBr$_3$ NPLs down to one monolayer when they worked with OA and octylamine.[33] Cho et al., on the other hand, conducted a systematic study on the LARP synthesis of MAPbBr$_3$ NPLs in which they used OA and tested many alkylamines with different chain lengths (such as butylamine, hexylamine, octylamine, dodecylamine, and OLA).[181] They revealed that both the chain length and the concentration of alkylamines played a fundamental role in determining the thickness of MAPbBr$_3$ NPLs. In detail, a high concentration of alkylammonium cations can efficiently passivate the surface of MAPbBr$_3$ NCs, precluding their growth along the vertical direction and yielding NPLs with tunable thicknesses. In this context, the amines with a longer chain have a better electrostatic interaction with perovskite NCs, providing, thus, a stronger passivation. In 2017, Levchuk et al., working with OLA and OA, achieved a good control over the thickness of MAPbI$_3$ NPLs by introducing chloroform as the bad solvent.[182] Ahmed et al. proposed using pyridine, together with OLA and OA, as an effective coligand for finely tuning the thickness of MAPbBr$_3$ NPLs (Figure 10).[183] Their DFT calculations revealed that pyridine molecules are able to bind to the Pb^{2+} ions that are present on the surface of the growing nanostructures, forming dative N → Pb bonds and slowing down the vertical growth rate, thus leading to the formation of 2D nanostructures.[183]

It should be noted that no control over the lateral dimensions of the NCs was demonstrated in any of these works. With the aim of addressing this problem, Kirakosyan et al. revealed that the way the precursor solution (ionic salts dissolved in DMF) is added to the bad solvent influences the size and shape of the final NCs.[184] By varying the amount of added precursor solution (from 1 to 8 drops at a constant rate of ~45 drops/min), they could tune the lateral size of MAPbBr$_3$ NPLs from ~3 to 8 nm, while the thickness remained unchanged (2.5−3 nm). In the same year, Huang et al. performed a systematic study on how the amount of ligands (OLA and OA), the precursors/ligands ratio and the reaction temperature affect MAPbBr$_3$ NCs.[185] Similar to what was reported by Cho et al.,[181] they observed that a fine-tuning of these parameters resulted in a control over the size, and, thus, of the quantum confinement of MAPbBr$_3$ NCs. More in detail, working with a high ligand/precursor ratio, they observed the formation of small NCs, while a high precursor/ligand ratio produced polydisperse micro- and NCs. At intermediate ligand/precursor ratios, the nucleation and growth of the
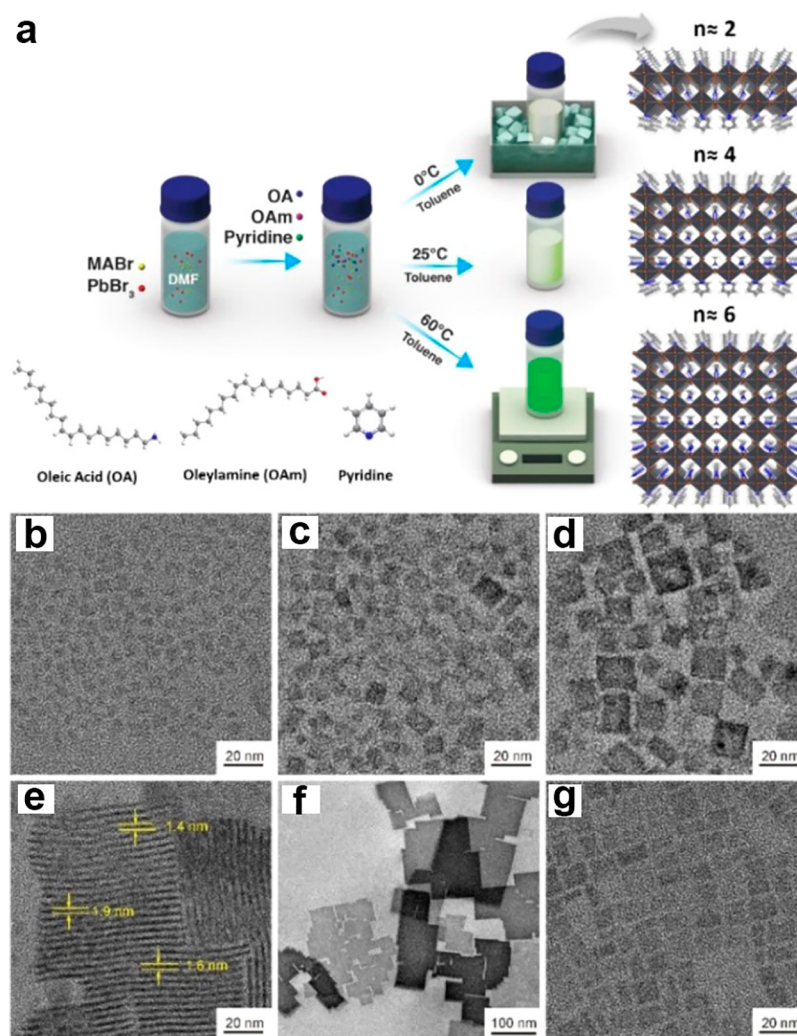
Scheme 4. Two Different Synthetic Routes, Both Employing NMF as the Source of MA$^+$ Ions, To Produce Either Perovskite NCs or Bulk Crystals^a

^{a}Reproduced from ref 178. Copyright 2016 American Chemical Society.

Figure 10. (a) Schematic illustration of a LARP synthesis of MAPbBr$_3$ nanostructures using oleic acid (OA), oleylamine (OLA), and pyridine as ligands. Representative TEM images of MAPbBr$_3$ NCs synthesized (b–d) without and (e–g) with pyridine at different precipitation temperatures: (b,e) 0 °C, (c,f) 25 °C, and (d,g) 60 °C, respectively. All panels are reproduced from ref 183. Copyright 2017 American Chemical Society.

NCs could be better controlled: the synthesis under such conditions produced small NCs that grew over time.

At this stage, we can tentatively summarize that the control over the size and thickness of MAPbBr$_3$ NPLs in the LARP approach can be achieved by using a sufficiently high ratio of long chain alkylammonium ions (or pyridine)/precursors. In this way, alkylammonium ligands (or pyridine) can significantly passivate the surface of MAPbBr$_3$ NCs, preferentially slowing down the vertical growth rate and allowing NCs to grow only along the lateral directions.

The LARP procedure, initially developed for MAPbX$_3$ NCs, was soon extended to all-inorganic CsBX$_3$ (B = Pb^{2+}, Bi^{3+}, and Sb^{3+}), Cs$_4$PbX$_6$, CsPb$_2$Br$_5$, and organic–inorganic FAPbX$_3$ NC systems. We will discuss the achievements in the synthesis of each system in separate sections.

3.2.3. FAPbX$_3$ NCs. In 2016, Weidman et al. were the first to report a LARP synthesis of both all-inorganic and organic–inorganic ABX$_3$ (A = Cs, MA, or FA; B = Pb or Sn) NPLs with 1 or 2 monolayer thicknesses.[186] In their work, the precursors (AX and BX$_2$ salts) were dissolved in DMF together with octylammonium and butylammonium halides (used in a 1:1 ratio). The precursor solution was added dropwise to toluene under vigorous stirring at RT to trigger an immediate

formation of NCs. To achieve colloidal stability and thickness homogeneity, an excess of ligands was used (in a 10:2:1 ligands/BX$_2$/AX).[186] A few months later, Perumal et al. reported the synthesis of FAPbBr$_3$ NCs. The focus of their work was mainly on achieving a bright PL emission rather than having tight control over the particle shape.[187] In their approach, FABr and PbBr$_2$ were dissolved in DMF and added dropwise to a solution consisting of toluene, butanol, octylamine, and OA under constant stirring.

The first LARP report on FAPbX$_3$ (X = Cl, Br, or I) NC systems was reported by Levchuk et al., who applied the same synthesis scheme that they had used for making MAPbX$_3$ NCs (which they had published some months before),[182] but with some minor modifications.[188] The synthesis relies on the rapid injection of a precursor solution, which is prepared by dissolving PbX$_2$ and FAX (X = Cl, Br, or I) salts in DMF, OA and OLA into chloroform at RT (Figure 11, panels a and b). With dependence on the OLA/OA ratio, the authors could produce either nanocubes or NPLs with control over their thickness (ranging from 2 to 4 monolayers, Figure 11, panels c and d). Interestingly, it was discovered that toluene prevented the formation of FAPbI$_3$ NCs, and it led to the immediate agglomeration of FAPbBr$_3$ or FAPbCl$_3$ NCs.
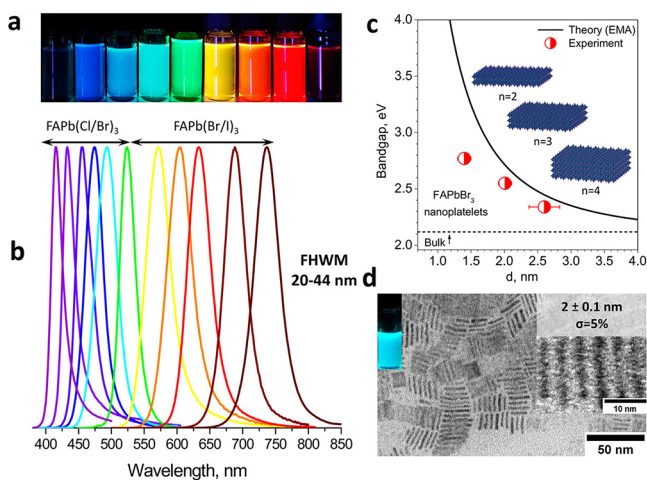
Figure 11. (a) Photograph of FAPbX$_3$ NC dispersions under UV-light and (b) the corresponding PL emission curves. (c) Theoretical effective mass approximation and experimental band gaps of FAPbBr$_3$ NPLs as a function of their thickness. (d) TEM characterization of vertically stacked FAPbBr$_3$ NPLs. All panels are reproduced with permission from ref 188. Copyright 2017 American Chemical Society.

Around the same time, Minh et al. reported the synthesis of FAPbX$_3$ nanocubes, introducing PbX$_2$–DMSO complexes as novel precursors.[189] In their approach, all the precursors (the PbX$_2$–DMSO complex and FAX) were dissolved in DMF together with OLA, and the corresponding solution was added to a mixture of toluene and OA. In this case, the formation of FAPbX$_3$ NCs is believed to occur via an intramolecular exchange reaction in which alkylammonium halides can replace DMSO molecules in the starting PbX$_2$-DMSO complex. Good control over the size distribution of the NCs was rendered possible by varying the relative amount of OLA.[189] Kumar et al. reported a slightly modified LARP procedure to create FAPbBr$_3$ NPLs with a very high PLQY which could be used in LED devices.[190] The difference here is that FABr and PbBr$_2$ salts were dissolved in ethanol and DMF, respectively, to form

two different polar solutions, which were then added simultaneously to a mixture of toluene, OA, and octylamine.[190]

3.2.4. All-Inorganic CsPbX$_3$ NCs. Until 2015, all-inorganic CsPbX$_3$ NCs could only be synthesized using the hot-injection approach.[26] However, in 2016, Li et al. showed that all-inorganic perovskite systems in the form of colloidal NCs could also be produced using the LARP approach at RT. Their synthesis resembles the one used for the organic–inorganic MAPbX$_3$ NC systems, with the only difference being that CsX is used rather than MAX in the precursor solution.[191] Moreover, in this case, the inorganic salts (CsX and PbX$_2$) are dissolved in DMF together with OLA and OA. They are then added to toluene, which results in an instantaneous formation of NCs. A few months later, Seth et al. further engineered this approach to achieve control over the morphology of CsPbX$_3$ NCs.[192] They found that the shape of the NCs could be controlled by varying the bad solvent (from toluene to ethyl acetate), the relative amount of ligands, and the reaction time: the use of ethyl acetate promotes the formation of quasi-cubic QDs, NPLs, or nanobars, while toluene can be used for the preparation of nanocubes, NRs, or NWs.[192] The authors tentatively attributed these different morphologies to the different ligand/nonpolar solvent interactions. Since ethyl acetate is more polar than toluene, it can act both as a solvent and a nucleophile, causing some OLA molecules to detach themselves from the surface of the growing nuclei, which, thus, undergo an oriented attachment (Figure 12a). In toluene, if the concentration of OLA is high enough, the NC surfaces become more protected in all directions, which consequently prevents both their attachment/merging and growth. However, if only a small amount of OLA is used in toluene, the NCs can grow anisotropically at longer reaction times, in the form of NRs and NWs, most likely as a consequence of an incomplete surface passivation of the facets (Figure 12b).

In 2017, Kostopoulou et al. reported a LARP synthesis of CsPbBr$_3$ NWs with micron-sized lengths.[193] The key feature of their approach is that they use anhydrous solvents and a low temperature: the precursor solution (CsBr, PbBr$_2$, DMF, OLA, and OA) is dropped into anhydrous toluene, which is kept in
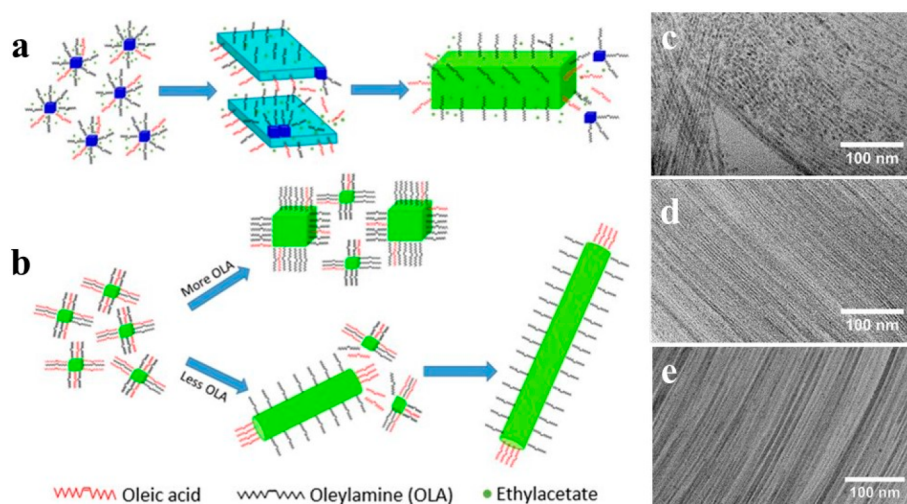
Figure 12. Sketch of the mechanism proposed for the formation of (a) NPLs (cyan) and nanobars (green) in ethyl acetate and (b) larger nanocubes, nanorods, and NWs from smaller nanocubes in toluene. (a–b) are reproduced with permission from ref 192. Copyright 2016 Macmillan Publishers Limited. (c–e) TEM images of CsPbBr$_3$ NWs at (c) 0 days, (d) 1 day, and (e) 7 days after leaving the colloidal toluene-based solution at RT without stirring. (c–e) are reproduced with permission from ref 193. Copyright 2017 Royal Society of Chemistry.

an iced water bath. Immediately after the injection, the resulting product consists of small-length, bullet-like NRs, which evolve into NWs with a width of 2.6 nm after 24h at RT, and to thicker NWs with a diameter of 6.1 nm after 1 week (Figure 12, panels c−e). Eventually, in 2018, Zhang et al. deliberately introduced water to the LARP synthesis of $CsPbBr_3$ NCs, demonstrating its influence on the growth rate and the shape of the resulting crystals.[194] The authors suggested that both H_3O^+ and OH^- may act as surface ligands with a higher activity than those of oleylammonium and oleate species. Consequently, this caused the perovskite NCs to grow in different directions.[194]

3.2.5. Mixed A-Cations APbX$_3$ NCs. With the aim of tuning the spectral response (i.e., the bandgap) of $APbX_3$ NCs, various groups started not only to vary the halide composition of those materials but also the A cations' composition.[74,195] There have been several reports on the synthesis of LHP NCs using the LARP method, with control over the composition of the A site. Mittal et al., for example, successfully tuned the bandgap of $APbBr_3$ NCs from 2.38 to 2.94 eV by varying the composition of the A site from pure MA to pure ethyl-ammonium (EA) [i.e., they synthesized $(EA)_x(MA)_{1-x}PbBr_3$ NCs].[196] In 2017, two different groups reported the synthesis of $Cs_{1-x}FA_xPbX_3$ NCs.[197,198] Xu et al. mixed Cs and MA ions to form $MA_{1-x}Cs_xPbBr_3$ NCs,[199] while Zhang et al. reported a LARP synthesis of mix-organic-cation $FA_xMA_{1-x}PbX_3$ NCs, achieving a continuously tunable PL emission from 460 to 565 nm.[200]

3.2.6. CsPb$_2$Br$_5$ NCs. In 2016, Wang et al. reported the first colloidal synthesis of perovskite-related $CsPb_2Br_5$ NPLs,[169] adopting the LARP approach that was proposed by Sichert et al.[17] In Wang et al.'s work, two different precursor solutions were prepared in DMF: one containing $PbBr_2$ and hexylammonium bromide, and one containing CsBr. These solutions were added to toluene to trigger the formation of the final NCs.[169] The authors also reported that such a synthetic procedure could not be used for the preparation of pure phase $CsPb_2Cl_5$ and $CsPb_2I_5$ NCs by substituting bromide salts ($PbBr_2$, CsBr, and HABr) with the corresponding chloride or iodide ones.[169]

Ruan et al. subsequently optimized the LARP strategy in order to control the morphology of $CsPb_2Br_5$ NCs.[201] This was achieved by introducing alkyl thiols (octanethiol) as ligands together with either alkylamines (OLA) or carboxylic-acids (Figure 13).[201] More precisely, under their experimental

conditions, $CsPb_2Br_5$ NWs were obtained by employing octanethiol and OLA, while $CsPb_2Br_5$ NSs required the use of alkyl-thiols and carboxylic-acids.[201] The following year, the same authors demonstrated that their approach could be used for a direct synthesis of tetragonal $CsPb_2X_5$ (X = Cl, Br, or I) NWs, even in mixed halide compositions.[202]

3.2.7. Pb-free perovskite-related NCs. Compared to the high number of works that report a colloidal synthesis of lead free perovskite NCs using the HI approach, there are very few examples of these compounds being produced by the LARP strategy. In 2016, Leng et al. proposed a LARP synthesis of $MA_3Bi_2X_9$ (X = Cl, Br, or I) perovskite-related NCs,[203] and, recently, of $Cs_3Bi_2X_9$ (X = Cl, Br, or I) NCs.[80,83] In their first work, octane was employed as the bad solvent, while DMF and ethyl acetate were used as good solvents for MAX and BiX_3 salts, respectively.[203] In their second work, they used DMSO to solubilize both CsX and BiX_3 salts and ethanol to trigger a recrystallization (Figure 14, panels a and b).[80] As in the case of Pb-based perovskite NCs, the amount of surfactants (octyl-amine and OA) was observed to play a major role in controlling the LARP synthesis of $Cs_3Bi_2X_9$ NCs. Interestingly, the use of toluene as a bad solvent, instead of ethanol, produced unstable NC solutions. In 2017, Zhang et al. adopted the LARP method to prepare blue-emitting $Cs_3Sb_2Br_9$ NCs. They dissolved $SbBr_3$ and CsBr salts in either DMF or DMSO in the presence of OLA to form a clear precursor solution, which was then dropped into a mixture of octane and OA (Figure 14, panels c and d).[76]

3.2.8. Disadvantages of LARP. Although it enables a direct synthesis of many different perovskite systems at RT under air, the LARP method also has some weak points. Perovskite NCs are very sensitive to polar solvents, therefore the polar solvents that are normally used in the LARP synthesis, for example DMF, can easily degrade and even dissolve the $CsPbX_3$ NCs, especially the $CsPbI_3$ ones.[168,171,204] Precursor-polar solvent interactions, indeed, were observed to play an important role in the formation of defective perovskite NCs. To elucidate this so-called "solvent effect", Zhang et al. investigated the effects of using different polar solvents on the crystallization of $MAPbI_3$ NCs.[205] They proved that PbI_2 generates stable intermediates in coordination solvents like DMSO, DMF, and tetrahydrofuran (THF), but it does not form complexes when it is dissolved in noncoordinating solvents, like γ-butyrolactone and acetonitrile.[205]

These different binding motifs have, in turn, different impacts on the crystal structure of the synthesized NCs: the strong bonding between PbI_2 and the coordinating solvents leads to the formation of defective $MAPbI_3$ NCs that contain residual solvent molecules on the surface and iodine vacancies in the bulk; when noncoordinating solvents are employed, PbI_2 units are able to crystallize into defect free $MAPbI_3$ NCs (Figure 15). Furthermore, DMF and DMSO, which are the typical polar solvents that are used in this approach, have a high boiling point and are toxic, therefore they are not suitable for large-scale production.

3.2.9. Alternative Approaches. While "typical" LARP syntheses rely on the use of miscible polar and nonpolar solvents, emulsion techniques are based on the use of nonmiscible liquids. The precursor's salts are dissolved in two different immiscible solvents with ligands and mixed together to form an emulsion. The reaction does not occur until later, when a demulsifier (which is miscible with both the two previous solvents) is added, immediately driving the
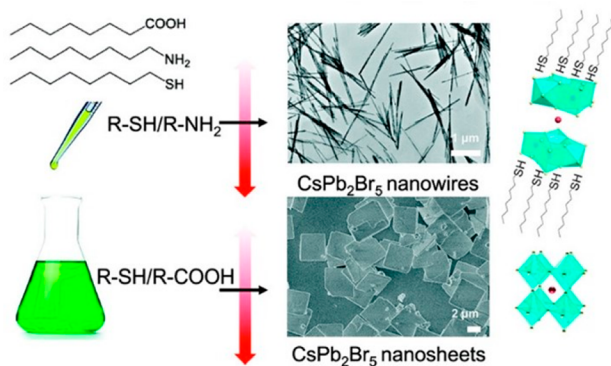

Figure 13. LARP synthesis of $CsPb_2Br_5$ NWs and NSs. Reproduced with permission from ref 201. Copyright 2017 American Chemical Society.
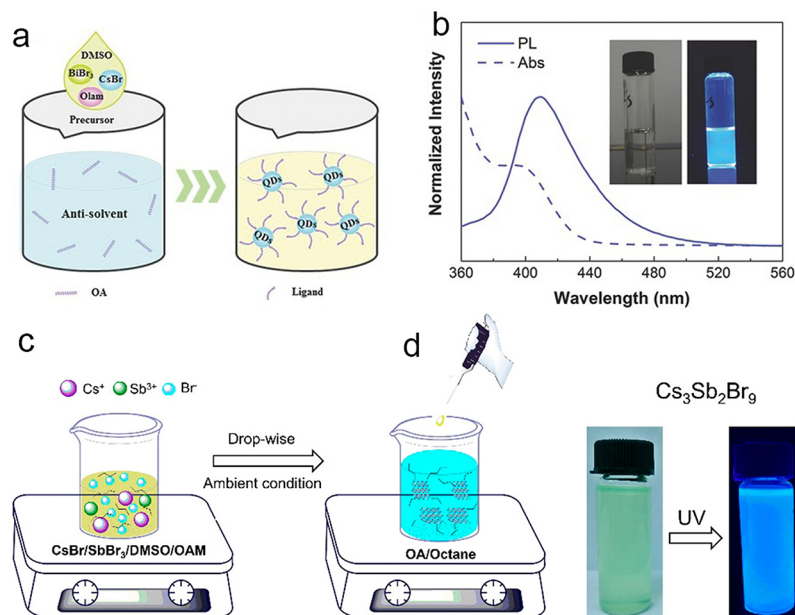
Figure 14. Illustration of the LARP approaches used for the synthesis of (a) $Cs_3Bi_2Br_9$ and (c) $Cs_3Sb_2Br_9$NCs. Photographs of vials containing colloidal (b) $Cs_3Bi_2Br_9$ and (d) $Cs_3Sb_2Br_9$ NCs dispersions with and without UV light excitation. (b) Absorption and PL spectra of $Cs_3Bi_2Br_9$ NC solutions. (a) and (b) are reproduced with permission from ref 80. Copyright 2018 Wiley-VCH. (c) and (d) are reproduced with permission from ref 76. Copyright 2017 American Chemical Society.
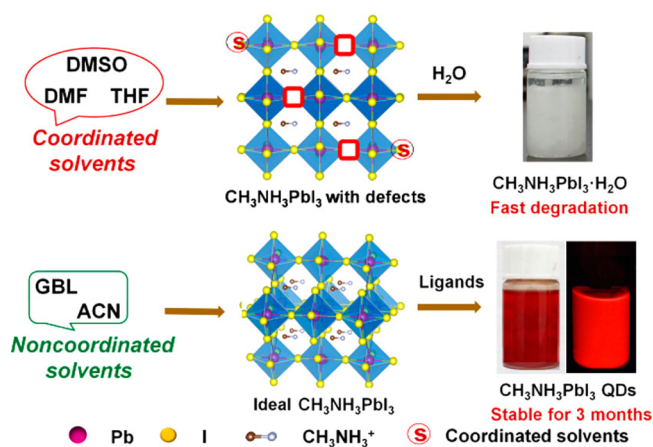

Figure 15. Effects of the solvents on the crystal structure of $CH_3NH_3PbI_3$ NCs: the use of coordinated solvents (top) leads to the formation NC defects, which are prone to degradation under humidity; noncoordinated solvents (bottom) allow for the formation of "defect-free" and stable NCs. Reproduced with permission from ref 205. Copyright 2017 American Chemical Society.

system into a state of supersaturation, causing the precipitation and nucleation of the $APbX_3$ NCs.[206,207] Henceforth, we will refer to this process as an "emulsion LARP". It is known that ligands in the polar-non polar systems can self-assemble into ordered structures called micelles.[206,207] In the microemulsion technique, such micelles are used as nanoreactors in which the precursors can diffuse and locally react to form the NCs. The process can be called a "microemulsion approach" if the micelles form within a bulk polar phase, where the hydrophobic carbon chains are turned inward to help stabilize the oil phase. However, the process can be called a "reverse microemulsion" approach if the main solvent is nonpolar and the micelles form with the hydrophilic head groups turned inward to help stabilize the aqueous phase (reverse

micelles).[208] In such syntheses, NC nucleation and growth is controlled by the diffusion of the precursors from the main phase into the micelles.[208] Once the NCs are formed inside the micelles, a demulsifier is added, enabling the product to be precipitated and cleaned. It should be noted that, in some cases, the difference between emulsion LARP approaches and the microemulsion (or inverted microemulsion) approach is very subtle. Indeed, if the emulsion is not properly characterized before the addition of the demulsifier, it is not always clear if the NCs nucleate inside the micelles before being precipitated or if their formation takes place in the very same moment that the demulsifier is added to the solution.

3.2.10. Emulsion LARP. In 2015, Huang et al. demonstrated that the emulsion LARP strategy could be used for the synthesis of $MAPbBr_3$ NCs.[209] They first prepared a solution of MABr and $PbBr_2$ in DMF, and then they mixed it with hexane, OA, and octylamine to form an emulsion. The subsequent addition of tert-butanol or acetone, which act as demulsifiers, initiated the recrystallization process with the formation of the NCs (Scheme 5).

Scheme 5. Emulsion LARP Synthesis[a]
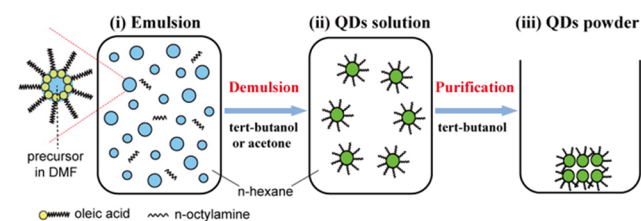
[a](i) Formation of the emulsion, (ii) demulsion by adding a demulsifier with the concomitant formation of perovskite NCs, and (iii) purification of the NCs. Reproduced from ref 209. Copyright 2015 American Chemical Society.

The following year, both Li et al. and Sun et al. reported the emulsion LARP synthesis of CsPbX$_3$ NCs.[191,210] They employed a solution of Cs-oleate, which had been dissolved in ODE, and added it to a solution of PbX$_2$ in DMF together with an alkylamine and a carboxylic acid. Such an emulsion was then added dropwise to toluene to start the nucleation process. In particular, Sun et al. tested different combinations of alkylamine and carboxylic acids and found that a systematic variation in the length of both the amine's alkyl chains and the carboxylic acid's alkyl chains resulted in a variation in the NCs' shape/size,[210] similar to what observed for organic−inorganic systems.[181] The use of hexanoic acid and octylamine produced spherical QDs, oleic acid and dodecylamine shaped the NCs into nanocubes, acetate acid and dodecylamine promoted the formation of NRs, while OA and octylamine produced NPLs (Figure 16). Akkerman et al. synthesized CsPbBr$_3$ NPLs using
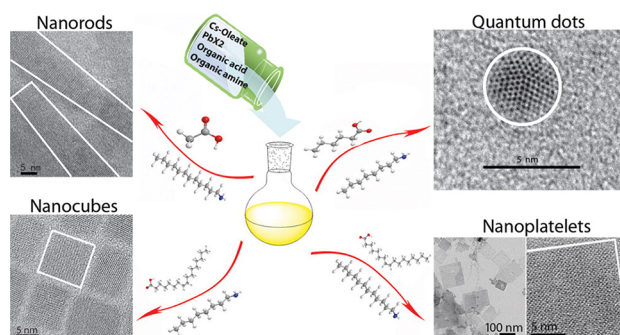

Figure 16. Differently shaped CsPbB$_3$ NCs, which can be achieved via an emulsion LARP approach at RT by varying the amount of organic acid and amine ligands. Reproduced from ref 210. Copyright 2016 American Chemical Society.

a similar approach, but they made some modifications: they solubilized Cs-oleate in ODE together with OA, OLA, and HBr, while PbBr$_2$ was dissolved in DMF. The two solutions were mixed together, consequently forming an emulsion. This emulsion was inert until acetone (which is miscible with both of the previous solvents) instantaneously induced the formation of perovskite NPLs.[19] Interestingly, the thickness of the NPLs could be finely tuned, down to only 3−5 monolayers, by varying the amount of HBr. A similar approach was then used to produce CsPbBr$_3$ NC inks for high-voltage solar cells.[28]

The same strategy was then used to synthesize ultrathin CsPbBr$_3$ nanowires and MAPbX$_3$ nanostructures.[211,212] The latter were synthesized by Liu et al., who prepared an oil phase solution by mixing OA, ODE, and hexadecylamonium halide and an aqueous phase by dissolving MAX and PbX$_2$ in different volumes of DMF. After mixing the two phases at RT, chloroform or acetone were used as demulsifiers, to quench the reaction and to collect the resulting nanostructures. Interestingly, the amount of DMF used in the aqueous phase dictated the shape of the final nanostructures (Figure 17).[212] In 2017, Kim et al. extended the emulsion LARP approach to make FAPbBr$_3$ NCs. This was achieved by dissolving FABr and PbBr$_2$ salts in DMF to form a precursor solution which was then added to a mixture of a desired alkylamine, OA, and hexane, yielding a milky emulsion.[213] The subsequent addition of tert-butanol to the emulsion solution caused the formation of perovskite NCs. The OA was observed to improve the stability of the FAPbBr$_3$ NCs, suppressing their reaggregation,
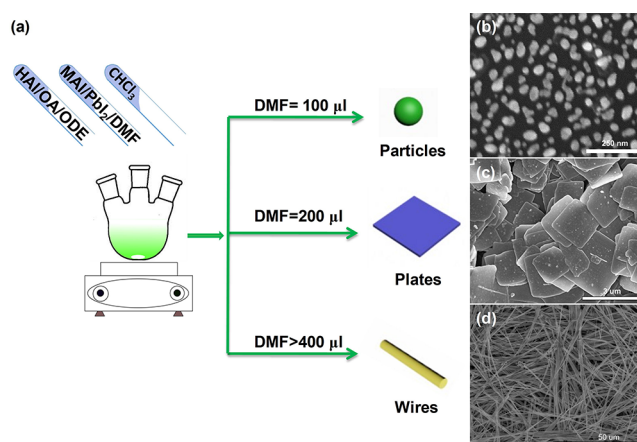

Figure 17. Schematic representation of the emulsion LARP synthesis of shape-controlled MAPbI$_3$ perovskites by employing hexadecyla-monium (HA) and varying the DMF volume, together with (b−d) the corresponding SEM pictures. All panels are reproduced with permission from ref 212. Copyright 2017 Elsevier.

while the amine ligands could prevent the formation of large crystals (>micrometer) by controlling the crystallization kinetics. More specifically, FAPbBr$_3$ NCs that were synthesized using n-butylamine had a diameter of ∼10 nm, but those that were synthesized using n-hexylamine and n-octylamine had a smaller diameter (d < 10 nm).

3.2.11. Reverse Microemulsion. The first reported approach for the synthesis of perovskite NCs in the form of MAPbBr$_3$ QDs was a reverse microemulsion technique developed in 2014 by Schmidt et al.[15] In their synthesis, octylammonium bromide was dissolved in a warm mixture (80 °C) of OA and ODE, followed by the addition of MABr and PbBr$_2$ which had previously been dissolved in a small amount of DMF. The mixing resulted in the formation of a reverse microemulsion in which NCs nucleated and grew. Eventually, the product NCs were precipitated and cleaned by adding acetone.[15] The same procedure worked for the synthesis of MAPbI$_3$ NCs, even though there was less control over the quality of the final NCs (in terms of size distribution and optical properties). In a subsequent work, the same group further improved the optical properties of these QDs by avoiding the use of OA and by finely adjusting the molar ratio between the bromide salts and the amount of nonpolar solvent (ODE).[214] Tyagi et al. adopted the same method to produce a mixture of NCs and NPLs, from which they could selectively precipitate and analyze MAPbBr$_3$ NPLs.[215] The following year, this approach was optimized so as to produce MAPbBr$_3$ with different morphologies. Yuan et al., for example, demonstrated that MAPbBr$_3$ NCs can be synthesized with control over the thickness down to one monolayer.[216] They prepared a transparent precursor solution by dissolving PbBr$_2$ and the desired amount of ammonium salts (methylammonium and alkylammonium bromides) in DMF. Next, they injected the solution into hexane, which was vigorously stirred at RT, leading to the formation of the NCs. These NCs were eventually precipitated and washed by the addition of acetone.[216] In this case, control over the size of the NCs was achieved by using different ligands: benzylamonium ions were employed to make confined NPLs (1 or 2 monolayers), while thicker nanostructures were obtained using octadecylammo-nium bromide. Teunis et al. synthesized MAPbBr$_3$ nano-clusters[217] and NWs[218] by adding a solution of MABr in DMF
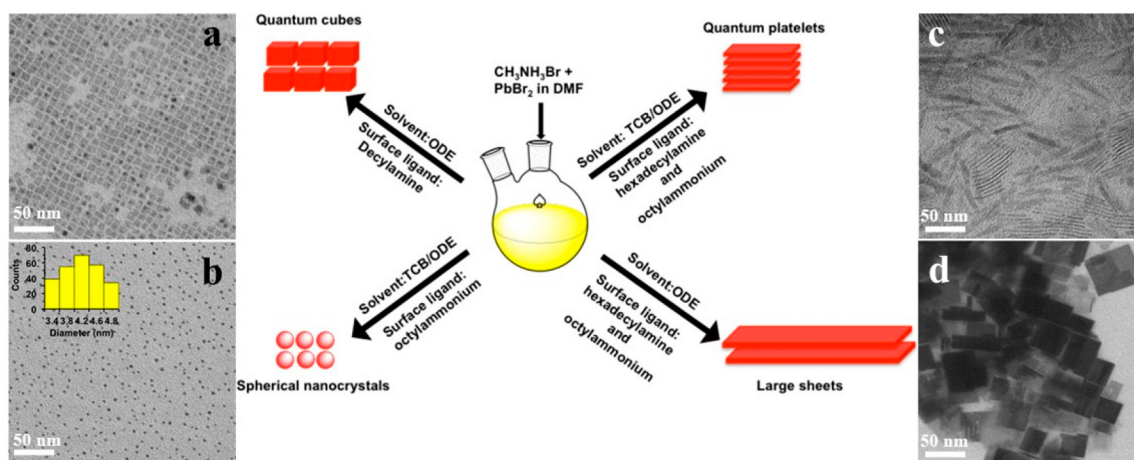
Figure 18. Shape control in the reverse microemulsion synthesis of colloidal MAPbBr$_3$ NCs. By controlling the nucleation and growth parameters (solvents, surface ligands, and temperature), the shape of the NCs can be systematically changed. Oleic acid is present in each synthesis. (a−d) TEM images of the corresponding nanostructures are also reported. The scale bars are 50 nm. All panels are reproduced from ref 219. Copyright 2017 American Chemical Society.
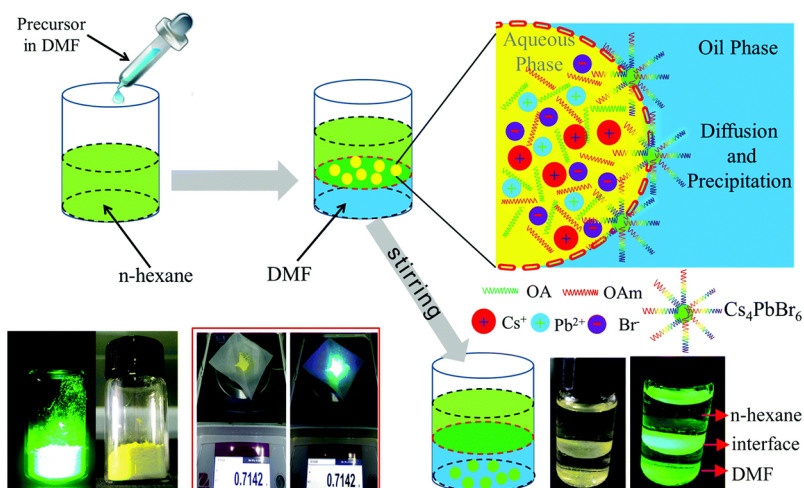

Figure 19. Reverse microemulsion synthesis of Cs$_4$PbBr$_6$ microcrystals. The inset shows the products prepared on a large scale without and with UV (365 nm) irradiation. Adapted with permission from ref 220. Copyright 2016 Royal Society of Chemistry.

and, in a second step, a solution of PbBr$_2$ in DMF to a hot (90 °C) mixture of ODE and alkylammonium bromide salts. The reaction was then allowed to run for a specific amount of time (3 or 4 min) to produce the NCs, which were precipitated and collected by the addition of acetone. In order to acquire nanoclusters, the alkylammonium bromide ligands used were hexylamine and diaminododecane,[217] while NWs were produced using octylammonium bromide only.[218] The following year, the same group demonstrated good shape control over MAPbBr$_3$ NCs via the reverse microemulsion approach.[219] In that work, a systematic variation in the solvent of the oil-phase, the temperature, and the ligand environment resulted in the formation of NPLs, NSs, nanocubes, or spherical nanoparticles (Figure 18).[219]

In 2016, Chen et al. reported a reverse microemulsion synthesis of 0D Cs$_4$PbBr$_6$ microcrystals employing DMF and n-hexane as the "aqueous phase" and the "oil phase", respectively:[220] PbBr$_2$ and CsBr were dissolved in DMF together with OLA and OA. This solution was then added to hexane under stirring, leading to the formation of the Cs$_4$PbBr$_6$ microcrystals over time (Figure 19).[220]

Zhang et al. used the same strategy and revised it in order to provide better control over the size distribution and, more importantly, over the optical properties of 0D Cs$_4$PbBr$_6$ NCs.[221] In their new approach, a solution of PbBr$_2$, hydrogen bromide (HBr) in DMF, OA, and OLA was injected into a solution of cesium oleate in hexane and OA under stirring. The introduction of HBr as an extra source of Br$^-$ ions helped to better control the anion/cation ratio in the synthesis.[221] Moreover, the separation of the Pb and Cs precursors in DMF and hexane, respectively, allowed for control over the nucleation rate of the NCs. Indeed, the nucleation rate is limited by the slow release of Cs$^+$ ions from the oil to the aqueous phase.[221] Importantly, control over the size of the NCs was possible by tuning the micelle size, which, in turn, depends on the amount of OA that is used to stabilize the microemulsion.[221] Thanks to the versatility of this approach, the same group extended it to the synthesis of 3D (CsPbBr$_3$) and 2D (CsPb$_2$Br$_5$) NC systems (Figure 20).[222] The key parameter for being able to fine-tune the stoichiometry and, thus, the crystal structure of the final NCs was the Cs:Pb:Br feed ratio.
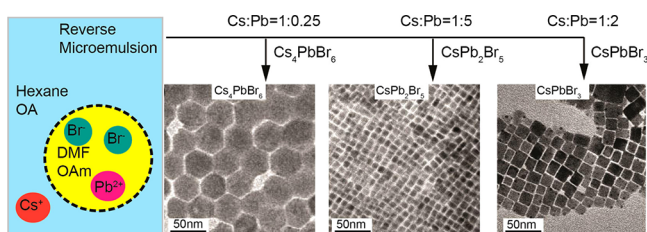
Figure 20. Illustration of the micelle structure that is formed in the reverse microemulsion process, which comprises an "oil" phase with *n*-hexane, and an "aqueous" phase with DMF. TEM images of Cs_4PbBr_6, $CsPb_2Br_5$, and $CsPbBr_3$ perovskite NCs formed with the different Cs:Pb:Br feed ratios. Reproduced from ref 222. Copyright 2017 American Chemical Society.

3.2.12. Polar Solvent Controlled Ionization. The polar solvent controlled ionization (PCI) can be seen as the "opposite" of the LARP technique.[223] In the LARP strategy, the starting precursors are dissociated into ions in polar solvents from the beginning of the synthesis (state C in Scheme 6). The polar solvent is then transferred into a large

Scheme 6. States Which Characterize the Polar Solvent Controlled Ionization and LARP Approaches[a]
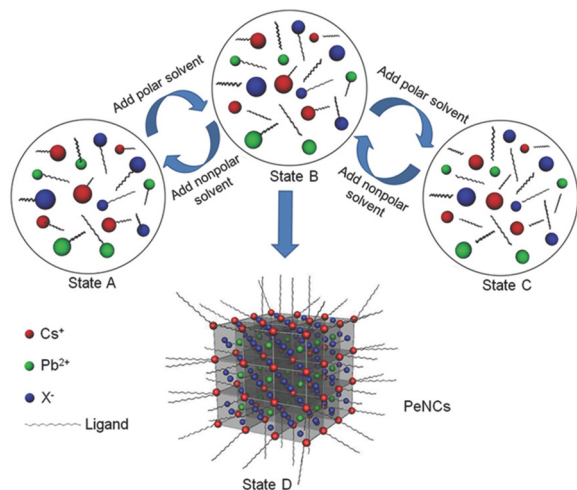
[a]Reproduced with permission from ref 223. Copyright 2018 Wiley-VCH.

amount of nonpolar solvent (state B), which inhibits the solubility of the ions and, thus, induces a rapid crystallization due to supersaturation (state D).[223] On the other hand, in the PCI method, none of the precursors are initially dissociated; they are in the form of metal oleates or alkylammonium halides dispersed in a nonpolar solvent (like hexane) (state A).

The subsequent addition of a polar solvent can induce the dissociation of the precursors (state B) until reaching a critical concentration of ions in solution, which results in the precipitation of the final NCs (state D). The main advantage of this method is clear: it uses a minimal amount of polar solvents. In 2018, Fang et al. demonstrated the synthesis of all-inorganic $CsPbX_3$ NCs via the PCI strategy.[223]

3.3. Alternative (Indirect) Synthesis Approaches

In addition to the synthetic approaches discussed so far, there have been a few two-step syntheses of LHP NCs in which the nucleation of LHPs take places within starting colloidal seeds.[97,224,225] For example, presynthesized PbI_2 NCs were

used as a colloidal template to form 2D and 3D LHP NCs when they were reacted with alkyl ammonium iodide or MAI.[224] Also, CsX NCs, which are easy to synthesize and for which size tunability is straightforward, were employed as monodisperse colloidal precursors to make LHP NCs (Figure 21).[225] Interestingly, it has been demonstrated that, when CsBr
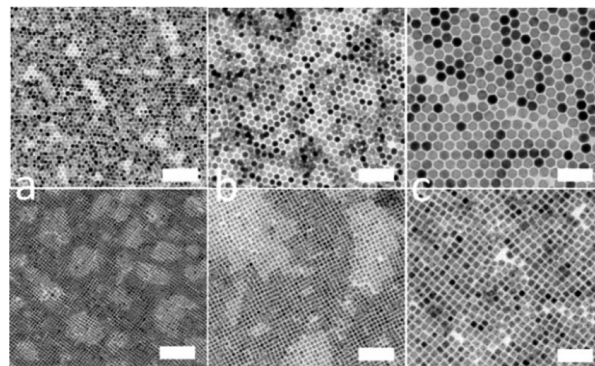
Figure 21. (a−c) TEM images of CsBr NCs of three representative sizes (top panels) and the resulting $CsPbBr_3$ NCs (bottom panels) that were obtained after the addition of Pb-oleate. Scale bars correspond to 50 nm in all panels. All panels are reproduced from ref 225. Copyright 2018 American Chemical Society.

NCs react with Pb-oleate, the CsBr → $CsPbBr_3$ transformation goes through CsBr/$CsPbBr_3$ core/shell NCs as intermediate structures.[225] The ternary 0D compound (e.g., Cs_4PbBr_6 NCs) is another colloidal candidate that transforms into the LHP NCs (e.g., $CsPbBr_3$ NCs) when it is reacted with $PbBr_2$ (dissolved in toluene/OLA/OA).[97]

A potential advantage of such indirect syntheses is that control over the size of LHP NCs is possible by tuning the size of the parent NCs. Also, monodisperse colloidal NCs can, in principle, serve as precursors for LHP NCs with more complex morphologies.

3.4. Summary of the Synthesis Approaches

Overall, from the colloidal chemistry point of view, the two-step standard HI technique has reached its maturity and it can now be used to produce nearly monodisperse LHP NCs, with, at the same time, an excellent control over the shape of the NCs, allowing for the production of QDs, NRs, NWs, NPLs, and NSs (see refs 16, 26, 43, 105, 106, 118−123, 125, 127, 131, and 226). However, this route has been mainly developed for $CsPbBr_3$ NCs, and it seems to be limited in producing MA-, FA-, or I-based NCs[67,96,112] with good control over the shape or optical properties, in terms of fwhm and PLQY. Also, as mentioned in section 3.1, this technique has some restrictions imposed by the use of metal halide salts as both metal and halide precursors. In order to circumvent this issue, the newly developed benzoyl or silyl halides based HI methods, in which any desired metals/halide precursors ratio can be employed, allow for a precise compositional control over the resulting NCs. Indeed, these new colloidal approaches yield not only $APbX_3$ (A = Cs, MA, or FA; X = Cl, Br, or I) NCs with a very good control over the size distribution and high PLQYs (which result as a consequence of the halide rich environment in which they are synthesized),[43,115,226] but also complex quaternary or quinary DP NC systems.[115,227]

While the aforementioned HI techniques are particularly appropriate for producing MHP NC samples with a high

degree of control, they have two main drawbacks: the synthesis needs to be performed in air-free conditions (air sensitive precursors); it is hard to scale up these techniques and, consequently, to employ them for a large-scale production. These problems can be avoided by employing alternative synthesis routes, such as the LARP[28,168,169,176,219] and the heat-up "related"[130,133] approaches, which can yield MHP NCs in gram scale even under air atmosphere. More in details, the heat-up, solvothermal, ultrasonication, and microwave techniques can easily be used to produce mainly CsPbX$_3$ NC systems in large quantities and with high PLQYs.[117,126,129,130,132,135] On the other hand, these techniques require a heating source and they are based on the same chemicals and solvents employed in the two-precursors HI methods, thus suffering from poor tunability of the metal/halide precursors ratio. Also, if compared to HI methods, the heat-up "related" techniques yield LHP NCs with much lower size and shape control, which might require different size selection steps.[117,127]

Conversely, a better versatility has been demonstrated for the LARP-related procedures, including the emulsion LARP, the reverse microemulsion, and the polar solvent controlled ionization. In fact, LARP-related techniques allow for the synthesis of all the APbX$_3$ (A = Cs, MA, or FA; X = Cl, Br, or I) NC systems at RT with a modest control over the shape of the NCs, which include, for example, MAPbBr$_3$, MAPbI$_3$, FAPbX$_3$ NPLs, and CsPbX$_3$ NPLs, NRs, and NWs.[19,178,179,182,188,210,219,228] Unfortunately, LARP-related procedures rely on metal halide salts as precursors, thus they provide a limited control over the composition of product NCs. Additionally, they are based on polar solvents which might eventually degrade or even dissolve the produced MHP NCs. Hence the NCs made with this method tend to have poor optical properties and stability.[168,171,204,205]

3.5. Complex Morphologies

A possible approach to improve the stability of MHP NCs is to grow a protective shell in order to isolate them from the environment. Unfortunately, the labile nature of LHP NCs makes them unsuitable for the fabrication of more complex morphologies, such as core–shell NCs and other NC heterostructures. However, due to their aforementioned defect-tolerance, such complex morphologies have been less in demand for MHP NCs than for more traditional NCs, for which core–shell geometries are indeed needed to achieve high PLQYs.[229,230]

The simplest approach to accommodate MHP NCs (i.e., LHP NCs) into a heterostructure is using halide perovskites as inorganic capping ligands for PbS NCs.[231−234] This strategy enables to modify the surface of PbS NCs and grow LHPs as shell via an approach that is similar to the LARP one,[235,236] reducing the rate of Auger recombination in infrared-emitting NCs.[237] Recently, a few strategies have been proposed to grow metal or semiconductor domains onto LHP NCs under mild conditions. In a very simple approach, the surface capping ligand (i.e., OLA) acts as a reducing agent for Au(III) cations (which are previously introduced to the LHP NC solution by adding AuBr$_3$ salt), consequently forming Au^0 onto the CsPbBr$_3$ NCs.[238] In such hybrid structures, the absorption spectrum shows little dampening of the excitonic band, and the absorption tail extends to longer wavelengths (similar to the modification of CdSe NCs with Au nanoparticles[239]). In addition, it has been observed that the PLQY decreases (e.g., from 80% to 60%) after the formation of Au domains, possibly

due to an excited-state interaction between LHP and Au NCs (the Au domains serve as charge recombination sites).[238] As the corner facets are expected to be less passivated than the lateral ones, Au domains grow mainly at the corners of LHP NCs (Figure 22a). In contrast to what was reported by
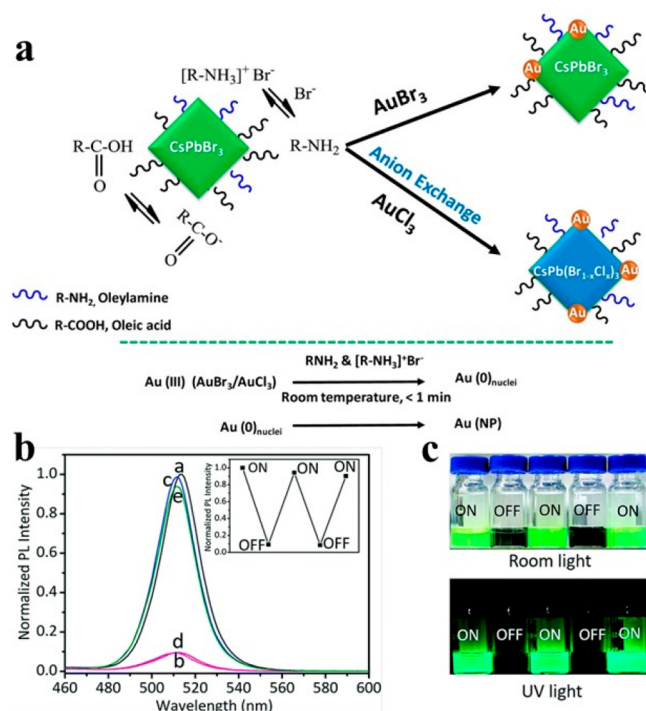
Figure 22. (a) Influence of ligands on the reduction of Au(III) at the surface CsPbBr$_3$ NCs to form Au-CsPbBr$_3$ hybrid structures. Reproduced from ref 238. Copyright 2017 American Chemical Society. (b) PL spectra of CsPbBr$_3$ NCs (a) before and after the sequential addition of (b and d) AuBr$_3$ and (c and e) 1-dodecanethiol. (c) Photographs depicting the modulation cycles of the system under room light and UV light, respectively. Reproduced with permission from ref 240. Copyright 2018 The Royal Society of Chemistry.

Balakrishnan et al.,[238] Chen et al. have observed the complete quenching of the PL of CsPbBr$_3$ upon the heteronucleation of Au^0 domains.[240] Interestingly, in this case the addition of a proper amount of 1-dodecanethiol can remove Au segments and consequently restore the PL of LHP NCs.[240] As is shown in Figure 22b, the consecutive modulation of CsPbBr$_3$/Au heterostructures by the addition of AuBr$_3$ and thiol ligands is reflected in the alternating weak and strong PL emission.[240]

It is worth noting that the addition of Au(III) to a LHP NC dispersion does not always result in the formation of Au-LHP heterostructures.[238,241] In fact, the addition of AuBr$_3$ solubilized in EtOH/toluene to LHP NCs results in a Pb^{2+} → Au^{3+} cation exchange reaction, producing Cs$_2$Au^{I}Au^{III}Br$_6$ NCs with a tetragonal crystal structure and a band gap of about 1.6 eV.[241]

Unlike the previous cases, a significant PL enhancement was reported when Ag domains were grown on CsPbBr$_3$ NCs.[242] Ag nanoparticles display a strong local surface plasmonic resonance absorption at ~410 nm (higher than the absorption onset of CsPbBr$_3$), therefore they can enhance the UV light absorption and further enhance the PL of the perovskite NCs.[242,243]

In order to improve the stability of LHP NCs, different attempts to cover them with inorganic shell materials have also been reported.[244] By adding proper amounts of zinc stearate and 1-dodecanethiol at a high temperature (e.g., 120 °C) to presynthesized CsPbX$_3$ NCs, ZnS domains could be grown on their surface, boosting their photostability.[244]

While 3D LHP NCs (e.g., CsPbBr$_3$ NCs) are extremely sensitive to water, treating Cs$_4$PbBr$_6$ NCs dispersed in a nonpolar solvent with water can trigger a 0D → 3D transformation.[245] This indirect method was then exploited in a new sol−gel approach for the surface modification of CsPbBr$_3$ NCs at a single particle level.[246] This method starts with a Cs$_4$PbBr$_6$ NC/hexane solution, to which tetramethoxysilane is added as a silica precursor. The addition of a small amount of water triggers two processes: (i) a large fraction of Cs$^+$ and Br$^-$ ions are stripped from the NCs so that the 0D NCs are transformed into 3D CsPbBr$_3$ NCs and (ii) OLA/OA is removed from the surface of the LHP NCs that are in contact with the water/hexane interface (Figure 23). After the
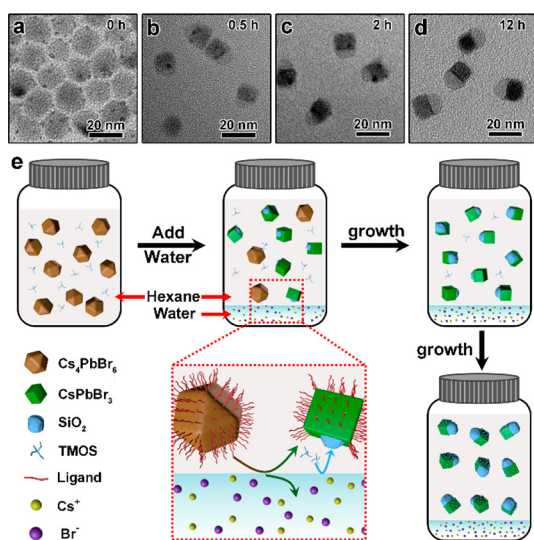

Figure 23. TEM images of the CsPbBr$_3$/SiO$_2$ Janus NCs obtained at different reaction times: (a) 0, (b) 0.5, (c) 2, and (d) 12 h. (e) Schematic illustration of the formation process. Reproduced from ref 245. Copyright 2017 American Chemical Society.

ligands have been removed, the silica can be deposited onto LHP NCs via a sol−gel method, resulting in highly stable CsPbX$_3$/oxide Janus-like NCs.[246] The same strategy has been used for the synthesis of CsPbBr$_3$/Ta$_2$O$_5$ NCs.[246]

Although such hybrid structures were characterized by an improved stability against degradation by air, water, and light irradiation, a core−shell architecture would be more favorable for a complete protection of LHP NCs from the environment (moisture, air, etc.). Octylammonium lead bromide,[247] amorphous CsPbBr$_x$,[248] TiO$_2$,[249] and recently SiO$_2$[250] have been reported as shelling materials for LHP NCs. The TiO$_2$ shell not only efficiently protects the NCs from degradation but also facilitates a charge carrier transfer.[249] As a result, the TiO$_2$ layer coated CsPbBr$_3$ NCs exhibit excellent water stability for at least three months, and their size, structure, morphology, and optical properties remain unchanged.[249] CsPbBr$_3$/TiO$_2$ core/shell NCs (Figure 24) can be simply synthesized by dissolving titanium butoxide in a CsPbBr$_3$ NC

toluene solution, followed by a calcination process at 300 °C.[249]
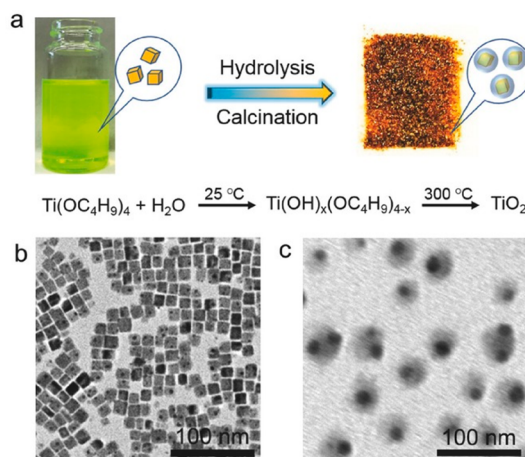
Figure 24. (a) Sketch of the fabrication process employed in the production of CsPbBr$_3$/TiO$_2$ core/shell NCs. TEM images of (b) CsPbBr$_3$ NCs and (c) CsPbBr$_3$/TiO$_2$ core/shell NCs after calcination at 300 °C for 5 h. Reproduced with permission from ref 249. Copyright 2018 Wiley-VCH.

4. ANION EXCHANGE

The major contribution to the valence band maximum (VBM) of LHP materials comes from the halide orbitals.[39] Thus, a systematic variation in the halide composition of such compounds allows for a fine adjustment of the VBM (Cl→ Br→ I or I→ Br→ Cl). One of the most effective ways to change the halide composition of preformed LHP NCs is to perform a postsynthetic anion-exchange (AE) reaction (Figure 25, panels a and b), which has been shown to be a versatile tool to tune the optical properties of both bulk and nanoscale LHPs.[251−253] Differently from what observed in cation exchange reactions in II−VI colloidal semiconductor NCs, the AE process in LHP NCs is completely reversible, suggesting that the solvation energy of the exchanging ions does not drive the process.[20,21,254,255] Also, the fast AE rate that is observed in such systems is indicative of the high mobility of anions in MHPs, which, indeed, are known to have high ionic conductivities.[256] In general, the presence of two types of mobile ions, namely the A-cations and halide anions, in both organic and inorganic lattices gives rise to a broad spectrum of lattice dynamics.[257,258] A key factor that affects the mobility of halide ions (as the main ionic carrier) is the high intrinsic concentration of halide vacancies in such materials,[259] and the associated high mobility of the halide ions, which is ultimately responsible for the hysteresis in the current−voltage curves from films of these materials.[8] The activation energies ascribed to the ion/defect migration have been experimentally determined, and they range from ∼0.1 eV to ∼0.6 eV.[260,261] In addition, it is well-documented that, among the various ions and defects,[262] halides and halide vacancies are the fastest migrating species.[263] These two intrinsic factors (the low defect formation energy and the fast ion/defect motion) facilitate the halide exchange reaction, which, in turn, can be easily exploited to tune the LHP NCs' emission spectra (in the range from 1.8 to 3.0 eV, Figure 25c) by simply exposing the NCs to specific amounts of the desired halide precur-

Figure 25. (a) Scheme of the AE reaction involving $CsPbX_3$ NCs. (b) XRD patterns and (c) PL spectra of $CsPbX_3$ (X = Br, Cl, or I) NCs prepared by AE from $CsPbBr_3$ NCs. Reproduced from ref 21. Copyright 2015 American Chemical Society.
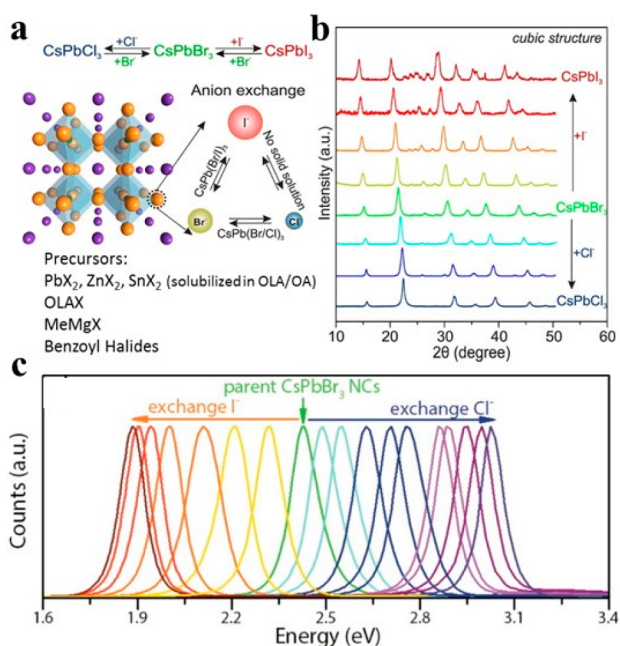
sor.[39,61,264,265] Interestingly, AE enables the PL to be tuned from blue (410 nm) directly to red (690 nm) or red to blue (Cl→ I or I→ Cl) without going through the intermediate colors. This can be explained by the large difference between the ionic radii of the Cl^- and I^- anions, which does not promote the stability of $CsPb(Cl/I)_3$ solid solutions.[21]

In practice, one of the simplest approaches consists of mixing two different preformed $CsPbX_3$ NC solutions that have different halide compositions: the two populations of NCs tend to blend, forming a homogeneous (Br/I) or (Br/Cl) composition in between the two parent NCs.[20] The most accurate way to control the extent of the AE in LHP NCs is to start with preformed NCs ($CsPbBr_3$ NCs) and to expose them to different types of halide sources, such as OLA-X, PbX_2, or SnX_2 (dissolved in OLA/OA/solvent), benzoyl halides, etc.[21,43,266−268] Overall, the size and shape of the parent LHP NCs are preserved, while their compositions are successfully tailored in a desired range.

The in situ synthesis of halide anions via a reductive dissociation of the solvent molecules (e.g., dihalomethane) is another less common approach to perform AE reactions.[269] In this technique, the reaction begins with a photoinduced electron transfer from $CsPbX_3$ (X = Cl, Br) NCs to dihalomethane solvent molecules, producing halide ions via a reductive dissociation (Scheme 7).

The halide ions generated in situ near the surface of the NCs drive the AE reaction efficiently, as long as the $CsPbX_3$ NCs are photoexcited above the bandgap. The extent of the anion-exchange reaction can be precisely controlled by adjusting either the photon dose or the wavelength of the excitation light that self-limits the reaction when the light becomes off-resonant with the absorption of the NCs. Salts added to the NC solutions can also act as halide sources. Some salts, such as PbX_2[20] and LiX_2,[270] lead either to a slow and incomplete exchange (the resulting NCs have a broadened PL spectra),

Scheme 7. Proposed Mechanism for the Photoinduced AE Process of Perovskite NCs in the Presence of Dihalomethane as the Solvent[a]
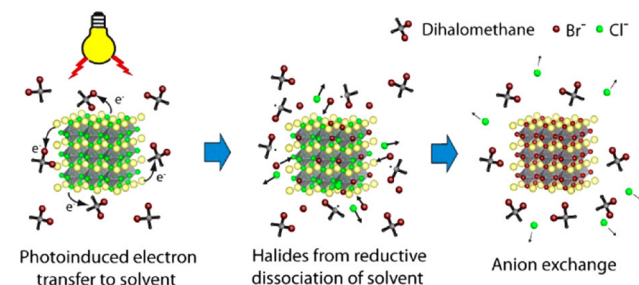
[a]Reproduced from ref 269. Copyright 2017 American Chemical Society.

while other salts, such as ZnX_2, trigger a fast (reversible) exchange at RT.[271,272]

It was initially hypothesized that the NCs produced by AE possessed a homogeneous composition, at least in the case of the $CsPbBr_3 \rightarrow CsPbI_3$ transformation, and the intermediate steps of the transformation were $CsPb(Br/I)_3$ homogeneous alloys (Scheme 8, path A).[21,273] However, further optical[267]

Scheme 8. Different Possible AE Pathways for a $CsPbBr_3$ NC and Iodide Anions[a]
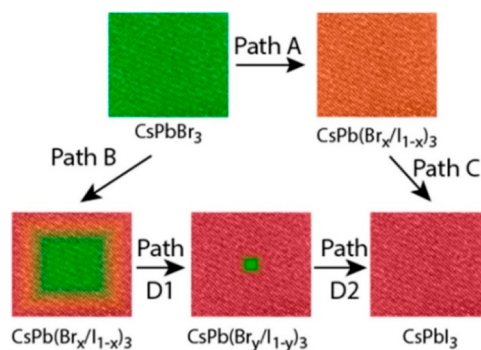
[a]Paths A + C describe the $CsPbBr_3 \rightarrow CsPbI_3$ conversion having as intermediate $CsPb(Br+I)_3$ alloyed structures. In the transformation that is depicted in paths B + D1 + D2, core@graded-shell heterostructures form as intermediate steps, and $CsPbI_3$ is the final product. Reproduced from ref 274. Copyright 2018 American Chemical Society.

and quantitative X-ray photoelectron[274] spectroscopy analyses indicated that the intermediate exchanged structures have radial gradient compositions, and the concentration of the iodide ions was higher at the surface (Scheme 8, path B).

AE reactions can also be performed in the solid state by immobilizing LHP NCs on fine KX (X = Cl, Br, or I) powders.[275] This was achieved by Guhrenz et al., who first added pure KX salts to LHP NC solutions in hexane and subsequently removed the solvent under vacuum. Upon the evaporation of the solvent, the resulting AE took place entirely in the solid state.[275] Even sintered NC thin films can undergo a halide exchange when they are submerged in a heated lead halide solution,[276] a process that can greatly facilitate a postsynthetic tuning of the optical properties of the LHP NCs for applications. AE can also take place at the solid/gas interface by treating NC thin films with volatile halide precursors. Organic ammonium halides with low molecular

weights (such as methylammonium halides or butylammonium halides) are normally used for this treatment because they slowly evaporate (decomposing to amine and hydrogen halides) under mild heating (~100 °C).[73]

A striking application of the AE has been demonstrated in the fabrication of multicolor $CsPbX_3$ (X = Cl, Br, I, or alloy of two halides) NW heterojunctions with a pixel size down to 500 nm and a PL that is tunable over the entire visible spectrum (Figure 26a).[277] After transferring an individual $CsPbBr_3$ NW

Figure 26. (a) Confocal image of a three-color heterojunction NW. Blue, green, and red represent the PL emissions at 410–450, 500–550, and 580–640 nm, respectively. Reproduced from ref 277. Copyright 2017 National Academy of Sciences. (b) Band edge energies of $CsPbX_3$ NCs extracted from cyclic voltammetry data. Reproduced from ref 279. Copyright 2016 American Chemical Society.

to a clean SiO_2/Si substrate, a thin layer of poly(methyl methacrylate) (PMMA) was spin-cast. A selected area of the PMMA was removed by e-beam l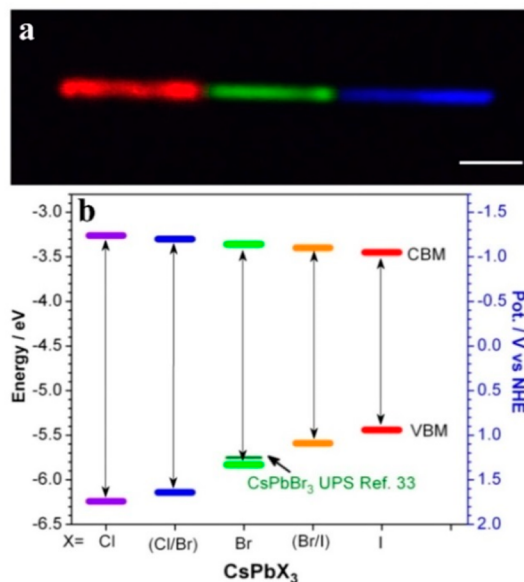ithography in order to expose a specific part of the NW. Next, the substrate was dipped into an OLA-X (X = Cl or I) solution. During the reaction, the PMMA layer remained intact. After the AE reaction, the PMMA layer was completely removed by washing with chlorobenzene and hexane.[277]

Very recently, a further step forward in controlling AE reactions was made by Ravi et al., who demonstrated that AE can be suppressed on $CsPbX_3$ NCs that have been passivated with $PbSO_4$-oleate.[278] This kind of protection could be utilized to deposit LHP NCs with different compositions as tandem layers to engineer an effective harvesting of light.[278] Finally, it is also worth mentioning that supplementary cyclic voltammetry studies showed that the conduction band minimum (CBM) also undergoes slight changes over a halide exchange, and it shifts systematically with the halide composition (Figure 26b), though the shift is small (0.19 eV).[279] This indeed highlights the dependency of band edge states on the halide composition of $CsPbX_3$ NCs, demonstrating that appropriate interfaces need to be designed both in new heterostructured materials and in optoelectronic devices.

5. CATION EXCHANGE

Cation-exchange (CE) reactions, in which the cations of preformed NCs are substituted with new cations in solution, have emerged as particularly powerful tools that can achieve precise control over NCs composition and access novel nanostructures.[254] Such transformations allow one to use NCs that are synthesized by conventional methods as templates for the production of nanoheterostructures or alloyed NCs while preserving the size and shape of the parent crystals.[280] In principle, both the A and B-cations in LHP NCs can be partially or totally replaced via CE reactions.[67,281−283]

The band gaps of LHPs weakly depend on A-cations as they do not contribute significantly to the density of states near the Fermi level. However, the nature of the A-cation might play an important role in determining the symmetry of the LHP's compounds. For example, organic cations (e.g., MA⁺ or FA⁺) are more dynamic than inorganic cations (e.g., Cs⁺), and they are able to bind $[PbBr_6]^{4-}$ octahedra through hydrogen bonds. Therefore, when organic cations replace inorganic ones via CE, they can induce symmetrical changes in LHP NCs, ultimately changing the vibrational modes.[64] Furthermore, exchanging the A cations in LHP NCs can lead to a variation in (I) the tolerance factor and consequently the stability of NCs, (II) the PL peak position (due to the tilting of the B-X-B bond) and lifetime, and (III) the dimensionality of LHPs. For example, Cs⁺ ions in $CsPbI_3$ NCs can be partially or fully exchanged with FA⁺ cations (by using FA-oleate as a precursor), which leads to the production of NCs with long-term stability and a near-IR emission.[67] Similarly, $FAPbX_3$ NCs can also be obtained through a solid−liquid−solid CE reaction by adding a FA-acetate salt to a solution of $MAPbX_3$ NCs.[281] Starting with 2D perovskites, replacing octadecylammonium (OA⁺) with Cs⁺ or FA⁺ in OA_2PbBr_4 microplatelets leads to a reorganization of the lattice. In this process, $[PbBr_6]^{4-}$ octahedra become corner-sharing; they form green emitting sheets with a 3D LHP phase, and they have both a high degree of crystallinity and excellent optoelectronic properties.[282,284,285] The reason behind such a 2D → 3D transformation, in which A-cations replace organic cations in the layered structures, is still not known, but its driving force is believed to be the formation of an extended 3D octahedral network.

The band gap of MHPs is known to widen when the electronegativity of both B and X atoms is increased, and the unit cell volume is decreased.[286] Therefore, a postsynthetic B-cation exchange can be used as an alternative route to tune the optical properties of LHP NCs. Considering that Pb^{2+} ions are surrounded by 6 halide anions (forming $[PbX_6]^{4-}$ octahedra) which are enclosed by 8 A-cations, it is easy to understand that a CE of the B cations in LHPs is rather difficult to achieve. However, a partial CE between the LHP NCs (e.g., $CsPbBr_3$ NCs) and different metal cations has been observed when employing MBr_2 solutions (i.e., $SnBr_2$, $ZnBr_2$, or $CdBr_2$ dissolved in OLA/toluene).[283] The resulting alloyed $CsPb_{1−x}M_xBr_3$ NCs show a blue-shift in the absorption and emission spectra, but the high PLQYs (>50%) and narrow PL line widths (80 meV) of the parent NCs remain intact. The observed blue-shift was explained as being a result of a lattice contraction induced by "guest" MBr_6 octahedra, which are electronically decoupled from the $PbBr_6$ framework. The contraction of the $PbBr_6$ octahedra leads to shorter Pb−Br bonds and, therefore, to stronger interactions between Pb and

Br orbitals. Since the CBM is composed of antibonding combinations of Pb(6p) and Br(4p) orbitals, a stronger interaction between the two atoms results in a shift in the CBM to higher energies, which, in turn, widens the band gap.

Similar to the AE process, the CE one was tentatively explained as being facilitated by the presence of halide vacancies in the parent $CsPbBr_3$ NCs.[283] Briefly, the exchange between M^{2+} and Pb^{2+} ions takes place through a halide vacancy-assisted migration (i.e., OLA molecules in solution remove Br^- ions from the NCs' surface and $PbBr_2$ units one after another), leaving vacancies behind. Subsequently, MBr_2 species occupy the vacant sites and diffuse inside the lattice.[283] A schematic representation of such a mechanism is given in Scheme 9.

Scheme 9. (a) Partial $Pb^{2+} \rightarrow M^{2+}$ (M= Sn, Cd, or Zn) CE in $CsPbBr_3$ NCs and the (b) Corresponding Proposed Reaction Mechanism[a]
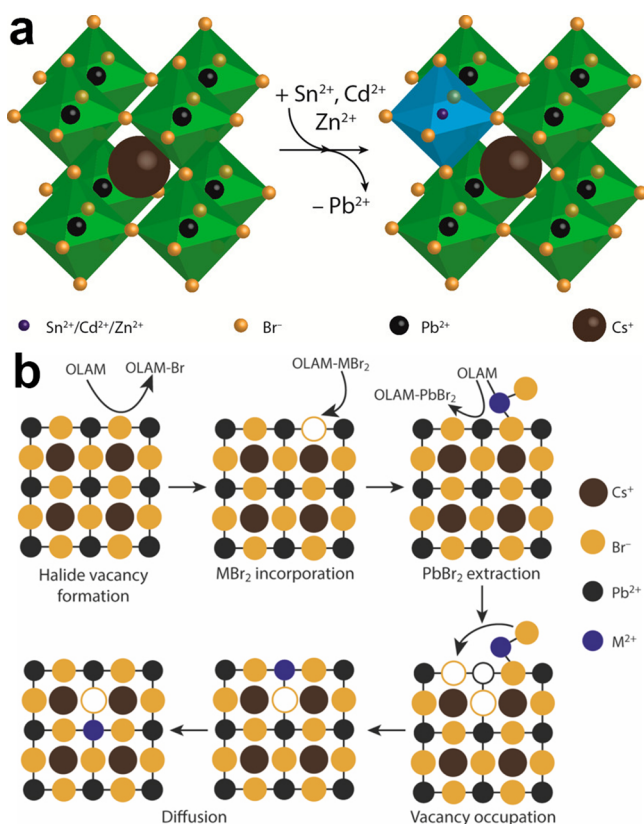
[a]Reproduced from ref 283. Copyright 2017 American Chemical Society.

CE can also be employed as an alternative approach to produce alloyed $CsPb_xMn_{1-x}Cl_3$ perovskite NCs that have the same shape and crystal structure as the parent $CsPbCl_3$ NCs.[287,288] Interestingly, the exchange between Pb^{2+} and Mn^{2+} is almost completely reversible[287] by treating "as prepared" $CsMnCl_3$ NCs with a $PbCl_2$ solution that has been dissolved in OLA/OA/ODE, following the reaction:

$$CsMnCl_3 + xPb^{2+} \leftrightarrow CsPb_xMn_{1-x}Cl_3 + xMn^{2+}$$

However, it is not possible to obtain pure $CsPbCl_3$ via CE from $CsMnCl_3$. This is perhaps related to the balance between the inward diffusion of Pb^{2+} and the outward diffusion of

Mn^{2+}.[287] These alloyed NCs severely suffer from photo oxidation. Interestingly, to protect such systems from photo-oxidation and thermodegradation, a one-step dual ion exchange reaction was proposed by Xu et al., who prepared $CsPb_xMn_{1-x}Cl_3$ NCs embedded in a KCl matrix. In their approach, preformed $CsPbBr_3$ NCs underwent both a cation and an anion exchange when they were exposed to $MnCl_2$ and KCl salts.[288] In such transformations, a partial exchange of Pb and Mn is likely to occur as a result of opening the rigid halide octahedron structure around Pb during the halide exchange. This unique exchange feature results in a series of unusual phenomena, including long reaction times, intermediate core−shell structures with triple emission bands, and dopant molecule composition-dependent doping processes (Figure 27).[289] Since the diffusion of large $MnCl_2$ species from the surface to the core of the NCs is quite difficult, the exchange requires extremely long reaction times (e.g., 40 h).
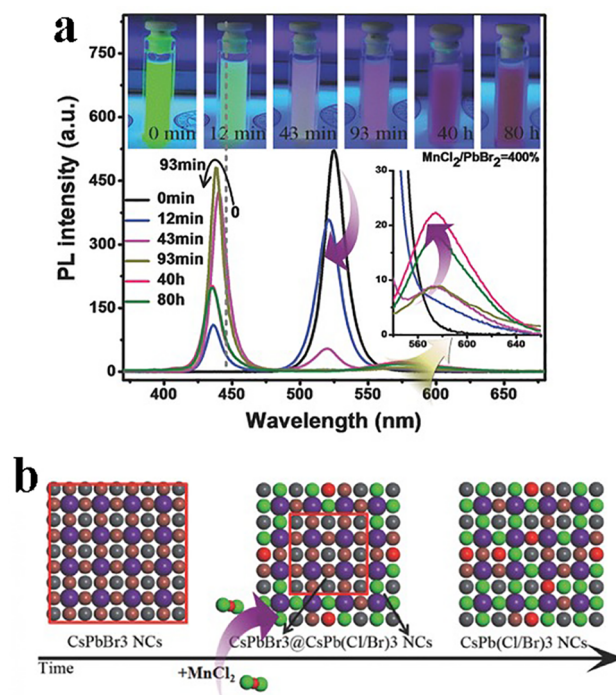
Figure 27. (a) Temporal evolution of the PL emission of $CsPbBr_3$ NCs after the addition of $MnCl_2$, together with (inset) the corresponding photographs taken under an UV lamp (365 nm). (b) Schematic representation of the ion exchange process from pure $CsPbBr_3$ NCs to Mn-doped $CsPb(Cl/Br)_3$ NCs obtained by the addition of $MnCl_2$. Reproduced with permission from ref 289. Copyright 2017 Wiley-VCH.

In a similar fashion, homogeneous $Cs(Pb_xMn_{1-x})(Cl_yBr_{1-y})_3$ NCs can be synthesized via a postsynthetic cation−anion cosubstitution reaction by mixing preprepared colloidal $CsPbBr_3$ and $CsPb_{1-x}Mn_xCl_3$ NCs in hexane.[290] The AE rate, which is much faster than that of the CE, can promote the Mn^{2+} substitution in $CsPb(Cl_yBr_{1-y})_3$ systems that are rich in Br.[291] Following a similar rationale, white light emitting $Cs(Pb_{1-x-z}Zn_z)(Cl_yBr_{1-y})_3{:}xMn^{2+}$ NCs were obtained by a controlled mixing of as-prepared $CsPb_{1-x}Mn_xCl_3$ NCs and $ZnBr_2$ (dissolved in OLA/hexane).[291]

6. SURFACE, SHAPE, AND PHASE POSTMODIFICATIONS

In addition to AE and CE reactions, several postsynthetic treatments have been investigated in order to modify the optical and the structural properties of LHP NCs and to increase their performance once they are implemented in devices. These modifications, which are "chemically" triggered, can be classified into three categories: surface, shape, and phase (and/or mixed) post-modifications.

6.1. Surface Chemistry of MHP NCs

Surface post-treatment is a convenient method to enhance the optical properties as well as make LHP NCs more robust under ambient conditions.[292,293] Similar to the internal bonding in LHPs, the bonding of ligands to the surface has a strong ionic character, and in solution, it is highly dynamic, resulting in a facile desorption of surface-capping molecules during the isolation and purification steps. In addition, the proton transfer between the oleate species in solution and oleylammonium capping ligands can neutralize surface-bound oleylammonium species, which will subsequently leave the A-site position on the surface of LHP NCs.[111] To prevent such a ligand loss, the surface of LHP NCs can be opportunely modified either in solution[294−296] or via a solid-state process.[293,297] Before discussing these surface treatments in detail, we will first summarize the main features of the possible surface terminations that characterize MHP NCs. As shown in Scheme 10 (panels a and b), MHP NCs can be terminated by

Scheme 10. Schematic Illustration of CsPbX$_3$ NCs That Have Been (a) CsX or (b) PbX$_2$ Surface Terminated; (c) the Dynamic Surface Stabilization of a CsPbBr$_3$ NC by Oleylammonium Bromide (OA is Not Part of the Ligand Shell); and (d) LHP NC That Has Been Passivated by OLA$^+$ Ions, Which Replace Surface Cs$^+$ Ions^a

^{a}(c) Reproduced with permission from ref 301. Copyright 2016 American Chemical Society.
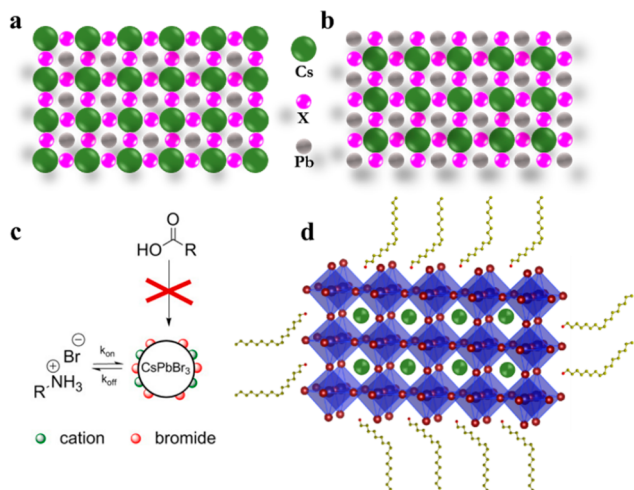
either AX[298,299] or MX$_2$[44,299] rich surfaces. It is worth mentioning that the different electronic and optical properties of MHPs correspond to specific surface-terminations.[299] For instance, a theoretical investigation indicated that a CsI-terminated γ-CsSnI$_3$ material exhibits a higher electron mobility than its SnI$_2$-terminated counterpart, thus highlighting the importance of surface termination in MHPs.[300] Regarding

CsPbBr$_3$ NCs, such as those reported by Protesescu et al.,[26] it was initially assumed that the oleylammonium cations bind to surface bromide anions, presumably through a hydrogen bridge or via electrostatic interactions. On the other hand, surface cesium or lead ions can be passivated only by bromide or oleate anions, resulting in a NC(X)$_2$ binding motif.[301] However, De Roo et al. demonstrated via nuclear Overhauser effect spectroscopy (NOESY) NMR analysis that OA does not bind to CsPbBr$_3$ NCs, therefore an oleylammonium oleate termination is not possible. Consequently, oleylammonium bromide was proposed as a capping layer (Scheme 10c)[301] since highly ionic CsPbBr$_3$ NCs prefer ionic ligands over those that bind with a more covalent character, such as lead oleate. However, further experimental works evidenced that the Cs/Pb ratio in CsPbBr$_3$ NCs is typically lower than 1 (especially in confined systems),[19,302] suggesting that the surface of small NCs is terminated by PbBr$_2$ and that surface Cs$^+$ cations are replaced by oleylammonium ions (Scheme 10d).[302]

Furthermore, DFT calculations showed that such a OLA$^+$→ Cs$^+$ substitution does not require much energy, and it stabilizes the system by forming three hydrogen bonds between the −NH$_3^+$ moiety and the surrounding Br$^−$ ions on the surface of the NCs.[303] In such a system, the occurrence of Br vacancies may leave naked Pb atoms on the surface of the NCs. These Pb atoms act as surface traps which may be responsible for the lower PLQY.[295]

The addition of PbBr$_2$ (dissolved in both an amine and a carboxylic acid) to as-prepared LHP NCs induced a strong ligand binding at the surface[25,301] and introduced an excess of Br$^−$.[25] These two effects essentially promote surface defect passivation and, consequently, result in a substantial enhancement of the PLQY.[25] Interestingly, the nonradiative pathways of carrier recombination can be effectively reduced by passivating the under-coordinated Pb ions with small molecules such as thiocyanate, leading to LHP NCs with near-unity PLQYs.[295] It should be noted that the size and shape of the parent NCs are preserved in all these post-treatments.

6.2. Ligand Exchange

Didodecyl dimethylammonium bromide (DDAB, which is relatively shorter than OLA) has been reported as a promising X-type ligand[304] to replace OLA on the surface of LHP NCs, leading to highly stable LHP NC films.[294] In order to achieve such an exchange, it is crucial to add OA, as it will protonate OLA and thus promote its desorption, otherwise adding DDAB directly to the purified NC solution would cause NC degradation.[294] Potassium-oleate (K-oleate) has also been introduced to protect and passivate the surface of LHP NCs, which leads to an enhancement of the optical properties and of the photo- and thermal stability of LHP NCs.[305]

In all these protocols, the presence of insulating long-chain aliphatic molecules impairs the exploitation of such NCs in optoelectronic applications. To overcome this issue, conventional short-chain solid-state ligand-exchange procedures have been proposed.[306] Unfortunately, the low stability of LHP NCs (LHP NCs are not stable when they are exposed to many polar antisolvents) in such processes limits their effectiveness. It has been found that short aromatic ligands can trigger the precipitation of LHP NCs in a proper solvent, such as benzene.[297] This could be attributed to the partial ligand exchange on the surface, which results in a low steric repulsive force and therefore a facile sedimentation. This observation

suggests that short aromatic ligands (e.g., benzoic acid or 4-phenylbutylamine) in an appropriate (co)solvent (e.g., octane and benzene) can be utilized as a safe medium to remove the long-chain aliphatic molecules that are present on the surface of the as-synthesized NCs.[297]

6.3. Phase Transformations

The introduction of "new" ligands to as-prepared LHP NC solutions not only modifies the surface of NCs, but also can trigger their phase transformation. Typically, phase transformations in LHP NCs are accompanied by shape evolution. The most common example is the 3D → 0D ($CsPbBr_3$ → Cs_4PbBr_6) NC transformation.[307−311] This is triggered by the extraction of $PbBr_2$ from the 3D $CsPbBr_3$ perovskite NCs that are operated by the excess amines.[70,307] It has been reported that, by adding alkyl-thiol ligands, the size uniformity and chemical stability of the as-transformed Cs_4PbBr_6 NCs can be greatly improved.[310] Intriguingly, the 3D → 0D transformation can be reversed by various methods, such as the addition of OA,[308] $PbBr_2$,[97] or by a chemical reaction with Prussian Blue.[312] These reactions are appealing for reversible patterning.[307] Another example is the 3D → 2D ($CsPbBr_3$ → $CsPb_2Br_5$) NCs phase transformation:[313−317] such a conversion can occur either in $PbBr_2$-rich conditions ($CsPbBr_3$ + $PbBr_2$ → $CsPb_2Br_5$)[311,313] or by destabilizing/removing Cs^+Br^- ($2CsPbBr_3$ → $CsPb_2Br_5$ + Cs^+Br^-) from the starting 3D NCs.[314] In practice, it has been found that the latter goes through a more complicated path when it is driven by ligands.[314] As is illustrated in Scheme 11, when employing

Scheme 11. Transformation of Cubic $CsPbBr_3$ Perovskite NCs into Tetragonal $CsPb_2Br_5$ NSs Which Takes Place by the Progressive Exfoliation of the Former[a]
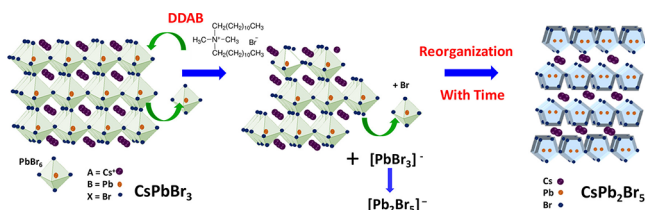
[a]Reproduced from ref 314. Copyright 2018 American Chemical Society.

DDAB, such a phase transformation starts with a ligand exchange step. Subsequently, the DDAB induces the initial formation of $[PbBr_3]^-$ and $[Pb_2Br_5]^-$ complexes, as is evidenced from the optical analysis of the exchanging solution: absorption bands at 320 and 345 nm appear at the early stages o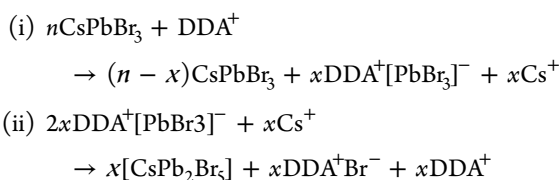f the process. The interaction between DDAB and $CsPbBr_3$ NCs results in a quick exfoliation of the starting material, in which Cs^+ ions are exchanged with alkylammonium ions:[314]

(i) $nCsPbBr_3 + DDA^+$

$\rightarrow (n-x)CsPbBr_3 + xDDA^+[PbBr_3]^- + xCs^+$

(ii) $2xDDA^+[PbBr3]^- + xCs^+$

$\rightarrow x[CsPb_2Br_5] + xDDA^+Br^- + xDDA^+$

As the system equilibrates, the lead halide complexes reorganize to form $CsPb_2Br_5$ NCs in solution.[314]

Interestingly, the shape of the original 3D NC is completely lost upon the phase transition, which, in fact, leads to the formation of a 2D NS. In addition to ligands, other external

agents can induce these shape/phase transformations.[38,130,318−320] It has been demonstrated that heat,[312,315] light,[316] pressure,[321] and water[245,317] can also cause perovskite NCs in the solid state phase-change. For example, thermal annealing facilitates a Cs_4PbBr_6 → $CsPbBr_3$ transformation, through physically extracting CsBr,[312] or a $CsPbBr_3$ → $CsPb_2Br_5$ transformation via a decomposition of the initial material (which is triggered by the desorption of weakly bound carboxylates).[315]
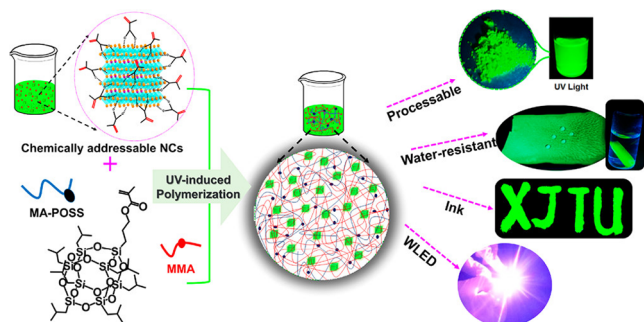
6.4. Self-Assembly

Thanks to postsynthesis techniques, it is also possible to induce a self-assembly of as-prepared NCs in which individual components arrange themselves into an ordered structure.[322] Various methods lead to 1D or 3D LHP NC superlattices, such as solvent/ligand-assisted,[323,324] templated,[325] and drying-mediated[39,226] self-assembly. Compared to the PL emission of the starting NCs, the PL of the superlattices generally red-shifts due to the cooperative emission of LHP NCs. Significant features of the cooperative emission in such superlattices are the modification of the radiative lifetime (e.g., from 148 to 400 ps for 3D superstructures of $CsPbBr_3$ NCs) and their superfluorescence (short, intense bursts of light).[326] It must be noted, however, that the ordered assemblies of these materials have yet to achieve the richness of structures that can be created using conventional NCs. For example, multinary superstructures have yet to be demonstrated.

7. COMPOSITES

Suffering from the poor stability, perovskite materials are sensitive to moisture, light, and temperature due to their low formation energy.[327,328] This chemical instability limits all technological applications in which the NC has to be processed into a composite or layer or in which NCs are exposed to an external source of energy for a long time.[329] Several chemical methodologies have been reported to improve the stability of LHP NCs by combining them with other classes of materials such as different types of polymers,[329−343] silica/alumina,[344−354] Cs_4PbBr_6,[355−358] graphene/2D materials,[359−362] and others.[363−371] Organic polymers with low levels of oxygen and moisture transmission rates have been widely investigated to serve as effective matrices for embedding LHP NCs.[53,264] The resulting nanocomposites can be fabricated mainly through two routes: (i) an in situ preparation of LHP NCs-polymer composites and (ii) a postencapsulation of LHP NCs into polymers. The in situ fabrication strategy basically consists of conducting a LARP or HI synthesis of LHP NCs and adding extra polymerizabile species to the reaction mixture. For example, poly(maleic anhydride-*alt*-1-octadecene)[329] or methacrylic acid (MtA)[343] can be simply integrated into the standard HI approach, resulting in polymer- or monomer-passivated (encapsulated) LHP NCs. Such surface-modified LHP NCs exhibit the same crystal structure, shape and emission peaks as the NCs prepared under the same conditions as those in the standard synthesis protocol, with no polymers added.[329,343] This approach may need further steps to polymerize the capping monomers. For example, the addition of 2,2-azobis(isobutyronitrile) (radical initiator) together with methyl methacrylate and methacrylisobutyl polyhedral oligomeric silsesquioxane leads to the copolymerization of MtA-LHP NCs under UV-light irradiation (Scheme 12).[343]

More complex systems (e.g., ternary graphene oxide-polymer-$CsPbX_3$ NC composites) can be achieved via the

Scheme 12. Copolymerization of Chemically Addressable NCs (Methacrylic Acid-Capped) with POSS-Appended Methacrylate Monomer (MA-POSS) and/or Methyl Methacrylate (MMA) to Produce Polymer Composites[a]
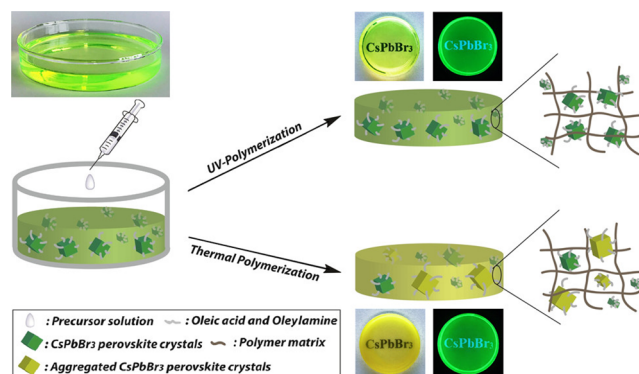

[a]Reproduced from ref 343. Copyright 2018 American Chemical Society.

Scheme 13. One-Pot Strategy Used to Prepare Perovskite-Polymer Composites (CsPbBr3-Polymer or MAPbBr3-Polymer)[a]

[a](a) Formation of perovskite crystals in liquid monomers. The digital picture under room light illustrates a dispersion of CsPbBr$_3$ crystals in styrene; (b) the subsequent UV- or thermal-initiated polymerization leads to the formation of perovskite-polymer composites. Representative disks (under room and UV light) are shown in the photos. Reproduced from ref 338. Copyright 2018 American Chemical Society.

HI process by functionalizing the constituent monomers and/ or adding extra components (e.g., graphene, etc) so as to deliver robust emissive materials.[372] Another example is to use the LARP synthesis of LHP NCs with DMF as the solvent and poly vinylpyrrolidone (PVP) as the only capping ligand.[342] PVP can be physically adsorbed on the surface of the product NCs, which not only protects them, but also makes them, compatible with polystyrene to fabricate water-resistant CsPbX$_3$@microhemispheres.[342] Recently, a universal "LARP related" strategy has been proposed by Xin et al. to prepare LHP NCs@polymer composites with many different polymers, such as poly(methyl methacrylate), poly(butyl methacrylate), and polystyrene in a one-pot chemical reaction.[338] In this approach, all required precursors (PbX$_2$ and CsX) are dissolved in DMF together with ligands (OLA and OA), and a mixture of ethylene dimethacrylate, 2,2′-azobis(2-methyl-propionitrile), and a chosen monomer was used as the bad solvent (instead of toluene).[338] The as-prepared solutions underwent UV or thermal polymerization, and the LHP NCs did not require any tedious purification or separation steps (Scheme 13).[338]

A very similar procedure was devised for preparing CsPbBr$_3$ NCs/ethylene vinyl acetate composites in which a EVA/ toluene solution was employed as the bad solvent.[373]

LHP NCs have been also embedded into different polymer matrices using two step approaches in which presynthesized samples are exposed to desired polymers: poly(methyl methacrylate)[26,337,340] (insulating polymer), polystyrene[330,341] (one of the most widely used plastics), poly(styrene-ethylene-butylene-styrene)[330] (which is highly ductile), poly(lauryl methacrylate)[330] (a highly viscous liquid), and poly(acrylic acid)[372] (a weak anionic polyelectrolyte). The so-called "swelling−shrinking" technique is one of the simplest strategies to mix presynthesized colloidal NCs with the desired polymers.[341] This approach is based on the fact that the cross-linked polymers swell in a good solvent and shrink in a theta solvent (a solvent in which polymer coils act like ideal chains).[374] For example, toluene and hexane are good solvents and theta solvents for polystyrene, respectively. Thus, LHP NCs@PS composites can be easily obtained, without having to use inert gas or baking/heating operations, by simply dispersing LHP NCs and polystyrene beads in toluene and, subsequently, adding hexane in order to shrink the polymer.[341]

Air stability and water resistance are the most remarkable characters of these reported perovskite@polymer composites.

Alternative matrices for stabilizing LHP NCs are oxide materials, such as silicon oxide (silica, SiO$_2$),[345−347,350,352,353,375−377] titanium oxide (titania, TiO$_2$),[366] and aluminum oxide (alumina, Al$_2$O$_3$),[344,348,351] as they present very low diffusion rates of ions or atoms (environmental effects). In a straightforward method, a precursor solution of LHPs (e.g., MAPbI$_3$ or CsPbBr$_3$) was found to directly fill the high-porous matrix of silica or alumina, without the use of colloidal stabilization.[344,375] This method normally requires a heating step to evaporate solvents and, consequently, to form the LHP crystals. It is worth noting that the pore size of the matrix determines the size and, therefore, the optical properties of the LHPs.

The formation of LHP@MO$_x$ heterostructures can also be achieved by using in situ (or one-step) approaches. For example, a modified LARP method, in which (3-aminopropyl) triethoxysilane (APTES) was added to the bad solvent (i.e., toluene), led to the encapsulation of MAPbBr$_3$[377] or CsPbBr$_3$@Cs$_4$PbBr$_6$[353] NCs in a silica matrix (Scheme 14).

APTES can also functionalize the surface of silica spheres with amino groups, facilitating the nucleation and growth of LHPs directly on the surfaces of silica particles.[378]

With regard to postsynthesis approaches, Hu et al. observed that adding an appropriate amount of a silica precursor (i.e., tetraethoxysilane, TEOS) to a solution of freshly synthesized LHP NCs (prepared by the HI method) led to the formation of micron-sized silica spheres in which LHP NCs are embedded.[350] However, it was observed that the NCs strongly aggregated in the resulting spheres.[350] Disec-butoxyaluminox-ytriethoxysilane is an interesting precursor for fabricating silica/alumina monoliths via a sol−gel process in toluene.[346] This single molecular precursor contains two alkoxide functionalities and a typical Al−O−Si linkage. The compatibility of this molecule with toluene enables the incorporation of presynthesized LHP NCs into silica/alumina monoliths, resulting in highly stable and homogeneous systems (no aggregation was observed).[346] Polysilazanes (PSZs) are

Scheme 14. Encapsulation of MAPbX₃ NCs in a Silica Matrix Using a LARP-Based Approach Together with Triethoxysilane (APTES)[a]
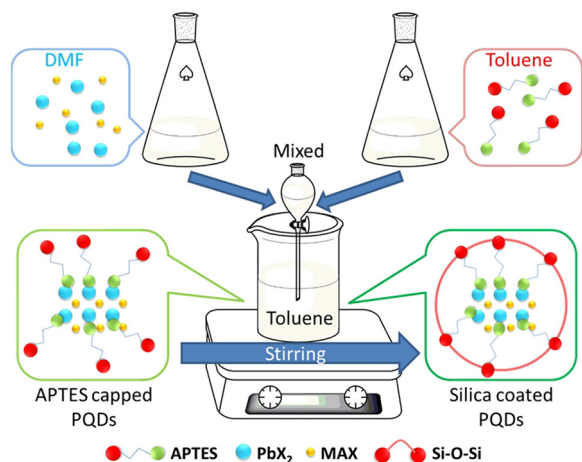
[a]Reproduced from ref 377. Copyright 2018 American Chemical Society.

classified as inorganic polymers in which Si and N atoms alternate to form the basic backbone. The nitrogen-based ligand groups of the PSZ matrix ($-H_2$-SiNH$-$) can be used as capping agents, and the remaining silazane moiety can be reacted with water to induce a hydrolysis condensation reaction which forms a PSZ inorganic matrix. LHP NCs@ PSZ nanocomposites can be synthesized simply by a hydrolysis and condensation reaction of liquid PSZ precursors and a small amount of water, as shown in Scheme 15.[349]

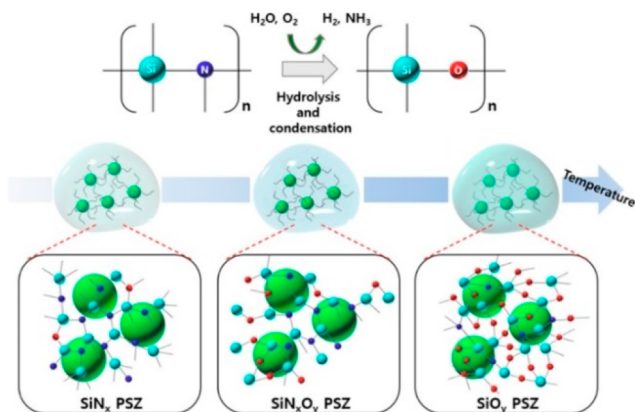## Scheme 15. Sol−Gel Route (Moisture-Induced Hydrolysis), Based On the Use of Liquid PSZ, Employed to Protect the Surface of LHP with Either SiN_x, SiN_xO_y, or SiO_y[a]

[a]Reproduced from ref 349. Copyright 2018 American Chemical Society.

Thanks to this approach, a SiN_x, SiN_xO_y, or SiO_y surface protection on LHP NCs can be selectively applied by manipulating the moisture-induced hydrolysis temperature.[349] Recently, a few groups have demonstrated other interesting two-step strategies for preparing LHP composites.[364,379] For example, Zhang et al. used a Pb-based metal-organic framework (MOF) as a starting precursor, which was then reacted with a MABr/n-butanol solution to form NCs@Pb-MOF composites (Figure 28).[379,380] This approach can be
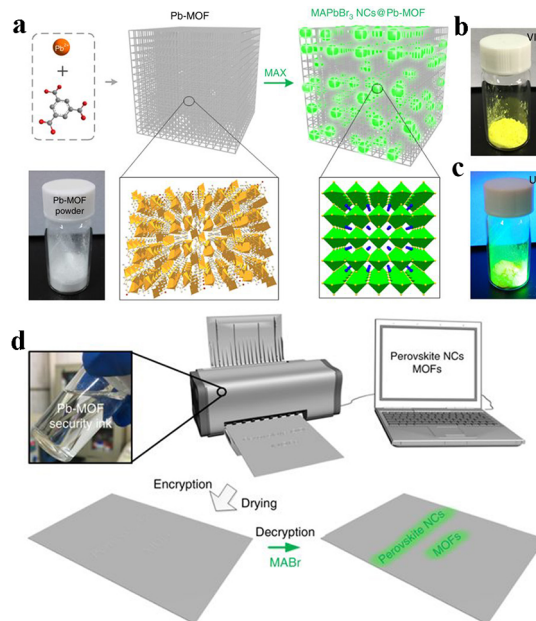
Figure 28. (a) Schematic representation of the conversion of a Pb-MOF into a luminescent MAPbBr₃/Pb-MOF composite. MAX is a halide salt (CH₃NH₃X, X = Cl, Br, or I), and the green spheres in the matrix are MAPbBr₃ NCs. The two black boxes show the crystal structures of the Pb-MOF (left) and the MAPbBr₃ (right). (b and c) Optical images of MAPbBr₃ NCs@Pb-MOF powder under (b) ambient light and (c) a 365 nm UV lamp. (d) Illustration of an inkjet setup based on Pb-MOF, which can be used for information encryption and decryption. Reproduced with permission from ref 379. Copyright 2017 Macmillan Publishers Limited.

exploited as a smart luminescent system for confidential information encryption and decryption: the Pb-MOF, which is transparent in the visible, can be easily printed and locally converted into luminescent LHP NCs (Figure 28).[379] Almost all LHP@oxide composites have a better thermal, photo, air, and humidity stability than standard NCs as well as a bright PL.

8. OPTICAL PROPERTIES OF HALIDE PEROVSKITE NCS

8.1. Linear Absorption and Emission

Since the first demonstration of halide perovskite NCs by Schmidt et al. in 2014 showing a remarkable PLQY of 20%, many groups have focused on improving the optical properties of these NCs for optoelectronic applications in terms of tunability, PLQY, stability, and excitonic properties.[15,381] One of the greatest advantages of MHPs is the ease with which the individual components can be exchanged to tune the bandgap of the resulting material (see previous sections). After the first report on MAPbBr₃ NCs, which had an absorption onset and a PL emission around 529 nm, it was quickly shown that modifying the halide composition could shift the optical properties of such NCs throughout the entire visible spectrum, as had been previously observed for bulk perovskite thin films.[251,382] Protesescu et al. showed that the emission wavelength for CsPbX₃ (with X = Cl, Br, or I) NCs could be shifted from 410 nm (X = Cl) to 512 nm (X = Br) to 685 nm (X = I), virtually going through all values in between by using mixed halide components (Figure 29).[26]
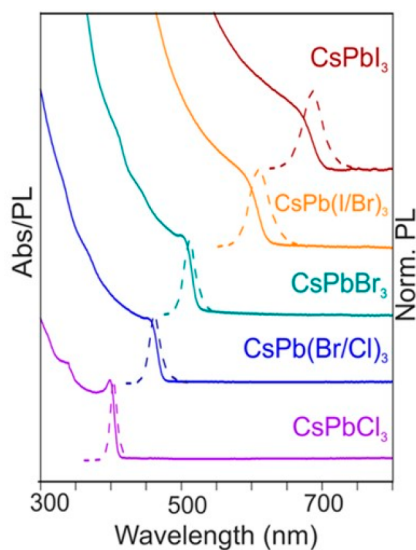
Figure 29. Bandgap tuning of CsPbX$_3$ NCs as a function of halide content, as demonstrated by UV−vis and PL spectra. Reproduced from ref 26. Copyright 2015 American Chemical Society.

The reason for this tunability lies in the nature of the electronic structure of halide perovskites, as is reported in Scheme 16. The conduction band forms from the antibonding

Scheme 16. Formation of Energetic Bands in a Lead Iodide Perovskite Material through the Hybridization of Lead and Iodide Orbitals

orbitals of the hybridization of the Pb 6p orbitals and the outer p orbitals of the halide (5p for I, 4p for Br, and 3p for Cl), and it is mostly p-like due to the high density of states (DOS) from the lead contribution. The valence band, on the other hand, forms from the antibonding states of the hybridization of the Pb 6s and the same halide p-orbitals.[383]

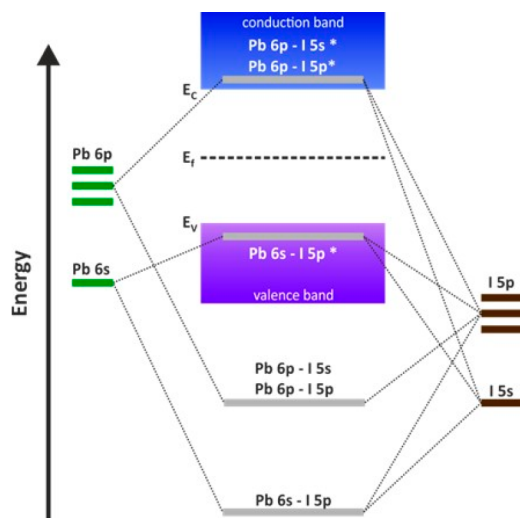This is in stark contrast to conventional semiconductor materials, such as gallium arsenide, whose bandgaps are formed between bonding and antibonding orbitals. Accordingly, the valence band edge shifts in energy as the halide component is changed, while there are only small changes to the conduction band edge.[384] The A-site cation does not contribute significantly to the conduction and valence bands in terms of

density of states, yet it does have a significant effect on the bandgap of the perovskite.[385] Three ions have been shown to satisfy the Goldschmidt tolerance factor when incorporated at the A-site of the perovskite crystal structure, namely inorganic cesium (Cs$^+$) and organic MA$^+$ and FA$^+$ cations. As the size of the A-cation decreases (from FA to MA to Cs), the bandgap of the corresponding LHP material blue shifts due to an increased tilting angle of Pb-X-Pb bonds and the concomitant distortion of the cubic crystal structure.[386] Consequently, the emission energies of MA-based perovskite NCs were shown to vary with the halide content from 407 to 734 nm.[171] In FA-based NCs, the PL emission shifts further to the red with reported values of 408 nm (Cl), 535 nm (Br), and 784 nm (I).[112,113,189] Furthermore, the B-site cation can also play a role in dictating the final optical properties of MHP NCs. For example, when Pb^{2+} is replaced with Sn^{2+} (one of the elements of choice for fabricating potentially environmentally friendly perovskites[387]), the bandgap and the PL emission of the resulting MHP NCs strongly red shift to 443 nm (Cl) and 953 nm (I), most likely as a consequence of the higher electronegativity of the Sn^{2+} in respect to Pb^{2+}.[78] However, the stability of Sn^{2+}- and, similarly, Ge^{2+}-based perovskite compounds is extremely poor due to a reduced inert electron pair effect, which corresponds to a decrease in the stability of the divalent oxidation state.[388] Consequently, only a single study on Ge-based perovskite NCs has been reported to date.[159] Whether the NCs are synthesized directly, or obtained through a subsequent anion or cation exchange process, their final bandgap or PL emission wavelengths depend only on their final stoichiometry for comparable sizes and shapes.[124]

Stokes shifts of LHP NCs are typically small, ranging from 20 to 85 meV.[127,389,390] Notably, the Stokes shift increases as the size of the NCs is reduced. This was explained by the formation of a confined hole state, which can delocalize across the entire NC, therefore it has size-dependent properties.[299] The PL line widths of MHPs are another critical parameter, especially for light-emitting applications. In most reports, PL spectra are displayed on wavelength scales, and their resulting line widths strongly vary according to the halide component (10−12 nm for Cl-perovskites and up to 40 nm for I-perovskites). However, as the wavelength of an energetic transition is related to the energy via the equation $E = \frac{hc}{\lambda}$, one should use an energy scale for comparing absolute values of line widths. Indeed, one finds that the line widths are typically on the order of 70−110 meV and do not vary noticeably in relation to the halide content. These are extremely narrow and comparable with the best CdSe-QD systems that are currently being used in commercially available lighting technologies.[38] In NC ensembles, two effects lead to the observed line widths: the homogeneous broadening, which is intrinsic to the perovskite material, and the inhomogeneous broadening, which depends on variations in the individual NCs. Two methods can be used to probe the origin of the broadening of absorption and PL line widths of NC ensembles, namely either measuring individual NCs or the so-called "four wave mixing" technique.[391] It was determined that, for CsPbX$_3$ NCs, inhomogeneous broadening only plays a minor role in shaping the total line widths when these methods are used at RT (as is shown in Figure 30a).[391] Rather, homogeneous broadening, which is largely due to the strong electronic-phononic coupling, is the predominant source of line width broadening.[391,392] As the temperature is lowered, the number of
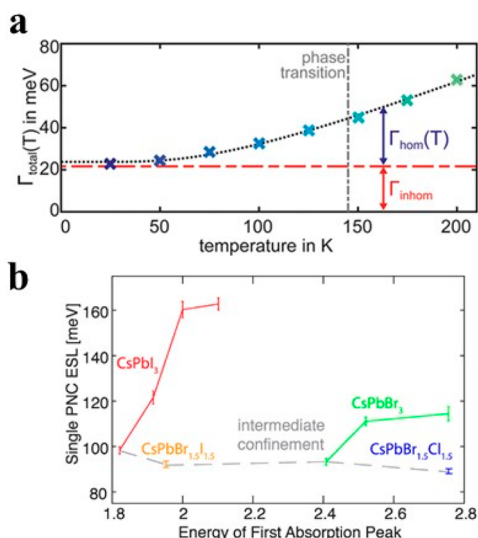
Figure 30. (a) Broadening of the 1s exciton level (Γ_{total}, fwhm of the absorption edge) of bulklike MAPbI$_3$ NPLs as a function of the temperature, together with the contribution of homogeneous and inhomogeneous broadening. Adapted from ref 391. Copyright 2018 American Chemical Society. (b) Effective spectral line width (ESL) of single nanocubes (PNC) as a function of their respective first absorption peaks. Adapted from ref 392. Copyright 2017 American Chemical Society.

occupied phonon modes decreases, leading to a reduction in the homogeneous broadening. At very low temperatures, the line widths are nearly exclusively inhomogeneously broadened. The effect of line width broadening is even enhanced in NCs that exhibit quantum confinement (Figure 30b).

In terms of PLQYs, LHP NCs typically exhibit extremely high values, even without an electronic surface passivation with wider-gap epitaxial shells, which is necessary for chalcogenide-based QDs.[113] Both Cs- and MA-based lead halide perovskites have been reported to have PLQY values of up to 80−95% for bromides and iodides.[24,45,117,295] These high values are a sign of the strong defect tolerance of halide perovskite materials, which arises as a result of their electronic structure and the bandgap that forms between two antibonding orbitals. Indeed, this characteristic, coupled with the fact that interstitial and antisite defects require very high formation energies, leads to the predominant formation of shallow traps.[393] FA-based NCs are not far behind their Cs- and MA-counterparts, with PLQY values of 70−90%. On the other hand, much lower PLQYs, typically below 20%, were reported for APbCl$_3$ systems.[43,188] This is likely due either to the small size of the chloride anions and their resulting effects on the crystal structure or due to the fact that defects in Cl-perovskites are not as shallow as in their Br and I counterparts, therefore they might act as electronic nonradiative traps.

An additional method to manipulate the optical emission of LHP NCs is by doping them with additional ions. This has been investigated in many recent publications, which have focused on the use of Cs-based Cl/Br perovskites. The introduction of Mn^{2+} ions, which partially replace Pb^{2+} cations in the LHP lattice, leads to a strongly Stokes-shifted emission, with the bandgap given by the perovskite matrix and the emission resulting from atomic states of Mn^{2+} ions (Figure 31a). Thanks to such features, these systems are particularly appealing for use in solar concentrators (Figure 31b).[31] A fine-
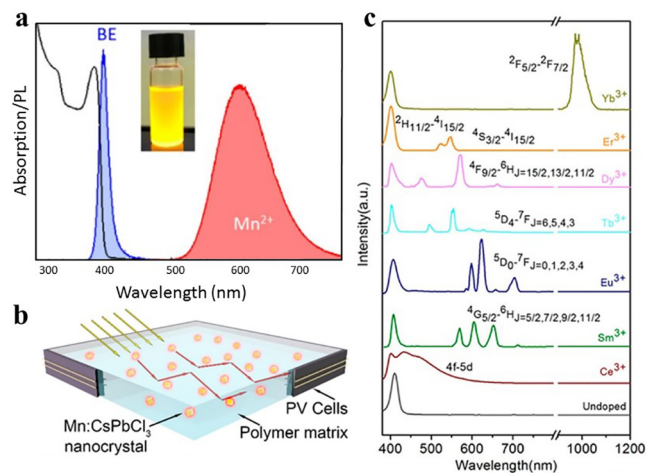
Figure 31. (a) Absorption and PL emission of Mn-doped CsPbCl$_3$ NCs: (b) the large Stokes shifts in these systems make them an ideal candidate material for solar concentrators. Adapted from ref 31. Copyright 2017 American Chemical Society. (c) PL curves of CsPbCl$_3$ NCs doped with different lanthanide ions. Adapted from ref 143. Copyright 2017 American Chemical Society.

tuning of the Mn^{2+} doping levels can also lead to a controllable dual emission from both the localized Mn^{2+} states and the bandgap recombination.[290,348] In contrast, doping CsPbBr$_3$ NCs with other divalent cations, such as Sn^{2+}, Cd^{2+}, and Zn^{2+}, was shown to lead to a blue shift in the band edge and PL emission.[283] In these cases, however, a significant fraction (0.2%−0.7%) of the original Pb ions was replaced by new metal cations, generating alloyed NCs. The blue shift in such systems can be rationalized, considering that upon alloying, the original perovskite lattice contracts, widening the bandgap.

The alloying CsPbBr$_3$ NCs with Al^{3+} ions (0.2% content) were shown to have similar effects: the resulting NCs had a blue-shifted PL emission centered at 456 nm and a surprisingly high PLQY of 42%.[394] In all of these cases, the perovskite NCs serve as an absorbing host which excites the dopants through energy transfer. Thus, even CsPbCl$_3$ NCs, which have very large absorption cross sections, but typically very low QYs, can be induced to emit strongly, provided that the energy transfer efficiency to the dopant ions is high. Furthermore, by specifically selecting the dopant atoms, the emission wavelengths of the resulting NCs can be easily tuned. As was demonstrated in the case of doping with lanthanide ions, the emission of CsPbCl$_3$ nanocubes could be shifted between 400 and 1000 nm with QYs in the order of 15−35% (as is shown in Figure 31c).[143]

8.2. Quantum Confinement

Regardless of the approach, the PLQY of blue-emitting perovskite NCs still lags significantly behind those of their red- and green-emitting counterparts. One additional method to obtain blue-emitting LHP NCs, which is commonly used for producing conventional semiconductive QDs, is the exploitation of quantum confinement.[395] In this process, one or more dimensions of a NC are shrunk down to or even below the size of the excitonic Bohr radius. Under these conditions, the wave functions of the charge carriers become confined, and, consequently, the absorption onset blue shifts, as the electron and the hole acquire confinement energies: $E_{onset} = E_G + E_e + E_h$. Upon confinement, the PL of LHP NCs also commonly exhibits a blue shift, although this shift is often not as large as

that of the absorption onset.[17] This is due to the interaction energy of the electron−hole pair, also known as the exciton binding energy, which leads to a modified optical transition energy: $E_{PL} = E_G + E_e + E_h − E_X$. The amount of binding energy in quantum-confined nanostructures can be several times higher than in bulk semiconductor materials.[17] This is due to changes in the dimensionality and the reduced screening of the Coulomb interaction through the surrounding, mainly weakly, polarizable ligands and organic media. In LHP materials, the excitonic Bohr radii are extremely small: in $CsPbX_3$, they range from 5 nm ($CsPbCl_3$) to 12 nm ($CsPbI_3$), while they are even smaller in their organic/inorganic hybrid counterparts, in the order of 1.5−3 nm.[26,382] Consequently, many of the reported LHP NC systems, even those with a high aspect ratio, such as NPLs or NWs/NRs, display only a weak quantum-confinement or no confinement at all.[124,396,397]

We will first discuss LHP NPLs, which can be considered effective colloidal quantum wells. Thanks to the use of long chain surfactants, which are too large to be incorporated into the crystal structure, it is possible to template the growth of LHP NCs, forming sheetlike morphologies with a high degree of control over the NPLs thickness.[50,117,122] A reduction in the NPLs thickness to below 4 or 5 monolayers leads to a quantum confinement that can be observed in a strong blue shift of the absorption onsets, as well as of the PL emission, by up to 0.8 eV, as is shown in Figure 32.[17,19,186] In the case of $MAPbI_3$ NPLs, this effect is quite striking: the bulk emission lies in the near-infrared, while the PL of the NPLs can be tuned almost throughout the visible range down to the green in the case of
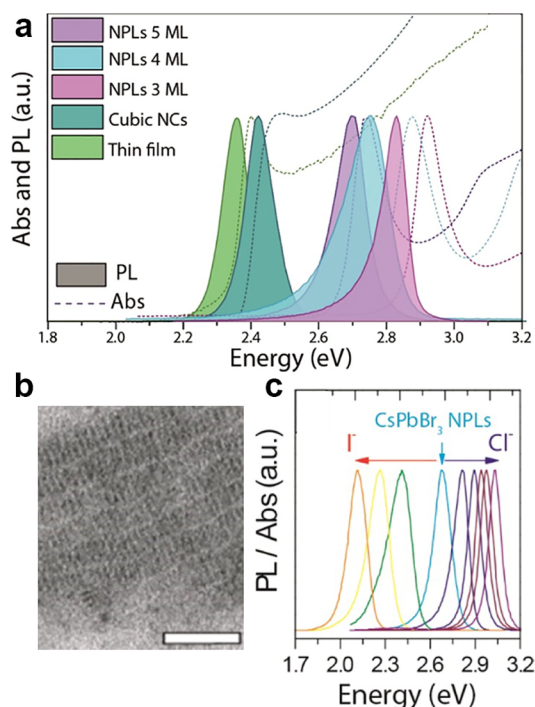
single-layered NPLs.[22] For Cs-based tin halide NPLs, it was demonstrated that the PL-emission can be tuned over a wide range in the near-infrared, from 950 nm down to 710 nm.[18]

Unfortunately, the high degree of tunability of the these strongly confined nanostructures' PL emission also has a significant drawback in that most NPLs exhibit low QYs, in the order of 5−20% when $n ≥ 2$ and only 1% when $n = 1$. This is likely a side-effect of the reduced dielectric screening of the electron−hole pair, which leads to an incomplete polaron formation around the charge carriers, leaving them more susceptible to scattering with defects and polar optical phonons.[50] However, recent publications have shown that this may only be part of the reason and that it is possible to mitigate some of the drops in the PLQY by limiting the number of surface defects through adequate surface passivation.[295] Bohn et al., for example, recently showed that the poor blue emission of $CsPbBr_3$ NPLs could be boosted by a postsynthesis treatment with a $PbBr_2$-ligand solution, and the PLQY increased from ∼7 to ∼70%.[398] This work suggests that, by carefully limiting the amount of surface defects (such as the Pb and Br vacancies in the aforementioned example) in halide perovskite NPLs, it is possible to obtain efficient blue-emitting nanostructures which can be integrated into electroluminescent devices.[135,398,399] Despite this, the QY is not constant for all NPLs, but it actually increases as the thickness increases. This is likely due to a dielectric screening effect of the charge carriers.

Importantly, the PL and absorption of NPLs are quantized according to the number of monolayers ($n = 1, 2, 3, \cdots$) that form the thickness of such nanostructures. Thus, if the elemental composition is known, the optical features of a NPL ensemble can be directly ascribed to those of a specific thickness. When NPLs are dispersed in organic solvents, they do not typically interact with each other. However, in the solid state, they tend to stack together so that the wave functions of neighboring NPLs (with a thickness lower than 4 monolayers) can overlap, leading to electronic coupling and to the formation of minibands, provided that the inorganic spacer layer is thin enough (in the order of 1.5 nm).[17,72,400]

There have been far fewer publications on perovskite quantum wires/rods and quantum dots than 2D nanostructures. This is likely due to the halide perovskites' tendency to form two-dimensional structures such as Ruddlesden−Popper perovskites. Furthermore, it is difficult to obtain 1D and 0D perovskite NCs with precisely tuned dimensions.[401] One-dimensional $CsPbBr_3$ NWs were first reported in 2016, and clear quantum confinement effects were visible in NWs with a diameter smaller than 10 nm (Figure 33).[16] As for 2D NPLs, typical colloidal approaches lead to NWs having a certain thickness distribution, which, in turn, results in multiple absorption and PL peaks.[16,17,402] It was found that the quantum confinement in 1D NWs is stronger for each given thickness than in their 2D counterparts. This is to be expected, as the NWs are confined in an additional dimension, further blue-shifting the PL and absorption onsets. PLQYs were also observed to decrease when the diameter of the NWs was reduced, an effect that was attributed to the higher concentration of surface defects in thinner NWs.[16] An alternative explanation for this observation is that there is an induced strain in NCs, which increases when the dimensionality is reduced and leads to the formation of defects inducing a nonradiative recombination.[403] It was also possible to tune the PL emission of these NWs through subsequent halide ion

Figure 32. (a) PL and absorption curves of $CsPbBr_3$ thin films, cubic NCs, and NPLs with different thicknesses. As the thickness is reduced, pronounced quantum confinement effects can be seen in the absorption and photoluminescence spectra. (b) TEM picture of 3 ML thick NPLs. (c) Postsynthesis AE reactions performed on NPLs lead to a wide tuning range of their PL, while retaining their size and shape. Adapted from ref 19. Copyright 2016 American Chemical Society.
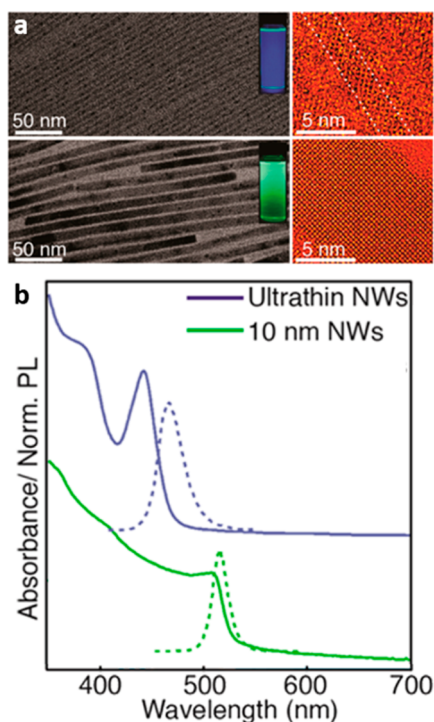
Figure 33. (a) TEM and HRTEM images of 10 nm and ultrathin (~2.2 nm, 4 ML) $CsPbBr_3$ NWs, and (b) their PL and absorption spectra. Similar to 2D NPLs, pronounced quantum confinement effects can be seen in these spectra. Adapted from ref 16. Copyright 2016 American Chemical Society.

exchange reactions.[16,126] In colloidal form, NWs are unstable, and they often merge together, as suggested by a subsequent redshift in their PL emission.[193,404]

In 2015, Protesescu et al. demonstrated that it is possible to tune the size of perovskite nanocubes down to 3.8 nm, which exhibited a noticeable quantum confinement (Figure 34, panels a and b). As for 1D NWs, though, especially for the smallest nanocubes, the increased width in the PL and absorption spectra indicates that the ensembles comprised nanocubes of various sizes, making it difficult to give a detailed analysis of the quantum confinement effects on 0D NCs.[26] Figure 35 depicts the quantum confinement for Cs–Pb–Br systems of varying dimensionalities. Here, it becomes apparent that, for a given size of the confined dimensions, there is an increase in the confinement as the dimensionality is reduced from 2D to 1D and, finally, to 0D. To date, only a few studies have focused on investigating the quantum confinement in perovskite nanocubes. Unfortunately, while a significant number of publications have been reported on perovskite QDs, there are significant discrepancies between the observed PL emission wavelengths and the size of the NCs. The reason behind this was attributed to the fact that the NCs, which were observed via TEM, were likely the degradation products of larger perovskite NCs that had been formed during the electron beam illumination.[46,103,405] While a monolayer constitutes the extreme case of a 2D perovskite system, the smallest possible 0D unit is a single $[PbX_6]^{4-}$ octahedron. In solution, these octahedra exhibit moleculelike excitonic absorption and emission spectra, with bandgaps far in the UV between 3.38 eV for PbI_6 and 4.37 eV for $PbCl_6$.[70] Balancing a strongly negative charge in the solid state requires a number of cations, for example Cs^+ ones, which would lead

to a Cs_4PbX_6 phase in this case. In this phase, the octahedra no longer share corners, but they are separated by cesium ions, eight of which surround each octahedron. The resulting optical properties do not differ much from those of the solvated octahedra. Since the charges are highly confined in the octahedra, A-cations play nearly no role in determining the spectral position of the optical features, in contrast to the halide ions. Additionally, as to be expected, Cs_4PbX_6 NCs show no size-dependence in their optical properties.[97] Interestingly, some publications have reported green-emitting Cs_4PbBr_6 NCs, despite their strong absorption in the UV.[221] While some works argue that such a green PL arises from defect states or from self-trapped excitons, the spectral position of the PL emission, its temperature-dependence, and, in some studies, also a strong absorption in the green suggest that these Cs_4PbBr_6 crystals are actually "contaminated" with small $CsPbBr_3$ inclusions.[406] Similar features were also observed in intentionally synthesized $Cs_4PbBr_6/CsPbBr_3$ composite materials, in which the Cs_4PbBr_6 perovskite acts as the strong absorber and transfers the energy to emissive $CsPbBr_3$ NCs.[356] This issue cannot be settled at the moment, as no clear evidence has been found that such $CsPbBr_3$ impurities are always present in samples of green-emitting Cs_4PbBr_6 materials. In order to get further insights into this subject, the reader is referred to recent articles focusing exclusively on 0D perovskites.[70,407,408]

One additional feature was observed in corrugated 2D, 1D, and 0D microstructure assemblies (Figure 34, panels d and e). In these microstructures, the individual quantum-confined nanostructures are electronically separated by organic spacer layers. Consequently, they retain the optical properties of their respective building blocks. An additional featureless and extremely broad PL emission, which was strongly red-shifted with respect to the expected perovskite emission, was observed and attributed to the formation and subsequent radiative recombination of self-trapped excitons.[409−411] These are produced through the excitation of a perovskite nanostructure, which then undergoes a physical reorientation to minimize the interaction energy with an adjacent nanostructure or within the crystal lattice. This reorientation significantly reduces the exciton energy, which is dubbed "self-trapped" as the radiative recombination must naturally accompany the physical reorganization of the perovskite structure. This consequently leads to a long-lived emission.[412] Interestingly, some of these structures are extremely efficient for light emission since they have QYs that are approaching unity.[413] Yet, a deeper knowledge still has to be acquired on the nature of the self-trapping exciton and the resulting optical properties of the nanostructured LHP material.

8.3. Exciton Binding Energies

The exciton binding energy is one of the most important parameters for an optoelectronic material, as it governs whether free electron–hole pairs or predominantly excitons generate the response of such materials when they are optically (or electrically) excited. Lately, many studies have focused on determining the exciton binding energy in bulk LHP and specifically in $MAPbI_3$, as this material exhibits very interesting properties in photovoltaic applications.[6] Generally, it has been agreed that the binding energy of excitons in LHPs is small enough (and the Bohr radius is large enough) that they can be considered Wannier-Mott excitons.
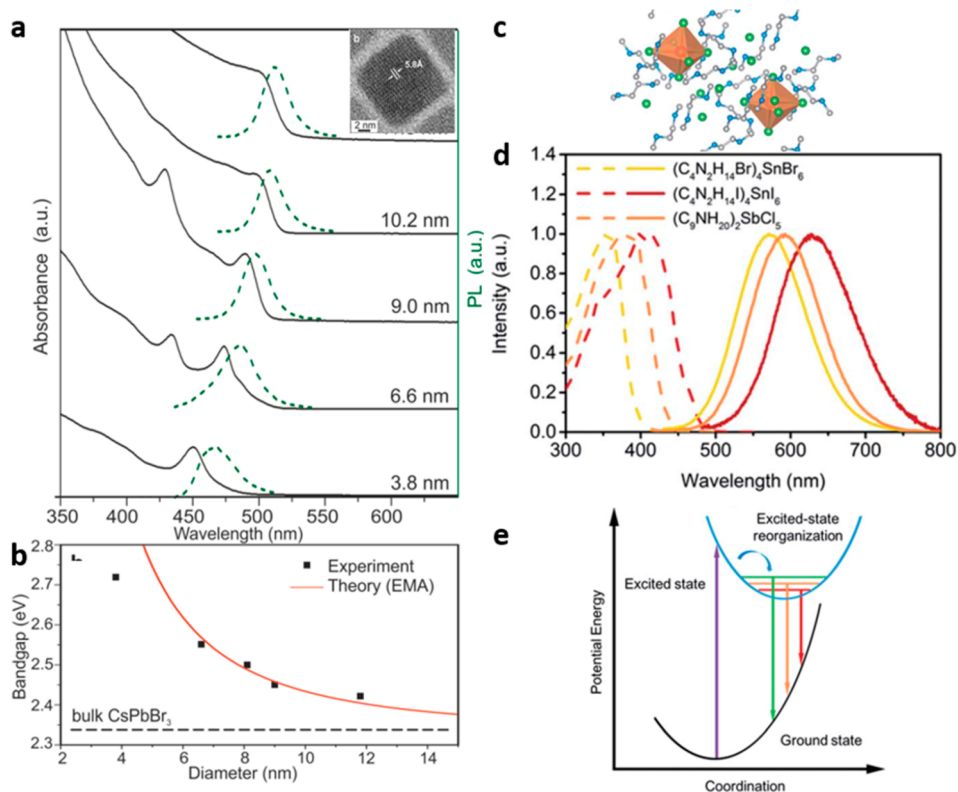
Figure 34. (a) PL and absorption spectra of CsPbBr$_3$ nanocubes of different sizes together with (b) the corresponding calculated bandgaps. Adapted from ref 26. Copyright 2015 American Chemical Society. (c) Depiction of corrugated 0D metal halide perovskite structures. (d) Corresponding excitation and PL spectra of these structures exhibiting a strong Stokes shift and a significant broadening of the PL, which are both induced by self-trapping excitons. (e) Energy diagram depicting the formation and recombination of self-trapped excitons. Adapted from ref 411 with permission from the Royal Society of Chemistry.
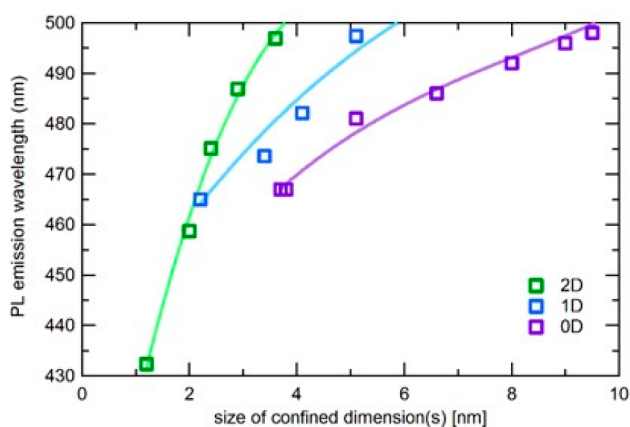
Figure 35. Variation in the PL emission as a function of the size of different CsPbBr$_3$ nanostructures: 2D, 1D, and 0D. Data extracted from refs 16, 26, 106, 123, and 398.

This means that the wave functions of such excitons are hydrogenic, and their respective Schrödinger equations can be solved analogously. Unfortunately, despite the plethora of studies on this issue, there are huge discrepancies on the reported values which, in the case of MAPbI$_3$, range from 2 to 60 meV at RT.[414] This is not due to the different methods that are employed in the experiments, as even similar experimental approaches have resulted in discrepancies. Additionally, some methods are at best problematic and more likely not applicable, as they deliver unreliable or even false values. For example, the dielectric function in LHPs is generally accepted

to be a function that strongly varies with the temperature and frequency. As such, it is also unclear which value of the function needs to be taken into account in order to obtain the binding energy, as this also depends on the relationship between the binding energy and the optical phonon energy of the material.[415] The application of Elliot's model to LHP absorption spectra can encounter severe problems. With the absorption features of a NC sample typically strongly broadened, it is hard to distinguish the contributions of excitonic and continuum absorption for small exciton binding energies.[416] Another commonly used method is to calculate the exciton binding energy from the temperature dependence of the PL intensity.[417] This model assumes that bound electron–holes pairs are luminescent, whereas unbound pairs recombine nonradiatively. Consequently, as the temperature is increased, the thermal energy dissociates a larger fraction of excitons, resulting in a quenching of the PL. However, it is known that halide perovskites (e.g., MAPbI$_3$) have quite an efficient luminescence from free electrons and holes even at RT. Hence, this method tends to lead to significantly higher and unreliable values, such as 50 meV for MAPbI$_3$ or 75 meV for MAPbBr$_3$.

Unfortunately, there are far fewer studies on the exciton binding energy of LHP NCs than on their bulk counterparts. For NCs with dimensions that are significantly larger than the exciton Bohr radius, which do therefore not exhibit any quantum confinement, the values should be identical to those of their bulk counterpart. Indeed, the study by Protesescu et al. reported calculated values for CsPbX$_3$ NCs of 20, 40, and 75 meV for X = I, Br, and Cl, respectively, which fit into the range

of those commonly accepted for the corresponding bulk materials. On the other hand, decreasing the size of LHP NCs should lead to an increase in the exciton binding energy. The most effective systems for determining the effects of quantum confinement on the exciton binding energy turned out to be 2D perovskites, such as Ruddlesden—Popper compounds or NPLs, as the thickness in these systems can be controlled with single monolayer precision.[401] Here, because of the 2D nature of the materials, the density of states in the continuum exhibits a steplike appearance, and quantum-confinement separates continuum and excitonic states progressively. This facilitates the determination of the exciton binding energy, and the Elliot model can be easily applied. Interestingly, for both NPLs and bulk thin films, values of up to several hundred meVs have been determined experimentally by applying the Elliot model to linear absorption spectra (Figure 36, panels a and b). These
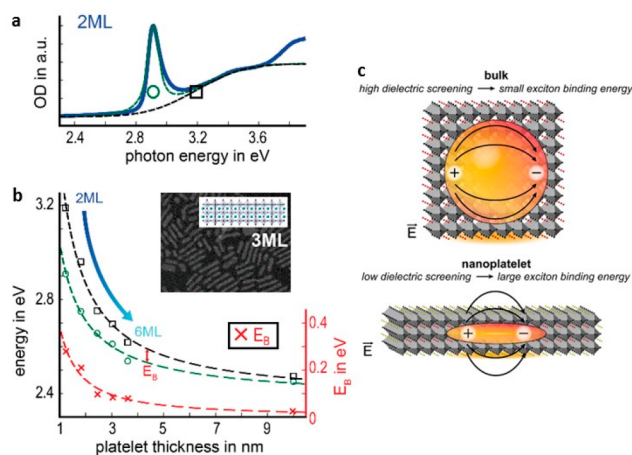

Figure 36. Determining the exciton binding energy in 2D LHP NPLs. (a) Optical density of 2 ML NPLs dispersed in toluene: the 1s exciton absorption peak (green ○) and continuum onset (black □) are determined by applying the Elliot's formula. The exciton binding energy is given by the energy difference between these two levels as a function of NPL thickness. Adapted from ref 398. Copyright 2018 American Chemical Society. (c) Scheme depicting that a reduced screening of the Coulombic electron—hole interaction in the thin NPLs strongly contributes to a large value in the hundreds of meV of the exciton binding energy. Adapted from ref 50. Copyright 2017 American Chemical Society.

values are more than ten times higher than those reported for perovskite bulk materials.[22,418,419] In the theoretical limit, due to geometric considerations, the binding energy should only be 4-fold enhanced: $E_B^{2D} = 4 \times E_B^{3D}$. However, this does not consider the dielectric surrounding of the 2D structures. As is shown in Figure 36c, the high-dielectric inorganic layers in perovskites are surrounded by low-dielectric organic ligands. Thus, as the thickness is reduced, the Coulomb interaction between the electron and the hole is progressively less screened. Consequently, the binding energy increases to the observed values.[420] With the excitons playing such a prominent role in LHPs even at RT, future work needs to focus on understanding the exciton binding energy in LHPs and how it is affected by composition, size, and dimensionality.

8.4. Nonlinear Effects

While most of the studies on LHP NCs have focused on their linear properties, several groups have also investigated the nonlinear effects of such systems. For high laser power

densities, multiple excitations can occur inside a single NC. Within these confined volumes, the excited carriers can interact with each other before decaying. One form of interaction is called the biexciton, in which two excitons bind together to form a coupled state comprising two electrons and two holes. As an exciton is electrically neutral, the binding energy of biexcitons is significantly lower than that of the "simple" exciton. Consequently, it is often not observable due to its thermal dissociation. However, in bulk and especially in quantum-confined LHP structures, which typically have large exciton binding energies, biexcitons can be stable at low temperatures or even at RT in some cases. Makarov et al. were the first to reveal that the biexcitons $CsPbI_3$ and $CsPbI_{1.5}Br_{1.5}$ NCs have a biexciton energy of approximately 11—12 meV, which is roughly half of the value of the simple exciton (Figure 37).[421] In more recent studies, discrepancies in the biexciton
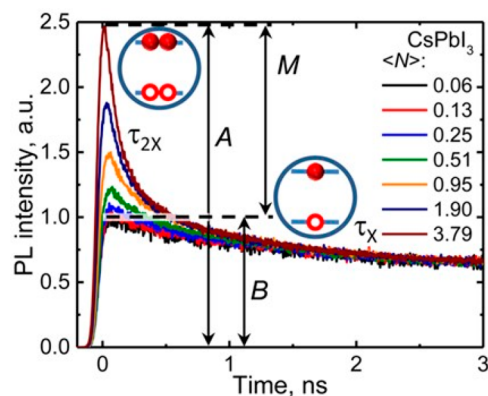
Figure 37. Biexctionic decay (lifetime τ_{2X}) in $CsPbI_3$ nanocubes for high pump intensities in time-resolved PL measurements. The late-time tail of the decay curve corresponds to a single exciton recombination (lifetime τ_X), while M and B correspond to the intensities of the multiexciton and single exciton signals, respectively. Adapted from ref 421. Copyright 2016 American Chemical Society.

binding energies have arisen, with some groups confirming the earlier values for pure $CsPbBr_3$ NCs[422] and others reporting significantly enhanced energies.[423,424] Additionally, these were shown to have energies that are dependent on the excitation power, although the studies failed to provide an explanation for this or an explanation for the contradictory reports on the binding energies.

While there are currently no reports on biexcitons in NPLs or in other strongly confined perovskite NCs, there have been two publications on bulk perovskite quantum wells.[425,426] In both works, biexciton energies of approximately 40—45 meV were reported for monolayer perovskites, which are roughly an order of magnitude below those of single excitons. Moreover, Elkins et al. revealed that increasing the thickness of such structures from one to two monolayers causes the corresponding biexciton energy to reduce to only 15 meV, which becomes insignificant when $n = 3$.[425] Consequently, such findings suggest that biexciton energies should be negligible in weakly or nonconfined LHP NCs. The ratio of photogenerated biexcitons to excitons seems to strongly depend on the halide composition and the size of NCs, as was reported by Utzat et al.[392] These authors revealed that quantum confinement plays a major role here, as it can enhance the electron—hole overlap, thus increasing the Auger recombination rate with respect to the radiative decay rate of biexcitons. Indeed, they were able to

determine $n_{biexciton}/n_{exciton}$ ratios of 2% for highly confined $CsPbBr_3$ NCs and 54% for weakly confined $CsPbI_3$ NCs. Their results illustrate possible applications for the individual types of NCs: I-containing NCs are an excellent choice for lighting applications that require high brightness LEDs, while Cl/Br and strongly confined Br variants are more attuned to single photon applications. Biexcitons in LHPs decay significantly faster than single excitons; the time constants are typically below 50−60 ps, which are substantially higher than those of conventional semiconductor QDs.[421,427] Additionally, as is depicted in Figure 38, LHP NCs appear to deviate from the
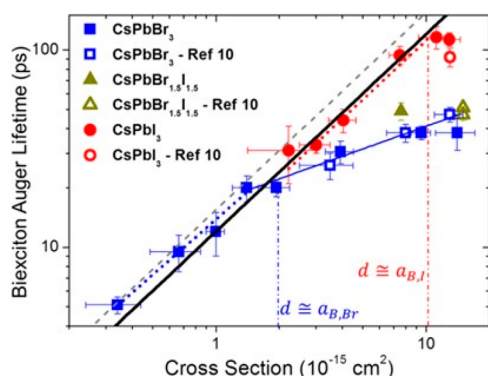
Figure 38. Biexciton Auger lifetimes of small LHP NCs and their dependence of the NCs size. A deviation from the universal volume scaling law can be observed for NCs when their diameter exceeds the exciton Bohr radius. Adapted from ref 423. Copyright 2016 American Chemical Society.

"universal volume scaling" law, which relates the Auger recombination lifetimes to the volume of the NC, irrespective of the material and composition. As the deviation appears for NCs whose diameter is larger than the excitonic Bohr radius, the reason for this discrepancy could be due to these NCs only being in the weakly confined regime (as a consequence of the small excitonic Bohr radii in LHPs).[423] Clearly, research needs to be conducted in order to understand the binding energies of biexcitons, their generation, and subsequent recombination in LHP NCs.

In some cases, photoexcited electron−hole pairs can be photoionized, whereby the electron, or the hole, leaves the NC before a radiative recombination occurs, resulting in a charged NC. A subsequent absorption process can induce the formation of another exciton in the same NC, which can then interact with the residual charge, resulting in the formation of a so-called "trion".[428,429] This quasiparticle typically recombines nonradiatively through Auger recombination, although radiative decay was also observed in LHP NCs, which had emission energies that were slightly red-shifted by about 15−20 meV from the excitonic transition energy.[428,429] The lifetimes of trions are typically 4−5 times longer than those of biexcitons, but their occurrence strongly depends on both the NCs surrounding and the excitation energy.[421,423,424] Yin et al. recently reported higher-order quasiparticles, such as charged biexcitons (XX^-, which is essentially a biexciton with an additional electron), or doubly charged single excitons (X^{2-}, which is an exciton with two additional electrons) in $CsPbI_3$ NCs, although only at ultralow temperatures due to their low binding energies (Figure 39).[430]

In that study, the authors observed a doublet emission, split by several hundred μeV, originating from the exciton. They
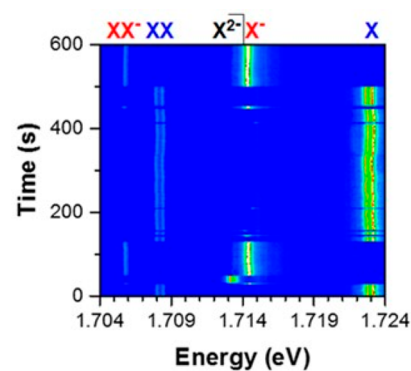
Figure 39. Time-dependent PL spectra of a single $CsPbI_3$ NC excited with an average of 1.5 excitons at 4K, revealing not only a single exciton recombination (X) but also singly charged (X^-) and doubly charged (X^{2-}) single excitons, biexcitons (XX), and charged biexcitons (XX^-). Adapted with permission from ref 430. Copyright 2017 American Physical Society.

further postulated that this large splitting could be caused by lattice anisotropy in the perovskite NCs. However, in a similar comprehensive single NC study, Becker et al. observed a fine-structure splitting into a triplet state (Figure 40).[428]
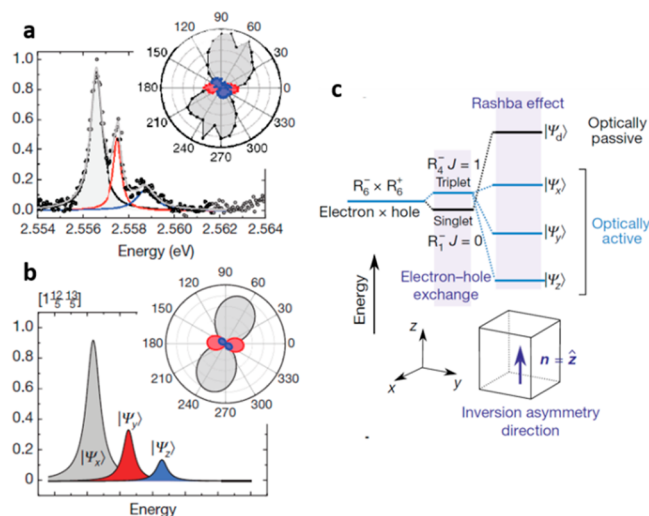
Figure 40. (a) Angular-resolved single NC PL measurements revealed a fine structure, which can be reproduced through simulations (b). (c) Energy scheme depicting the splitting of energetic states into cubic NCs. The Rashba effect is introduced to explain the experimental findings. This results in the lowest energetic state being optically active in contrast to common semiconducting NCs. Adapted with permission from ref 428. Copyright 2018 Macmillan Publishers Limited.

Combining PL measurements with theoretical calculations and employing Rashba splitting, the authors concluded that the lowest energetic states in LHP NCs are, in fact, emissive triplets. The Rashba effect is a splitting of initially degenerate spin states in a k-space in materials that exhibit large spin−orbit coupling and an inversion asymmetry.[431] This is in stark contrast to conventional semiconductor QDs, whose lowest state is typically dark, rendering them only weakly emissive at low temperatures.[432] Further work needs to determine the exact cause of the Rashba effect and to investigate other materials in which this might play a similarly important role.

Instead of exciting a material with photons that have a higher amount of energy than the bandgap ($\hbar\omega \geq E_G$) to generate an electron–hole pair, photons with an energy below the bandgap can also be used. Provided that these carry at least half of the bandgap energy ($\hbar\omega \geq \frac{1}{2}E_G$), a two-photon absorption (TPA) process, via virtual states, can be observed in a given material at very high excitation densities. This phenomenon is especially interesting for photovoltaic applications, as more of the solar spectrum could be used to generate a current, boosting the efficiency of solar cells. TPA was first observed in CsPbBr$_3$ NCs by Wang et al. in 2016, and they had enormous absorption cross sections which were 2 orders of magnitude larger than that observed in conventional semiconductor QDs.[433] In organic MA-based NCs, the absorption cross-section was determined to be 1 order of magnitude larger still.[434] In LHP NCs, even higher orders of absorption were observed by Chen et al., with optical cross sections determined for up to five-photon absorption processes in both MA- and Cs-containing bromide perovskite NCs.[435] Interestingly, the authors found that core–shell structures, comprising a MAPbBr$_3$ core and a (OA)$_2$PbBr$_4$ shell, to be the most efficient structure for such high-order absorption processes, and they suggested that these structures could possibly be used in multiphoton imaging applications.

Carrier multiplication (CM), also known as "multiexciton generation" (MEG), is a process by which one high-energy photon is converted into multiple electron–hole pairs. This is an additional method that can be used to boost the efficiency of photovoltaic devices, and it has been demonstrated to have a high efficiency in PbSe and CdSe QDs.[436] Unfortunately, this process was not observed in halide perovskites NCs even at energies as high as 2.65 × E_G. This could be due to the fact that the effective electron and hole masses are similar. Consequently, due to optical selection rules, the excitation energy is split equally between the hot electron and the hot hole, increasing, in turn, the threshold for carrier multiplication to ≈3 × E_G. For CsPbI$_3$ NCs, this corresponds to 5.5 eV or roughly to an excitation wavelength of 230 nm.[421] This energy lies far outside the PV-relevant region of the solar spectrum, therefore researchers are not very interested in investigating the CM process in MHP materials. Interestingly, Manzi et al. observed a combined effect of multiphoton absorption leading to multiple excitons generation in thin films of all-inorganic Cs-based LHP NCs (Br and I), as is shown in Figure 41.[437] The authors observed a strong nonlinear absorption for a wide range of photon energies below the bandgap ($0.5E_G < \hbar\omega < 0.8E_G$). Importantly, they determined that the absorption processes was higher at specific energies, so that $p \times \hbar\omega = n \times E_X$ wherein E_X is the exciton transition energy and p, n are whole integer numbers. This process uses below-band gap photons to create excitons, and the excess energy of the absorption process is turned into multiple electron–hole pairs. As these two processes are the biggest source of energy loss in a PV device, the study presents a possibility to enhance the efficiency of a PV-device past the Schokley-Queisser limit. It will be interesting to see in the future whether this phenomenon is restricted to LHP NCs or whether it can be observed in other materials, being consequently a general phenomenon in semiconducting NCs.

Another interesting nonlinear phenomenon, capable of overcoming the Shockley-Queisser limit, is the so-called quantum cutting effect. In this process, first observed in the
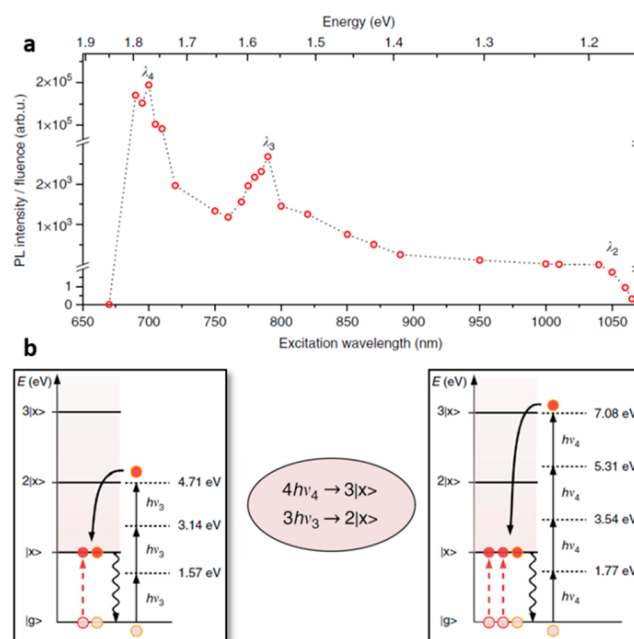
Figure 41. (a) Interesting resonances appear in wavelength-dependent below bandgap excitation spectra of LHP NC films. (b) This occurs whenever an integer multiple of the exciting photon energy equals an integer multiple of the exciton energy. This is explained with a multiphoton absorption, leading to multiple excitons being generated. Adapted with permission from ref 437. Copyright 2018 Macmillan Publishers Limited.

1970s in bulk crystals containing rare earth ions,[438,439] a high-energy photon is converted into two or more lower-energy photons, with consequent PLQY values far surpassing unity.[440] The quantum cutting effect, which is also defined as a particular case of a downconversion process, is typically achieved by codoping a material with two different impurities: the first one, called the donor or sensitizer, is able to absorb the light from the source and to transfer its excitation energy to the second impurity, called the acceptor, which is responsible for the final luminescence.[441] Typical luminescent impurities are trivalent rare-earth ions as they exhibit stability, small reabsorption losses, high PLQY, and, in addition, their 4f energy levels offer a large variety of energy transfer possibilities between different rare-earth ions.[442] Among them, Yb^{3+} ions are of particular interest for photovoltaic applications, as they are characterized by a luminescent emission at 1.24 eV (~1000 nm), an energy that can be easily absorbed by silicon.[30]

Quantum cutting has also been observed in NCs comprising a single rare earth impurity and a suitable host material, which should be characterized by a low electron–phonon coupling to prevent nonradiative decay of the high-energy excitation.[443] Halide perovskites as well constitute an interesting choice as host matrices, due to their enormous absorption cross sections and, in comparison to conventional inorganic semiconductors, a relatively low electron–phonon coupling.[444] This was first demonstrated in 2017 by Song and co-workers,[30,143] who not only explored the possibility of including rare earth ions into CsPbX$_3$ NCs (with X= Br, Cl, and mixtures thereof), but also demonstrated a PLQY in the NIR of nearly 150%. In particular, it was shown that CsPbCl$_{1.5}$Br$_{1.5}$:Yb^{3+}, Ce^{3+} NCs could boost the efficiency of commercial silicon solar cells from 18.8 to 21.5%. In a more recent publication, Milstein et al. investigated the quantum cutting effect in Yb-doped perovskite

NCs having PLQY up to 170%:[157] it was found that, upon excitation of the perovskite host, a picosecond nonradiative energy-transfer process to shallow Yb^{3+}-induced defects takes place, simultaneously exciting two Yb^{3+} ions. Given these promising results, rare earth doped MHP NCs hold great promise for improving existing photovoltaic applications, both for conventional silicon based and all-perovskite solar cells.

9. OUTLOOK

This review has covered many aspects concerning the synthesis methods, postsynthesis treatments, and optical properties of metal halide perovskite NCs. While this field is reaching maturity, there are several open issues that require attention, which we will outline here. Bound to these issues are the most promising future research directions from a materials' chemist perspective.

Surface Chemistry, Lattice Defects, and How to Investigate them

Currently, we need to reach a deeper understanding of the surface chemistry of MHP NCs, in terms of the type of ligands that can bind to their surface and how they interact with it. For example, it is still not clear how different types of ligands influence the surface termination and the stability of the NCs, nor which ligands passivate trap states and which ones possibly introduce new traps. We also have little knowledge of how ligands control nucleation, growth, and shape evolution, all aspects that remain obscure to date. In this regard, it is important to underline that there are huge differences in the surface chemistry, and in the nature and energetics of trap states when going from chlorides to bromides and iodides, meaning that what we learn from a specific halide system is not automatically valid for the other halides.

In terms of surface chemistry, the standard $CsPbBr_3$ NCs (synthesized by OLA and OA) have been studied the most, and consensus has been reached on the presence of oleylammonium as the A-cation on surface of the NCs.[301,303] Unfortunately, the nature of the bonding between the NC surface and such capping ligands[38,53] is very dynamic. In this respect, alkylammonium species are much more mobile and susceptible than carboxylates to washing with polar solvents.[120] Such dynamics leads to a major drawback: these materials are still colloidally and structurally instable, and this problem has not been entirely addressed to date. For instance, LHPs NCs can exhibit near-unity PLQY, but such optimal optical properties deteriorate drastically upon washing with polar solvents, during long-term storage or even after deposition on a substrate to form a dry film. Promising approaches here are, for example, the use of less aggressive washing procedures, such as those employing methyl acetate, or the use of zwitterionic ligands.[137] We believe that a more systematic exploration of alternative halide precursors, solvents, such as tri-*n*-octyl phospine oxide[445] or benzyl ether, and ligands, such as secondary or tertiary amines,[226] phosphonic acids, thiols or sulfonic acids, could be another exciting direction for achieving a more "static" surface passivation and/or to gain a more complete understanding of the surface stabilization of MHP NCs.[446] Among the aforementioned ligands, phosphonic acids are promising ones since they have a strong capability of forming organo-phosphonates with metal cations.[447−450]

In terms of energetics, we still have to elucidate how the surface energy of NCs changes depending on the type of surface termination and on what ligand molecules are passivating it. In addition, it would be interesting to understand what is the overall contribution of ligands to the electronic band structure of MHP NCs. At the moment, most published works dealing with these topics focus primarily on lead-based halide perovskites, and not much is known about the other MHP systems. From a computational point of view, a more extensive version of the recent work by ten Brinck and Infante on LHPs would be a good start.[299] Hand-in-hand with computation, a combination of traditional surface analysis techniques, vibrational spectroscopy, and nuclear magnetic resonance spectroscopy is steadily unfolding the surface chemistry of these NCs. An important technique that has not yet been applied to study the surface of halide perovskite NCs is that of small-angle neutron scattering. Such technique, supported by extensive modeling, has been employed to quantitatively determine the assembly of organic ligands on the surface of metal nanoparticles.[451] Such studies will additionally help in shedding light on the factors governing nucleation and growth in these types of NCs, for example the influence of the alkyl chain length and the role of acid−base equilibria. Addressing the surface chemistry of MHP NCs will remain a hot topic in the coming years.

The types of defects in MHPs in general, and then in NCs, need to be well-understood. For example, do vacancies or other types of defects promote anion exchange? Are they involved in the green light emission of the otherwise nonemitting $CsPb_2Br_5$ and Cs_4PbBr_6 materials? Lately, Ruddlesden−Popper phases were discovered in all-inorganic halide perovskites ($CsPbBr_3$), but the mechanism triggering their formation has not been clarified.[452] Such phases, which can be considered as "extended planar defects" in the lattice of $CsPbBr_3$, might originate upon the fusion of different NCs, as indicated by a recent work.[453] These extended "defects" do not seem as rare as initially thought, and their role in the overall reactivity and electronic properties of MHPs will have to be investigated. Other open questions are whether impurities, dopants, or other species segregate at these planar defects. Also, can we effectively tune density of halide vacancies in NCs by working under halide rich-poor conditions? These questions will remain partially unanswered until we have identified structural analysis techniques that will be less destructive toward these NCs, which for example are very sensitive to electron beam irradiation.

Emission in the Blue, Green, and Red That Meets the Standards

There is no doubt that the major field of application of halide perovskite NCs will be in light emission. In accordance with the International Telecommunication Union (ITU) and the International Commission on Illumination (CIE) recommendations, the three primary emission peaks for displays and for the wide-gamut colorimetry are centered at 630 nm (red), 532 nm (green), and 467 nm (blue).[454] In this regard, color-tunable perovskite NCs are particularly promising for LEDs, given their high PLQY and narrow emission line width. However, closer scrutiny of LHP systems revealed that each of the three emission colors is facing unsolved issues. We start with the blue. As a general trend, the PLQY of LHP NCs generally decreases for larger bandgaps, meaning that blue-emitting NC based devices will have lower performances than the corresponding green or red ones. Also, in order to achieve blue emission from LHP NCs, mixed halide systems have to be employed (i.e., Cl/Br mixed halide systems), which,

unfortunately, suffer from phase segregation.[113] This explains why LHP NC based devices with a blue emission suffer from poor efficiency and stability. Another appealing option would be the use of $APbBr_3$ (A = Cs, MA, and FA) NPLs, whose emission can be shifted toward the blue by means of quantum confinement; that is by reducing their thickness down to a few monolayers. Unfortunately, NPLs are highly susceptible to surface defects due to their large surface-to-volume ratio, and as a result, they feature lower PLQY values compared to the standard perovskite nanocubes. Even though recent studies have addressed their low PLQY,[398,455] the tendency of the NPLs to coalesce, with the consequent emergence of an undesired green emission, represents a roadblock to their application as blue emitters. Thus, in order to implement these nanostructures into devices, future research directions must address their instability, while retaining a high PLQY. Turning to green emission, the PL of $CsPbBr_3$ NCs is shifted toward the blue (505−520 nm) if compared to the desired target (532 nm). On the other hand, $FAPbBr_3$ NCs whose PL is peaked around 530 nm suffer from poor stability. One straightforward solution would consist in doping/alloying $CsPbBr_3$ NCs with other "A" or "B" cations in order to slightly red-shift their emission without compromising their PLQY and stability. Lastly, red-emitting NCs, for example $CsPbI_3$, are facing serious issues of structural stability, with a strong tendency to undergo phase transition into the nonemitting "yellow phase". To this regard, different strategies, mainly based on alloying/doping $CsPbI_3$ NCs with various A and B cations, have been demonstrated to efficiently improve the stability of these NCs.[456,457] Unfortunately, none of these alloyed/doped systems (e.g., $CsPb_xMn_{1-x}I_3$[154] or $SrCl_2-CsPbI_3$[458] is characterized by a proper red emission (630 nm), and, to date, stable iodide-based perovskite NC emitters have not been fabricated. Future research on red-emitting devices will be therefore aimed at finding other strategies in order to shift the PL of $CsPbI_3$ NCs and, at the same time, at increasing their stability.

Long-Term Stability, Encapsulation, Heterostructures

Long-term stability issues under harsh conditions (for example high temperatures and humidity) need to be carefully addressed, especially for applications in lighting applications, such as down-converting LEDs. The encapsulation of NCs in various inorganic matrixes has been actively pursued (for example, amorphous $CsPbBr_x$,[248] TiO_2,[249] SiO_2,[250] alumina,[344,348,351] and $PbSO_4$-oleate,[278] as discussed in this review), but what is not known is if such a "shelling" entirely prevents oxygen and moisture from accessing the NCs over extended periods of time. This leads us to another challenge: that of creating stable heterostructures between halide perovskite NCs and inorganic compounds. Encouraging results have been reported on stable epitaxial interfaces between lead halide perovskites and Pb chalcogenides,[234,459] ZnS,[244] and, recently, Cs_4PbBr_6.[460] The final target would be, undoubtedly, the production of core/shell nanostructures in which MHP NCs will be completely covered by a shell of a robust inorganic material, such as metal chalcogenides, oxides, or fluorides.

Beyond Lead, Seriously and Systematically

Turning to a more explorative materials science, one exciting direction is represented by the so-called "elpasolite" materials. This area of research is primarily motivated by the need to start using compounds that are more environmentally friendly than Pb-based ones. Even if at least 350 compounds of such a family

of materials have been synthesized so far, most of them remain unexplored.[79] Indeed, as was highlighted by Giustino and Snaith, the possible combinations of A, B^+, B^{3+}, and X^- ions correspond to a total of more than 9000 hypothetical quaternary halide compounds.[461] Among them, even in the least optimistic case, at least 900 would satisfy the Goldschmidt tolerance factor.[461] We can therefore assume that, to date, more than 600 compounds have not yet been investigated. In 2017, after a first screening performed via first-principle calculations, Zhao et al. proposed 11 nontoxic candidates as promising absorbers to replace $APbX_3$ in PV solar cells.[79] Among those, $Cs_2InSbCl_6$ and $Cs_2InBiCl_6$, have shown theoretical maximum solar cell efficiencies that are comparable to that of $CH_3NH_3PbI_3$. Until recently, the main challenge was to develop effective and versatile synthesis methods for the preparation of such complex compounds.[461] However, as is shown in this review, new efficient synthetic approaches for the colloidal synthesis of perovskite NCs have finally been developed over the past few years. These new strategies have already delivered Cs_2AgBiX_6,[115] $Cs_2AgInCl_6$,[227] and Mn-doped $Cs_2AgInCl_6$[227] DP NCs. These materials represent only the tip of the iceberg, and the real potential of double perovskites is yet to be fully revealed.[462,463] Also, it is likely that several elpasolite materials, which are predicted to be unstable in the bulk, could still be synthesized in the form of NCs, due to the significant contribution of the surface energy to the total energy balance in nanoscale materials. When this is coupled with the possibility to dope NCs with various ions, the potential for developing new materials for tailored optoelectronic applications is still enormous and remains vastly untapped to date.

Fundamental Properties

With the aim of improving and optimizing MHP NCs for optoelectronics, an in-depth understanding of their fundamental properties is essential. One of the trickiest parameters that still has to be determined is the exciton binding energy due to a both frequency- and temperature-dependent dielectric function. One strategy that could be now pursued, thanks to the new synthesis tools that have been developed recently, would be to finely tune the size of colloidal NCs from the smallest one accessible up to the bulk. Moreover, the observed fine structure and matching theory for cubic NCs will need to be verified, as do the existence and the magnitude of the Rashba effect, for other compositions and crystal morphologies, such as NPLs or nanowires. Parameters such as Auger recombination rates, exciton versus biexciton formation rates, and gain profiles will need to be determined if these NCs are to be used in high-power LEDs and lasers. Multiple carrier generation is also of great interest for photovoltaic applications, as it could help to shatter the Shockley-Queisser limit. Also, we have only begun to understand the realm of possibilities that can be offered by quantum-cutting effects in nanoscale halide perovskites.

AUTHOR INFORMATION

Corresponding Authors

*E-mail: luca.detrizio@iit.it.
*E-mail: liberato.manna@iit.it.

ORCID

Javad Shamsi: 0000-0003-4684-5407
Alexander S. Urban: 0000-0001-6168-2509

Muhammad Imran: 0000-0001-7091-6514
Luca De Trizio: 0000-0002-1514-6358
Liberato Manna: 0000-0003-4386-7985

Present Address

[1]J.S. is now working as a research associate (post doc) at the Department of Physics, University of Cambridge.

Notes

The authors declare no competing financial interest.

Biographies

Javad Shamsi received his Ph.D. in Nanochemistry from the Italian Institute of Technology in 2018, where he worked on colloidal synthesis of lead halide perovskite nanocrystals for optoelectronic applications under the supervision of Prof. Liberato Manna. He is now continuing as a postdoc to pursue his passion for the fundamental research in quantum-confined perovskite nanocrystals at the Department of Physics, University of Cambridge.

Alexander S. Urban studied Physics at the University of Karlsruhe (Germany) obtaining an equivalent to a M.Sc. degree (German: Dipl. Phys.) at the University of Karlsruhe (Germany) in 2006. During his studies he spent a year at Heriot Watt University (UK), where he obtained an M.Phys. in Optoelectronics and Lasers in 2005. He then joined the Photonics and Optoelectronics Chair of Jochen Feldmann at the Ludwig-Maximilians-University (LMU) Munich (Germany) in 2007, where he worked on the optothermal manipulation of plasmonic nanoparticles, earning his Ph.D. summa cum laude in 2010. He expanded his expertise in the fields of plasmonics and nanophotonics in the group of Naomi J. Halas at the Laboratory for Nanophotonics at Rice University (Houston, TX), beginning in 2011. He returned to the LMU in 2014 to become a junior group leader with Jochen Feldmann, where he led the research thrusts on optical spectroscopy, focusing on hybrid nanomaterials such as halide perovskite nanocrystals and carbon dots. In 2017, he was awarded a prestigious Starting Grant from the European Research Council, and shortly after that, in 2018, he became a Full Professor of Physics (W2) at LMU. Here, he now leads his own research group working on nanospectroscopy in novel hybrid nanomaterials.

Muhammad Imran received his M.S. degree in Energetic Materials Engineering from National University of Science and Technology (NUST), Pakistan, in 2013. He is currently a Ph.D. student under the supervision of Prof. Liberato Manna at the Nanochemistry Department, the Italian Institute of Technology (IIT), Genova. His research focuses on synthesis and post synthesis transformations of colloidal semiconductor nanocrystals.

Luca De Trizio graduated in Materials Science in 2008 from the University of Milano Bicocca and obtained his Ph.D. in Nanostructures and Nanotechnology from the same institution in 2013. During his Ph.D., in 2010−2011, he worked as a collaborator at the Italian Institute of Technology in Genova with Liberato Manna and, in 2012, at the Molecular Foundry at the Lawrence Berkeley National Laboratory with Delia Milliron. From 2013 to now, he has been working as a postdoc researcher at the Nanochemistry Department in the Italian Institute of Technology in Genova under the supervision of Liberato Manna. His research interests include the colloidal synthesis of transparent conductive oxides, plasmonic materials, luminescent semiconductors, electrocatalytic materials, and the study of postsynthetic chemical transformations of nanocrystals.

Liberato Manna received his Ph.D. in Chemistry in 2001 from the University of Bari (Italy) and worked at U.C. Berkeley (USA) as a Visiting Student and subsequently at the Lawrence Berkeley National Laboratory (USA) as a Postdoc until 2003. He was then Scientist at the National Nanotechnology Lab in Lecce (Italy), and he moved to the Istituto Italiano di Tecnologia (IIT), Genova (Italy), in 2009 as Director of the Nanochemistry Department. Since 2010, he has also been a part-time Professor at TU Delft (The Netherlands). Currently, he is also Deputy Director of IIT for the Materials and Nanotechnology programs at IIT. His research interests include the synthesis and assembly of colloidal nanocrystals, the study (including modeling) of structural, chemical, and surface transformations in nanoscale materials, and their applications in energy, photonics, and electronics. He currently teaches theoretical chemistry and electronic structure of solids at the University of Genova.

ABBREVIATIONS

0D	zero-dimensional
1D	one-dimensional
2D	two-dimensional
3D	three-dimensional
AE	anion exchange
APTES	(3-aminopropyl) triethoxysilane
CBM	conduction band minimum
CE	cation exchange
CM	carrier multiplication
DDAB	di-dodecyl dimethyl ammonium bromide
DFT	density-functional theory
DMF	dimethylformamide
DMSO	dimethylsulfoxide
DOS	density of states
DP	double perovskite
EA	ethyl ammonium
EtOH	ethanol
FA	formamidinium
FAX	formamidinium halide (X = Cl, Br, I)
fcc	face-centered cubic
FWHM	full width at half maximum
HI	hot injection
LARP	ligand assisted re-precipitation
LED	light-emitting diode
LHP	lead-based halide perovskite
MA	methylammonium
MAX	methylammonium halide (X = Cl, Br, I)
MEG	multiexciton generation
MHP	metal halide perovskite
MOF	metal-organic framework
MtA	methacrylic acid
NC	nanocrystal
NMF	N-methylformamide
NMR	nuclear magnetic resonance
NPL	nanoplatelet
NR	nanorod
NS	nanosheet
NW	nanowire
OA	oleic acid
ODE	octadecene
OLA	oleylamine
PCI	solvent controlled ionization
PL	photoluminescence
PLQY	photoluminescence quantum yield

PMMA   poly(methyl methacrylate)
POSS   polyhedral oligomeric silsesquioxane
PS   polystyrene
PSCI   polar solvent controlled ionization
PSZ   polysilazane
PVP   poly-vinyl pyrrolidone
QD   quantum dot
RE   rare earth
RT   room temperature
SEM   scanning electron micrococopy
TEM   transmission electron microscopy
TEOS   tetraethoxysilane
THF   tetrahydrofuran
TOA   tetraoctylammonium
TPA   two-photon absorption
TOP   tri-n-octylphosphine
UV   ultraviolet
VBM   valence band maximum
XRD   X-ray diffraction

REFERENCES

(1) Wells, H. L. Über die Cäsium- und Kalium-Bleihalogenide. *Z. Anorg. Chemie* **1893**, *3*, 195−210.

(2) Kojima, A.; Teshima, K.; Shirai, Y.; Miyasaka, T. Organometal Halide Perovskites as Visible-Light Sensitizers for Photovoltaic Cells. *J. Am. Chem. Soc.* **2009**, *131*, 6050−6051.

(3) Chung, I.; Lee, B.; He, J. Q.; Chang, R. P. H.; Kanatzidis, M. G. All-solid-state dye-sensitized solar cells with high efficiency. *Nature* **2012**, *485*, 486−489.

(4) Kim, H. S.; Lee, C. R.; Im, J. H.; Lee, K. B.; Moehl, T.; Marchioro, A.; Moon, S. J.; Humphry-Baker, R.; Yum, J. H.; Moser, J. E.; et al. Lead Iodide Perovskite Sensitized All-Solid-State Submicron Thin Film Mesoscopic Solar Cell with Efficiency Exceeding 9%. *Sci. Rep.* **2012**, *2*, 591.

(5) Lee, M. M.; Teuscher, J.; Miyasaka, T.; Murakami, T. N.; Snaith, H. J. Efficient Hybrid Solar Cells Based on Meso-Superstructured Organometal Halide Perovskites. *Science* **2012**, *338*, 643−647.

(6) Correa-Baena, J. P.; Saliba, M.; Buonassisi, T.; Gratzel, M.; Abate, A.; Tress, W.; Hagfeldt, A. Promises and challenges of perovskite solar cells. *Science* **2017**, *358*, 739−744.

(7) Park, N.-G. Perovskite solar cells: an emerging photovoltaic technology. *Mater. Today* **2015**, *18*, 65−72.

(8) Petrus, M. L.; Schlipf, J.; Li, C.; Gujar, T. P.; Giesbrecht, N.; Müller-Buschbaum, P.; Thelakkat, M.; Bein, T.; Hüttner, S.; Docampo, P. Capturing the Sun: A Review of the Challenges and Perspectives of Perovskite Solar Cells. *Adv. Energy Mater.* **2017**, *7*, 1700264.

(9) D'Innocenzo, V.; Srimath Kandada, A. R.; De Bastiani, M.; Gandini, M.; Petrozza, A. Tuning the Light Emission Properties by Band Gap Engineering in Hybrid Lead Halide Perovskite. *J. Am. Chem. Soc.* **2014**, *136*, 17730−17733.

(10) Deschler, F.; Price, M.; Pathak, S.; Klintberg, L. E.; Jarausch, D.-D.; Higler, R.; Hüttner, S.; Leijtens, T.; Stranks, S. D.; Snaith, H. J.; et al. High Photoluminescence Efficiency and Optically Pumped Lasing in Solution-Processed Mixed Halide Perovskite Semiconductors. *J. Phys. Chem. Lett.* **2014**, *5*, 1421−1426.

(11) Tan, Z. K.; Moghaddam, R. S.; Lai, M. L.; Docampo, P.; Higler, R.; Deschler, F.; Price, M.; Sadhanala, A.; Pazos, L. M.; Credgington, D.; et al. Bright light-emitting diodes based on organometal halide perovskite. *Nat. Nanotechnol.* **2014**, *9*, 687−692.

(12) Stranks, S. D.; Snaith, H. J. Metal-halide perovskites for photovoltaic and light-emitting devices. *Nat. Nanotechnol.* **2015**, *10*, 391−402.

(13) Yin, W. J.; Shi, T. T.; Yan, Y. F. Unusual defect physics in $CH_3NH_3PbI_3$ perovskite solar cell absorber. *Appl. Phys. Lett.* **2014**, *104*, No. 063903.

(14) deQuilettes, D. W.; Vorpahl, S. M.; Stranks, S. D.; Nagaoka, H.; Eperon, G. E.; Ziffer, M. E.; Snaith, H. J.; Ginger, D. S. Solar cells. Impact of microstructure on local carrier lifetime in perovskite solar cells. *Science* **2015**, *348*, 683−686.

(15) Schmidt, L. C.; Pertegas, A.; Gonzalez-Carrero, S.; Malinkiewicz, O.; Agouram, S.; Espallargas, G. M.; Bolink, H. J.; Galian, R. E.; Perez-Prieto, J. Nontemplate Synthesis of $CH_3NH_3PbBr_3$ Perovskite Nanoparticles. *J. Am. Chem. Soc.* **2014**, *136*, 850−853.

(16) Zhang, D.; Yu, Y.; Bekenstein, Y.; Wong, A. B.; Alivisatos, A. P.; Yang, P. Ultrathin Colloidal Cesium Lead Halide Perovskite Nanowires. *J. Am. Chem. Soc.* **2016**, *138*, 13155−13158.

(17) Sichert, J. A.; Tong, Y.; Mutz, N.; Vollmer, M.; Fischer, S.; Milowska, K. Z.; García Cortadella, R.; Nickel, B.; Cardenas-Daw, C.; Stolarczyk, J. K.; et al. Quantum Size Effect in Organometal Halide Perovskite Nanoplatelets. *Nano Lett.* **2015**, *15*, 6521−6527.

(18) Wong, A. B.; Bekenstein, Y.; Kang, J.; Kley, C. S.; Kim, D.; Gibson, N. A.; Zhang, D.; Yu, Y.; Leone, S. R.; Wang, L. W.; et al. Strongly Quantum Confined Colloidal Cesium Tin Iodide Perovskite Nanoplates: Lessons for Reducing Defect Density and Improving Stability. *Nano Lett.* **2018**, *18*, 2060−2066.

(19) Akkerman, Q. A.; Motti, S. G.; Srimath Kandada, A. R.; Mosconi, E.; D'Innocenzo, V.; Bertoni, G.; Marras, S.; Kamino, B. A.; Miranda, L.; De Angelis, F.; et al. Solution Synthesis Approach to Colloidal Cesium Lead Halide Perovskite Nanoplatelets with Monolayer-Level Thickness Control. *J. Am. Chem. Soc.* **2016**, *138*, 1010−1016.

(20) Akkerman, Q. A.; D'Innocenzo, V.; Accornero, S.; Scarpellini, A.; Petrozza, A.; Prato, M.; Manna, L. Tuning the Optical Properties of Cesium Lead Halide Perovskite Nanocrystals by Anion Exchange Reactions. *J. Am. Chem. Soc.* **2015**, *137*, 10276−10281.

(21) Nedelcu, G.; Protesescu, L.; Yakunin, S.; Bodnarchuk, M. I.; Grotevent, M. J.; Kovalenko, M. V. Fast Anion-Exchange in Highly Luminescent Nanocrystals of Cesium Lead Halide Perovskites ($CsPbX_3$, X = Cl, Br, I). *Nano Lett.* **2015**, *15*, 5635−5640.

(22) Hintermayr, V. A.; Richter, A. F.; Ehrat, F.; Döblinger, M.; Vanderlinden, W.; Sichert, J. A.; Tong, Y.; Polavarapu, L.; Feldmann, J.; Urban, A. S. Tuning the Optical Properties of Perovskite Nanoplatelets through Composition and Thickness by Ligand-Assisted Exfoliation. *Adv. Mater.* **2016**, *28*, 9478−9485.

(23) Tong, Y.; Ehrat, F.; Vanderlinden, W.; Cardenas-Daw, C.; Stolarczyk, J. K.; Polavarapu, L.; Urban, A. S. Dilution-Induced Formation of Hybrid Perovskite Nanoplatelets. *ACS Nano* **2016**, *10*, 10936−10944.

(24) Gonzalez-Carrero, S.; Francés-Soriano, L.; González-Béjar, M.; Agouram, S.; Galian, R. E.; Pérez-Prieto, J. The Luminescence of $CH_3NH_3PbBr_3$ Perovskite Nanoparticles Crests the Summit and Their Photostability under Wet Conditions is Enhanced. *Small* **2016**, *12*, 5245−5250.

(25) Di Stasio, F.; Christodoulou, S.; Huo, N.; Konstantatos, G. Near-Unity Photoluminescence Quantum Yield in $CsPbBr_3$ Nanocrystal Solid-State Films via Postsynthesis Treatment with Lead Bromide. *Chem. Mater.* **2017**, *29*, 7663−7667.

(26) Protesescu, L.; Yakunin, S.; Bodnarchuk, M. I.; Krieg, F.; Caputo, R.; Hendon, C. H.; Yang, R. X.; Walsh, A.; Kovalenko, M. V. Nanocrystals of Cesium Lead Halide Perovskites ($CsPbX_3$, X = Cl, Br, and I): Novel Optoelectronic Materials Showing Bright Emission with Wide Color Gamut. *Nano Lett.* **2015**, *15*, 3692−3696.

(27) Swarnkar, A.; Marshall, A. R.; Sanehira, E. M.; Chernomordik, B. D.; Moore, D. T.; Christians, J. A.; Chakrabarti, T.; Luther, J. M. Quantum dot-induced phase stabilization of alpha-$CsPbI_3$ perovskite for high-efficiency photovoltaics. *Science* **2016**, *354*, 92−95.

(28) Akkerman, Q. A.; Gandini, M.; Di Stasio, F.; Rastogi, P.; Palazon, F.; Bertoni, G.; Ball, J. M.; Prato, M.; Petrozza, A.; Manna, L. Strongly emissive perovskite nanocrystal inks for high-voltage solar cells. *Nat. Energy* **2017**, *2*, 16194.

(29) Li, B.; Zhang, Y.; Fu, L.; Yu, T.; Zhou, S.; Zhang, L.; Yin, L. Surface passivation engineering strategy to fully-inorganic cubic

CsPbI$_3$ perovskites for high-performance solar cells. *Nat. Commun.* **2018**, *9*, 1076.

(30) Zhou, D.; Liu, D.; Pan, G.; Chen, X.; Li, D.; Xu, W.; Bai, X.; Song, H. Cerium and Ytterbium Codoped Halide Perovskite Quantum Dots: A Novel and Efficient Downconverter for Improving the Performance of Silicon Solar Cells. *Adv. Mater.* **2017**, *29*, 1704149.

(31) Meinardi, F.; Akkerman, Q. A.; Bruni, F.; Park, S.; Mauri, M.; Dang, Z.; Manna, L.; Brovelli, S. Doped Halide Perovskite Nanocrystals for Reabsorption-Free Luminescent Solar Concentrators. *ACS Energy Lett.* **2017**, *2*, 2368−2377.

(32) Dursun, I.; Shen, C.; Parida, M. R.; Pan, J.; Sarmah, S. P.; Priante, D.; Alyami, N.; Liu, J.; Saidaminov, M. I.; Alias, M. S.; et al. Perovskite Nanocrystals as a Color Converter for Visible Light Communication. *ACS Photonics* **2016**, *3*, 1150−1156.

(33) Kumar, S.; Jagielski, J.; Yakunin, S.; Rice, P.; Chiu, Y.-C.; Wang, M.; Nedelcu, G.; Kim, Y.; Lin, S.; Santos, E. J. G.; et al. Efficient Blue Electroluminescence Using Quantum-Confined Two-Dimensional Perovskites. *ACS Nano* **2016**, *10*, 9720−9729.

(34) Congreve, D. N.; Weidman, M. C.; Seitz, M.; Paritmongkol, W.; Dahod, N. S.; Tisdale, W. A. Tunable Light-Emitting Diodes Utilizing Quantum-Confined Layered Perovskite Emitters. *ACS Photonics* **2017**, *4*, 476−481.

(35) Zhang, J. R.; Wang, Q.; Zhang, X. S.; Jiang, J. X.; Gao, Z. F.; Jin, Z. W.; Liu, S. Z. High-performance transparent ultraviolet photodetectors based on inorganic perovskite CsPbCl$_3$ nanocrystals. *RSC Adv.* **2017**, *7*, 36722−36727.

(36) Gao, G.; Xi, Q.; Zhou, H.; Zhao, Y.; Wu, C.; Wang, L.; Guo, P.; Xu, J. Novel inorganic perovskite quantum dots for photocatalysis. *Nanoscale* **2017**, *9*, 12032−12038.

(37) Kovalenko, M. V.; Bodnarchuk, M. I. Lead Halide Perovskite Nanocrystals: From Discovery to Self-assembly and Applications. *Chimia* **2017**, *71*, 461−470.

(38) Akkerman, Q. A.; Raino, G.; Kovalenko, M. V.; Manna, L. Genesis, challenges and opportunities for colloidal lead halide perovskite nanocrystals. *Nat. Mater.* **2018**, *17*, 394−405.

(39) Kovalenko, M. V.; Protesescu, L.; Bodnarchuk, M. I. Properties and potential optoelectronic applications of lead halide perovskite nanocrystals. *Science* **2017**, *358*, 745−750.

(40) Egger, D. A.; Bera, A.; Cahen, D.; Hodes, G.; Kirchartz, T.; Kronik, L.; Lovrincic, R.; Rappe, A. M.; Reichman, D. R.; Yaffe, O. What Remains Unexplained about the Properties of Halide Perovskites? *Adv. Mater.* **2018**, *30*, 1800691.

(41) Martiradonna, L. Riddles in perovskite research. *Nat. Mater.* **2018**, *17*, 377−377.

(42) Stranks, S. D.; Plochocka, P. The influence of the Rashba effect. *Nat. Mater.* **2018**, *17*, 381−382.

(43) Imran, M.; Caligiuri, V.; Wang, M.; Goldoni, L.; Prato, M.; Krahne, R.; De Trizio, L.; Manna, L. Benzoyl Halides as Alternative Precursors for the Colloidal Synthesis of Lead-Based Halide Perovskite Nanocrystals. *J. Am. Chem. Soc.* **2018**, *140*, 2656−2664.

(44) Pan, J.; Shang, Y.; Yin, J.; De Bastiani, M.; Peng, W.; Dursun, I.; Sinatra, L.; El-Zohry, A. M.; Hedhili, M. N.; Emwas, A. H.; et al. Bidentate Ligand-Passivated CsPbI$_3$ Perovskite Nanocrystals for Stable Near-Unity Photoluminescence Quantum Yield and Efficient Red Light-Emitting Diodes. *J. Am. Chem. Soc.* **2018**, *140*, 562−565.

(45) Liu, F.; Zhang, Y.; Ding, C.; Kobayashi, S.; Izuishi, T.; Nakazawa, N.; Toyoda, T.; Ohta, T.; Hayase, S.; Minemoto, T.; et al. Highly Luminescent Phase-Stable CsPbI$_3$ Perovskite Quantum Dots Achieving Near 100% Absolute Photoluminescence Quantum Yield. *ACS Nano* **2017**, *11*, 10373−10383.

(46) Polavarapu, L.; Nickel, B.; Feldmann, J.; Urban, A. S. Advances in Quantum-Confined Perovskite Nanocrystals for Optoelectronics. *Adv. Energy Mater.* **2017**, *7*, 1700267.

(47) Wang, H. C.; Bao, Z.; Tsai, H. Y.; Tang, A. C.; Liu, R. S. Perovskite Quantum Dots and Their Application in Light-Emitting Diodes. *Small* **2018**, *14*, 1702433.

(48) Wang, N.; Liu, W.; Zhang, Q. Perovskite-Based Nanocrystals: Synthesis and Applications beyond Solar Cells. *Small Methods* **2018**, *2*, 1700380.

(49) Wang, Y.; Sun, H. All-Inorganic Metal Halide Perovskite Nanostructures: From Photophysics to Light-Emitting Applications. *Small Methods* **2018**, *2*, 1700252.

(50) Weidman, M. C.; Goodman, A. J.; Tisdale, W. A. Colloidal Halide Perovskite Nanoplatelets: An Exciting New Class of Semiconductor Nanomaterials. *Chem. Mater.* **2017**, *29*, 5019−5030.

(51) Shi, E.; Gao, Y.; Finkenauer, B. P.; Akriti; Coffey, A. H.; Dou, L. Two-dimensional halide perovskite nanomaterials and heterostructures. *Chem. Soc. Rev.* **2018**, *47*, 6046−6072.

(52) Sun, J.; Yang, J.; Lee, J. I.; Cho, J. H.; Kang, M. S. Lead-Free Perovskite Nanocrystals for Light-Emitting Devices. *J. Phys. Chem. Lett.* **2018**, *9*, 1573−1583.

(53) Yang, D.; Li, X.; Zeng, H. Surface Chemistry of All Inorganic Halide Perovskite Nanocrystals: Passivation Mechanism and Stability. *Adv. Mater. Interfaces* **2018**, *5*, 1701662.

(54) Zhang, Q.; Yin, Y. All-Inorganic Metal Halide Perovskite Nanocrystals: Opportunities and Challenges. *ACS Cent. Sci.* **2018**, *4*, 668−679.

(55) Rossetti, R.; Nakahara, S.; Brus, L. E. Quantum size effects in the redox potentials, resonance Raman spectra, and electronic spectra of CdS crystallites in aqueous solution. *J. Chem. Phys.* **1983**, *79*, 1086−1088.

(56) Brus, L. Electronic wave functions in semiconductor clusters: experiment and theory. *J. Phys. Chem.* **1986**, *90*, 2555−2560.

(57) Nikl, M.; Nitsch, K.; Polak, K.; Pazzi, G. P.; Fabeni, P.; Citrin, D. S.; Gurioli, M. Optical properties of the Pb^{2+}-based aggregated phase in a CsCl host crystal: Quantum-confinement effects. *Phys. Rev. B: Condens. Matter Mater. Phys.* **1995**, *51*, 5192−5199.

(58) Nikl, M.; Polak, K.; Nitsch, K.; Pazzi, G. P.; Fabeni, P.; Gurioli, M. Optical properties of Pb^{2+}-based aggregated phase in NaCl and CsCl alkali halide hosts. *Radiat. Eff. Defects Solids* **1995**, *135*, 289.

(59) Nikl, M.; Nitsch, K.; Polák, K.; Mihókova, E.; Zazubovich, S.; Pazzi, G. P.; Fabeni, P.; Salvini, L.; Aceves, R.; Barbosa-Flores, M.; et al. Quantum size effect in the excitonic luminescence of CsPbX$_3$-like quantum dots in CsX (X = Cl, Br) single crystal host. *J. Lumin.* **1997**, *72−74*, 377−379.

(60) Im, J. H.; Lee, C. R.; Lee, J. W.; Park, S. W.; Park, N. G. 6.5% efficient perovskite quantum-dot-sensitized solar cell. *Nanoscale* **2011**, *3*, 4088−4093.

(61) He, X.; Qiu, Y.; Yang, S. Fully-Inorganic Trihalide Perovskite Nanocrystals: A New Research Frontier of Optoelectronic Materials. *Adv. Mater.* **2017**, *29*, 1700775.

(62) Zhao, Y.; Zhu, K. Organic-inorganic hybrid lead halide perovskites for optoelectronic and electronic applications. *Chem. Soc. Rev.* **2016**, *45*, 655−689.

(63) Manser, J. S.; Christians, J. A.; Kamat, P. V. Intriguing Optoelectronic Properties of Metal Halide Perovskites. *Chem. Rev.* **2016**, *116*, 12956−13008.

(64) Li, W.; Wang, Z.; Deschler, F.; Gao, S.; Friend, R. H.; Cheetham, A. K. Chemically diverse and multifunctional hybrid organic−inorganic perovskites. *Nat. Rev. Mater.* **2017**, *2*, 16099.

(65) Correa-Baena, J.-P.; Saliba, M.; Buonassisi, T.; Grätzel, M.; Abate, A.; Tress, W.; Hagfeldt, A. Promises and challenges of perovskite solar cells. *Science* **2017**, *358*, 739−744.

(66) Travis, W.; Glover, E. N. K.; Bronstein, H.; Scanlon, D. O.; Palgrave, R. G. On the application of the tolerance factor to inorganic and hybrid halide perovskites: a revised system. *Chem. Sci.* **2016**, *7*, 4548−4556.

(67) Protesescu, L.; Yakunin, S.; Kumar, S.; Bar, J.; Bertolotti, F.; Masciocchi, N.; Guagliardi, A.; Grotevent, M.; Shorubalko, I.; Bodnarchuk, M. I.; et al. Dismantling the ″Red Wall″ of Colloidal Perovskites: Highly Luminescent Formamidinium and Formamidinium-Cesium Lead Iodide Nanocrystals. *ACS Nano* **2017**, *11*, 3119−3134.

(68) Bartel, C. J.; Sutton, C.; Goldsmith, B. R.; Ouyang, R.; Musgrave, C. B.; Ghiringhelli, L. M.; Scheffler, M. New Tolerance

Factor to Predict the Stability of Perovskite Oxides and Halides. *arXiv* **2018**, arXiv:1801.07700.

(69) Snaith, H. J. Present status and future prospects of perovskite photovoltaics. *Nat. Mater.* **2018**, *17*, 372−376.

(70) Akkerman, Q. A.; Abdelhady, A. L.; Manna, L. Zero-Dimensional Cesium Lead Halides: History, Properties, and Challenges. *J. Phys. Chem. Lett.* **2018**, *9*, 2326−2337.

(71) Iyikanat, F.; Sari, E.; Sahin, H. Thinning CsPb$_2$Br$_5$ perovskite down to monolayers: Cs-dependent stability. *Phys. Rev. B: Condens. Matter Mater. Phys.* **2017**, *96*, 155442.

(72) Dou, L.; Wong, A. B.; Yu, Y.; Lai, M.; Kornienko, N.; Eaton, S. W.; Fu, A.; Bischak, C. G.; Ma, J.; Ding, T.; et al. Atomically thin two-dimensional organic-inorganic hybrid perovskites. *Science* **2015**, *349*, 1518−1521.

(73) Fu, Y.; Zhu, H.; Stoumpos, C. C.; Ding, Q.; Wang, J.; Kanatzidis, M. G.; Zhu, X.; Jin, S. Broad Wavelength Tunable Robust Lasing from Single-Crystal Nanowires of Cesium Lead Halide Perovskites (CsPbX$_3$, X = Cl, Br, I). *ACS Nano* **2016**, *10*, 7963−7972.

(74) Ono, L. K.; Juarez-Perez, E. J.; Qi, Y. Progress on Perovskite Materials and Solar Cells with Mixed Cations and Halide Anions. *ACS Appl. Mater. Interfaces* **2017**, *9*, 30197−30246.

(75) Dolzhnikov, D. S.; Wang, C.; Xu, Y.; Kanatzidis, M. G.; Weiss, E. A. Ligand-Free, Quantum-Confined Cs$_2$SnI$_6$ Perovskite Nanocrystals. *Chem. Mater.* **2017**, *29*, 7901−7907.

(76) Zhang, J.; Yang, Y.; Deng, H.; Farooq, U.; Yang, X.; Khan, J.; Tang, J.; Song, H. High Quantum Yield Blue Emission from Lead-Free Inorganic Antimony Halide Perovskite Colloidal Quantum Dots. *ACS Nano* **2017**, *11*, 9294−9302.

(77) Park, B.-W.; Philippe, B.; Zhang, X.; Rensmo, H.; Boschloo, G.; Johansson, E. M. J. Bismuth Based Hybrid Perovskites A$_3$Bi$_2$I$_9$ (A: Methylammonium or Cesium) for Solar Cell Application. *Adv. Mater.* **2015**, *27*, 6806−6813.

(78) Jellicoe, T. C.; Richter, J. M.; Glass, H. F. J.; Tabachnyk, M.; Brady, R.; Dutton, S. E.; Rao, A.; Friend, R. H.; Credgington, D.; Greenham, N. C.; et al. Synthesis and Optical Properties of Lead-Free Cesium Tin Halide Perovskite Nanocrystals. *J. Am. Chem. Soc.* **2016**, *138*, 2941−2944.

(79) Zhao, X. G.; Yang, J. H.; Fu, Y.; Yang, D.; Xu, Q.; Yu, L.; Wei, S. H.; Zhang, L. Design of Lead-Free Inorganic Halide Perovskites for Solar Cells via Cation-Transmutation. *J. Am. Chem. Soc.* **2017**, *139*, 2630−2638.

(80) Leng, M. Y.; Yang, Y.; Zeng, K.; Chen, Z. W.; Tan, Z. F.; Li, S. R.; Li, J. H.; Xu, B.; Li, D. B.; Hautzinger, M. P.; et al. All-Inorganic Bismuth-Based Perovskite Quantum Dots with Bright Blue Photoluminescence and Excellent Stability. *Adv. Funct. Mater.* **2018**, *28*, 1704446.

(81) Wei, F.; Brivio, F.; Wu, Y.; Sun, S.; Bristowe, P. D.; Cheetham, A. K. Synthesis, crystal structure, magnetic and electronic properties of the caesium-based transition metal halide Cs$_3$Fe$_2$Br$_9$. *J. Mater. Chem. C* **2018**, *6*, 3573−3577.

(82) Zhang, Y.; Yin, J.; Parida, M. R.; Ahmed, G. H.; Pan, J.; Bakr, O. M.; Bredas, J. L.; Mohammed, O. F. Direct-Indirect Nature of the Bandgap in Lead-Free Perovskite Nanocrystals. *J. Phys. Chem. Lett.* **2017**, *8*, 3173−3177.

(83) Yang, B.; Chen, J.; Hong, F.; Mao, X.; Zheng, K.; Yang, S.; Li, Y.; Pullerits, T.; Deng, W.; Han, K. Lead-Free, Air-Stable All-Inorganic Cesium Bismuth Halide Perovskite Nanocrystals. *Angew. Chem., Int. Ed.* **2017**, *56*, 12471−12475.

(84) Hu, Y. Q.; Zhang, S. F.; Miao, X. L.; Su, L. S.; Bai, F.; Qiu, T.; Liu, J. Z.; Yuan, G. L. Ultrathin Cs$_3$Bi$_2$I$_9$ Nanosheets as an Electronic Memory Material for Flexible Memristors. *Adv. Mater. Interfaces* **2017**, *4*, 1700131.

(85) Protesescu, L.; Yakunin, S.; Nazarenko, O.; Dirin, D. N.; Kovalenko, M. V. Low-Cost Synthesis of Highly Luminescent Colloidal Lead Halide Perovskite Nanocrystals by Wet Ball Milling. *ACS Appl. Nano Mater.* **2018**, *1*, 1300−1308.

(86) de Weerd, C.; Gregorkiewicz, T.; Gomez, L. All-Inorganic Perovskite Nanocrystals: Microscopy Insights in Structure and Optical Properties. *Adv. Opt. Mater.* **2018**, *6*, 1800289.

(87) Yang, C.; Wu, Y.; Ma, Q.; Zhang, W.-H. Nanocrystals of halide perovskite: Synthesis, properties, and applications. *J. Energy Chem.* **2018**, *27*, 622−636.

(88) Kovalenko, M. V.; Manna, L.; Cabot, A.; Hens, Z.; Talapin, D. V.; Kagan, C. R.; Klimov, V. I.; Rogach, A. L.; Reiss, P.; Milliron, D. J.; et al. Prospects of Nanoscience with Nanocrystals. *ACS Nano* **2015**, *9*, 1012−1057.

(89) Li, X.; Cao, F.; Yu, D.; Chen, J.; Sun, Z.; Shen, Y.; Zhu, Y.; Wang, L.; Wei, Y.; Wu, Y.; et al. All Inorganic Halide Perovskites Nanosystem: Synthesis, Structural Features Optical Properties and Optoelectronic Applications. *Small* **2017**, *13*, 1603996.

(90) Murray, C. B.; Norris, D. J.; Bawendi, M. G. Synthesis and characterization of nearly monodisperse CdE (E = sulfur, selenium, tellurium) semiconductor nanocrystallites. *J. Am. Chem. Soc.* **1993**, *115*, 8706−8715.

(91) Yu, W. W.; Peng, X. Formation of High-Quality CdS and Other II−VI Semiconductor Nanocrystals in Noncoordinating Solvents: Tunable Reactivity of Monomers. *Angew. Chem., Int. Ed.* **2002**, *41*, 2368−2371.

(92) Bullen, C. R.; Mulvaney, P. Nucleation and Growth Kinetics of CdSe Nanocrystals in Octadecene. *Nano Lett.* **2004**, *4*, 2303−2307.

(93) Deka, S.; Genovese, A.; Zhang, Y.; Miszta, K.; Bertoni, G.; Krahne, R.; Giannini, C.; Manna, L. Phosphine-Free Synthesis of p-Type Copper(I) Selenide Nanocrystals in Hot Coordinating Solvents. *J. Am. Chem. Soc.* **2010**, *132*, 8912−8914.

(94) Li, X.; Zhang, K.; Li, J.; Chen, J.; Wu, Y.; Liu, K.; Song, J.; Zeng, H. Heterogeneous Nucleation toward Polar-Solvent-Free, Fast, and One-Pot Synthesis of Highly Uniform Perovskite Quantum Dots for Wider Color Gamut Display. *Adv. Mater. Interfaces* **2018**, *5*, 1800010.

(95) Manna, L.; Milliron, D. J.; Meisel, A.; Scher, E. C.; Alivisatos, A. P. Controlled growth of tetrapod-branched inorganic nanocrystals. *Nat. Mater.* **2003**, *2*, 382−385.

(96) Vybornyi, O.; Yakunin, S.; Kovalenko, M. V. Polar-solvent-free colloidal synthesis of highly luminescent alkylammonium lead halide perovskite nanocrystals. *Nanoscale* **2016**, *8*, 6278−6283.

(97) Akkerman, Q. A.; Park, S.; Radicchi, E.; Nunzi, F.; Mosconi, E.; De Angelis, F.; Brescia, R.; Rastogi, P.; Prato, M.; Manna, L. Nearly Monodisperse Insulator Cs$_4$PbX$_6$ (X = Cl, Br, I) Nanocrystals, Their Mixed Halide Compositions, and Their Transformation into CsPbX3 Nanocrystals. *Nano Lett.* **2017**, *17*, 1924−1930.

(98) Han, C.; Li, C.; Zang, Z.; Wang, M.; Sun, K.; Tang, X.; Du, J. Tunable luminescent CsPb$_2$Br$_5$ nanoplatelets: applications in light-emitting diodes and photodetectors. *Photonics Res.* **2017**, *5*, 473.

(99) Lignos, I.; Stavrakis, S.; Nedelcu, G.; Protesescu, L.; deMello, A. J.; Kovalenko, M. V. Synthesis of Cesium Lead Halide Perovskite Nanocrystals in a Droplet-Based Microfluidic Platform: Fast Parametric Space Mapping. *Nano Lett.* **2016**, *16*, 1869−1877.

(100) Maceiczyk, R. M.; Dümbgen, K.; Lignos, I.; Protesescu, L.; Kovalenko, M. V.; deMello, A. J. Microfluidic Reactors Provide Preparative and Mechanistic Insights into the Synthesis of Formamidinium Lead Halide Perovskite Nanocrystals. *Chem. Mater.* **2017**, *29*, 8433−8439.

(101) Koolyk, M.; Amgar, D.; Aharon, S.; Etgar, L. Kinetics of cesium lead halide perovskite nanoparticle growth; focusing and de-focusing of size distribution. *Nanoscale* **2016**, *8*, 6403−6409.

(102) Udayabhaskararao, T.; Kazes, M.; Houben, L.; Lin, H.; Oron, D. Nucleation, Growth, and Structural Transformations of Perovskite Nanocrystals. *Chem. Mater.* **2017**, *29*, 1302−1308.

(103) Dang, Z.; Shamsi, J.; Palazon, F.; Imran, M.; Akkerman, Q. A.; Park, S.; Bertoni, G.; Prato, M.; Brescia, R.; Manna, L. In Situ Transmission Electron Microscopy Study of Electron Beam-Induced Transformations in Colloidal Cesium Lead Halide Perovskite Nanocrystals. *ACS Nano* **2017**, *11*, 2124−2132.

(104) Dang, Z.; Shamsi, J.; Akkerman, Q. A.; Imran, M.; Bertoni, G.; Brescia, R.; Manna, L. Low-Temperature Electron Beam-Induced Transformations of Cesium Lead Halide Perovskite Nanocrystals. *ACS Omega* **2017**, *2*, 5660−5665.

(105) Almeida, G.; Goldoni, L.; Akkerman, Q.; Dang, Z.; Khan, A. H.; Marras, S.; Moreels, I.; Manna, L. Role of Acid-Base Equilibria in the Size, Shape, and Phase Control of Cesium Lead Bromide Nanocrystals. *ACS Nano* **2018**, *12*, 1704−1711.

(106) Dong, Y.; Qiao, T.; Kim, D.; Parobek, D.; Rossi, D.; Son, D. H. Precise Control of Quantum Confinement in Cesium Lead Halide Perovskite Quantum Dots via Thermodynamic Equilibrium. *Nano Lett.* **2018**, *18*, 3716−3722.

(107) Yuan, L.; Patterson, R.; Wen, X.; Zhang, Z.; Conibeer, G.; Huang, S. Investigation of anti-solvent induced optical properties change of cesium lead bromide iodide mixed perovskite (CsPbBr$_{3-x}$I$_x$) quantum dots. *J. Colloid Interface Sci.* **2017**, *504*, 586−592.

(108) Woo, J. Y.; Kim, Y.; Bae, J.; Kim, T. G.; Kim, J. W.; Lee, D. C.; Jeong, S. Highly Stable Cesium Lead Halide Perovskite Nanocrystals through in Situ Lead Halide Inorganic Passivation. *Chem. Mater.* **2017**, *29*, 7088−7092.

(109) Su, Y.; Chen, X.; Ji, W.; Zeng, Q.; Ren, Z.; Su, Z.; Liu, L. Highly Controllable and Efficient Synthesis of Mixed-Halide CsPbX$_3$ (X = Cl, Br, I) Perovskite QDs toward the Tunability of Entire Visible Light. *ACS Appl. Mater. Interfaces* **2017**, *9*, 33020−33028.

(110) Liu, P.; Chen, W.; Wang, W.; Xu, B.; Wu, D.; Hao, J.; Cao, W.; Fang, F.; Li, Y.; Zeng, Y.; et al. Halide-Rich Synthesized Cesium Lead Bromide Perovskite Nanocrystals for Light-Emitting Diodes with Improved Performance. *Chem. Mater.* **2017**, *29*, 5168−5173.

(111) Yassitepe, E.; Yang, Z.; Voznyy, O.; Kim, Y.; Walters, G.; Castañeda, J. A.; Kanjanaboos, P.; Yuan, M.; Gong, X.; Fan, F.; et al. Amine-Free Synthesis of Cesium Lead Halide Perovskite Quantum Dots for Efficient Light-Emitting Diodes. *Adv. Funct. Mater.* **2016**, *26*, 8757−8763.

(112) Protesescu, L.; Yakunin, S.; Bodnarchuk, M. I.; Bertolotti, F.; Masciocchi, N.; Guagliardi, A.; Kovalenko, M. V. Monodisperse Formamidinium Lead Bromide Nanocrystals with Bright and Stable Green Photoluminescence. *J. Am. Chem. Soc.* **2016**, *138*, 14202−14205.

(113) Lignos, I.; Protesescu, L.; Emiroglu, D. B.; Maceiczyk, R.; Schneider, S.; Kovalenko, M. V.; deMello, A. J. Unveiling the Shape Evolution and Halide-Ion-Segregation in Blue-Emitting Formamidinium Lead Halide Perovskite Nanocrystals Using an Automated Microfluidic Platform. *Nano Lett.* **2018**, *18*, 1246−1252.

(114) Li, Q.; Li, H.; Shen, H.; Wang, F.; Zhao, F.; Li, F.; Zhang, X.; Li, D.; Jin, X.; Sun, W. Solid Ligand-Assisted Storage of Air-Stable Formamidinium Lead Halide Quantum Dots via Restraining the Highly Dynamic Surface toward Brightly Luminescent Light-Emitting Diodes. *ACS Photonics* **2017**, *4*, 2504−2512.

(115) Creutz, S. E.; Crites, E. N.; De Siena, M. C.; Gamelin, D. R. Colloidal Nanocrystals of Lead-Free Double-Perovskite (Elpasolite) Semiconductors: Synthesis and Anion Exchange To Access New Materials. *Nano Lett.* **2018**, *18*, 1118−1123.

(116) Kim, Y.; Yassitepe, E.; Voznyy, O.; Comin, R.; Walters, G.; Gong, X.; Kanjanaboos, P.; Nogueira, A. F.; Sargent, E. H. Efficient Luminescence from Perovskite Quantum Dot Solids. *ACS Appl. Mater. Interfaces* **2015**, *7*, 25007−25013.

(117) Tong, Y.; Bladt, E.; Ayguler, M. F.; Manzi, A.; Milowska, K. Z.; Hintermayr, V. A.; Docampo, P.; Bals, S.; Urban, A. S.; Polavarapu, L.; et al. Highly Luminescent Cesium Lead Halide Perovskite Nanocrystals with Tunable Composition and Thickness by Ultrasonication. *Angew. Chem., Int. Ed.* **2016**, *55*, 13887−13892.

(118) Bekenstein, Y.; Koscher, B. A.; Eaton, S. W.; Yang, P.; Alivisatos, A. P. Highly Luminescent Colloidal Nanoplates of Perovskite Cesium Lead Halide and Their Oriented Assemblies. *J. Am. Chem. Soc.* **2015**, *137*, 16008−16011.

(119) Zhang, D.; Eaton, S. W.; Yu, Y.; Dou, L.; Yang, P. Solution-Phase Synthesis of Cesium Lead Halide Perovskite Nanowires. *J. Am. Chem. Soc.* **2015**, *137*, 9230−9233.

(120) Pan, A.; He, B.; Fan, X.; Liu, Z.; Urban, J. J.; Alivisatos, A. P.; He, L.; Liu, Y. Insight into the Ligand-Mediated Synthesis of Colloidal CsPbBr$_3$ Perovskite Nanocrystals: The Role of Organic Acid, Base, and Cesium Precursors. *ACS Nano* **2016**, *10*, 7943−7954.

(121) Song, J.; Xu, L.; Li, J.; Xue, J.; Dong, Y.; Li, X.; Zeng, H. Monolayer and Few-Layer All-Inorganic Perovskites as a New Family of Two-Dimensional Semiconductors for Printable Optoelectronic Devices. *Adv. Mater.* **2016**, *28*, 4861−4869.

(122) Shamsi, J.; Dang, Z.; Bianchini, P.; Canale, C.; Di Stasio, F.; Brescia, R.; Prato, M.; Manna, L. Colloidal Synthesis of Quantum Confined Single Crystal CsPbBr$_3$ Nanosheets with Lateral Size Control up to the Micrometer Range. *J. Am. Chem. Soc.* **2016**, *138*, 7240−7243.

(123) Imran, M.; Di Stasio, F.; Dang, Z.; Canale, C.; Khan, A. H.; Shamsi, J.; Brescia, R.; Prato, M.; Manna, L. Colloidal Synthesis of Strongly Fluorescent CsPbBr$_3$ Nanowires with Width Tunable down to the Quantum Confinement Regime. *Chem. Mater.* **2016**, *28*, 6450−6454.

(124) Zhang, D.; Yang, Y.; Bekenstein, Y.; Yu, Y.; Gibson, N. A.; Wong, A. B.; Eaton, S. W.; Kornienko, N.; Kong, Q.; Lai, M.; et al. Synthesis of Composition Tunable and Highly Luminescent Cesium Lead Halide Nanowires through Anion-Exchange Reactions. *J. Am. Chem. Soc.* **2016**, *138*, 7236−7239.

(125) Dutta, A.; Dutta, S. K.; Das Adhikari, S.; Pradhan, N. Tuning the Size of CsPbBr$_3$ Nanocrystals: All at One Constant Temperature. *ACS Energy Lett.* **2018**, *3*, 329−334.

(126) Chen, M.; Zou, Y. T.; Wu, L. Z.; Pan, Q.; Yang, D.; Hu, H. C.; Tan, Y. S.; Zhong, Q. X.; Xu, Y.; Liu, H. Y.; et al. Solvothermal Synthesis of High-Quality All-Inorganic Cesium Lead Halide Perovskite Nanocrystals: From Nanocube to Ultrathin Nanowire. *Adv. Funct. Mater.* **2017**, *27*, 1701121.

(127) Tong, Y.; Bohn, B. J.; Bladt, E.; Wang, K.; Muller-Buschbaum, P.; Bals, S.; Urban, A. S.; Polavarapu, L.; Feldmann, J. From Precursor Powders to CsPbX$_3$ Perovskite Nanowires: One-Pot Synthesis, Growth Mechanism, and Oriented Self-Assembly. *Angew. Chem., Int. Ed.* **2017**, *56*, 13887−13892.

(128) Tang, X.; Zu, Z.; Shao, H.; Hu, W.; Zhou, M.; Deng, M.; Chen, W.; Zang, Z.; Zhu, T.; Xue, J. All-inorganic perovskite CsPb(Br/I)$_3$ nanorods for optoelectronic application. *Nanoscale* **2016**, *8*, 15158−15161.

(129) Pan, Q.; Hu, H.; Zou, Y.; Chen, M.; Wu, L.; Yang, D.; Yuan, X.; Fan, J.; Sun, B.; Zhang, Q. Microwave-assisted synthesis of high-quality "all-inorganic" CsPbX$_3$ (X = Cl, Br, I) perovskite nanocrystals and their application in light emitting diodes. *J. Mater. Chem. C* **2017**, *5*, 10947−10954.

(130) Shamsi, J.; Rastogi, P.; Caligiuri, V.; Abdelhady, A. L.; Spirito, D.; Manna, L.; Krahne, R. Bright-Emitting Perovskite Films by Large-Scale Synthesis and Photoinduced Solid-State Transformation of CsPbBr$_3$ Nanoplatelets. *ACS Nano* **2017**, *11*, 10206−10213.

(131) Liu, W.; Zheng, J.; Cao, S.; Wang, L.; Gao, F.; Chou, K. C.; Hou, X.; Yang, W. General Strategy for Rapid Production of Low-Dimensional All-Inorganic CsPbBr$_3$ Perovskite Nanocrystals with Controlled Dimensionalities and Sizes. *Inorg. Chem.* **2018**, *57*, 1598−1603.

(132) Liu, H.; Wu, Z.; Gao, H.; Shao, J.; Zou, H.; Yao, D.; Liu, Y.; Zhang, H.; Yang, B. One-Step Preparation of Cesium Lead Halide CsPbX$_3$ (X = Cl, Br, and I) Perovskite Nanocrystals by Microwave Irradiation. *ACS Appl. Mater. Interfaces* **2017**, *9*, 42919−42927.

(133) Long, Z.; Ren, H.; Sun, J.; Ouyang, J.; Na, N. High-throughput and tunable synthesis of colloidal CsPbX$_3$ perovskite nanocrystals in a heterogeneous system by microwave irradiation. *Chem. Commun.* **2017**, *53*, 9914−9917.

(134) Jang, D. M.; Kim, D. H.; Park, K.; Park, J.; Lee, J. W.; Song, J. K. Ultrasound synthesis of lead halide perovskite nanocrystals. *J. Mater. Chem. C* **2016**, *4*, 10625−10629.

(135) Yang, D.; Zou, Y. T.; Li, P. L.; Liu, Q. P.; Wu, L. Z.; Hu, H. C.; Xu, Y.; Sun, B. Q.; Zhang, Q.; Lee, S. T. Large-scale synthesis of ultrathin cesium lead bromide perovskite nanoplates with precisely tunable dimensions and their application in blue light-emitting diodes. *Nano Energy* **2018**, *47*, 235−242.

(136) Zhai, W.; Lin, J.; Li, Q.; Zheng, K.; Huang, Y.; Yao, Y.; He, X.; Li, L.; Yu, C.; Liu, C.; et al. Solvothermal Synthesis of Ultrathin Cesium Lead Halide Perovskite Nanoplatelets with Tunable Lateral

Sizes and Their Reversible Transformation into Cs_4PbBr_6 Nanocrystals. *Chem. Mater.* **2018**, *30*, 3714−3721.

(137) Krieg, F.; Ochsenbein, S. T.; Yakunin, S.; Ten Brinck, S.; Aellen, P.; Süess, A.; Clerc, B.; Guggisberg, D.; Nazarenko, O.; Shynkarenko, Y.; et al. Colloidal $CsPbX_3$ (X = Cl, Br, I) Nanocrystals 2.0: Zwitterionic Capping Ligands for Improved Durability and Stability. *ACS Energy Lett.* **2018**, *3*, 641−646.

(138) Amgar, D.; Binyamin, T.; Uvarov, V.; Etgar, L. Near ultraviolet to mid-visible band gap tuning of mixed cation $Rb_xCs_{1-x}PbX_3$ (X = Cl or Br) perovskite nanoparticles. *Nanoscale* **2018**, *10*, 6060−6068.

(139) Wu, H.; Yang, Y.; Zhou, D.; Li, K.; Yu, J.; Han, J.; Li, Z.; Long, Z.; Ma, J.; Qiu, J. Rb^+ cations enable the change of luminescence properties in perovskite $(Rb_xCs_{1-x}PbBr_3)$ quantum dots. *Nanoscale* **2018**, *10*, 3429−3437.

(140) Wang, H. C.; Wang, W.; Tang, A. C.; Tsai, H. Y.; Bao, Z.; Ihara, T.; Yarita, N.; Tahara, H.; Kanemitsu, Y.; Chen, S.; et al. High-Performance $CsPb_{1-x}Sn_xBr_3$ Perovskite Quantum Dots for Light-Emitting Diodes. *Angew. Chem., Int. Ed.* **2017**, *56*, 13650−13654.

(141) Wang, C. Y.; Zhang, Y. K.; Wang, A. F.; Wang, Q.; Tang, H. Y.; Shen, W.; Li, Z.; Deng, Z. T. Controlled Synthesis of Composition Tunable Formamidinium Cesium Double Cation Lead Halide Perovskite Nanowires and Nanosheets with Improved Stability. *Chem. Mater.* **2017**, *29*, 2157−2166.

(142) Vashishtha, P.; Metin, D. Z.; Cryer, M. E.; Chen, K.; Hodgkiss, J. M.; Gaston, N.; Halpert, J. E. Shape-, Size-, and Composition-Controlled Thallium Lead Halide Perovskite Nanowires and Nanocrystals with Tunable Band Gaps. *Chem. Mater.* **2018**, *30*, 2973−2982.

(143) Pan, G.; Bai, X.; Yang, D.; Chen, X.; Jing, P.; Qu, S.; Zhang, L.; Zhou, D.; Zhu, J.; Xu, W.; et al. Doping Lanthanide into Perovskite Nanocrystals: Highly Improved and Expanded Optical Properties. *Nano Lett.* **2017**, *17*, 8005−8011.

(144) Hu, Q.; Li, Z.; Tan, Z.; Song, H.; Ge, C.; Niu, G.; Han, J.; Tang, J. Rare Earth Ion-Doped $CsPbBr_3$ Nanocrystals. *Adv. Opt. Mater.* **2018**, *6*, 1700864.

(145) Biswas, A.; Bakthavatsalam, R.; Kundu, J. Efficient Exciton to Dopant Energy Transfer in Mn^{2+}-Doped $(C_4H_9NH_3)_2PbBr_4$ Two-Dimensional (2D) Layered Perovskites. *Chem. Mater.* **2017**, *29*, 7816−7825.

(146) Wang, P.; Dong, B.; Cui, Z.; Gao, R.; Su, G.; Wang, W.; Cao, L. Synthesis and characterization of Mn-doped $CsPb(Cl/Br)_3$ perovskite nanocrystals with controllable dual-color emission. *RSC Adv.* **2018**, *8*, 1940−1947.

(147) Shao, H.; Bai, X.; Cui, H.; Pan, G.; Jing, P.; Qu, S.; Zhu, J.; Zhai, Y.; Dong, B.; Song, H. White light emission in Bi^{3+}/Mn^{2+} ion co-doped $CsPbCl_3$ perovskite nanocrystals. *Nanoscale* **2018**, *10*, 1023−1029.

(148) Xu, K.; Lin, C. C.; Xie, X.; Meijerink, A. Efficient and Stable Luminescence from Mn^{2+} in Core and Core-Isocrystalline Shell $CsPbCl_3$ Perovskite Nanocrystals. *Chem. Mater.* **2017**, *29*, 4265−4272.

(149) Liu, W.; Lin, Q.; Li, H.; Wu, K.; Robel, I.; Pietryga, J. M.; Klimov, V. I. Mn^{2+}-Doped Lead Halide Perovskite Nanocrystals with Dual-Color Emission Controlled by Halide Content. *J. Am. Chem. Soc.* **2016**, *138*, 14954−14961.

(150) Parobek, D.; Roman, B. J.; Dong, Y.; Jin, H.; Lee, E.; Sheldon, M.; Son, D. H. Exciton-to-Dopant Energy Transfer in Mn-Doped Cesium Lead Halide Perovskite Nanocrystals. *Nano Lett.* **2016**, *16*, 7376−7380.

(151) Das Adhikari, S.; Dutta, S. K.; Dutta, A.; Guria, A. K.; Pradhan, N. Chemically Tailoring the Dopant Emission in Manganese-Doped $CsPbCl_3$ Perovskite Nanocrystals. *Angew. Chem., Int. Ed.* **2017**, *56*, 8746−8750.

(152) Parobek, D.; Dong, Y. T.; Qiao, T.; Son, D. H. Direct Hot-Injection Synthesis of Mn-Doped $CsPbBr_3$ Nanocrystals. *Chem. Mater.* **2018**, *30*, 2939−2944.

(153) Zou, S.; Liu, Y.; Li, J.; Liu, C.; Feng, R.; Jiang, F.; Li, Y.; Song, J.; Zeng, H.; Hong, M.; et al. Stabilizing Cesium Lead Halide

Perovskite Lattice through Mn(II) Substitution for Air-Stable Light-Emitting Diodes. *J. Am. Chem. Soc.* **2017**, *139*, 11443−11450.

(154) Akkerman, Q. A.; Meggiolaro, D.; Dang, Z.; De Angelis, F.; Manna, L. Fluorescent Alloy $CsPb_xMn_{1-x}I_3$ Perovskite Nanocrystals with High Structural and Optical Stability. *ACS Energy Lett.* **2017**, *2*, 2183−2186.

(155) Yao, J.; Ge, J.; Han, B. N.; Wang, K. H.; Yao, H. B.; Yu, H. L.; Li, J. H.; Zhu, B. S.; Song, J.; Chen, C.; et al. Ce^{3+}-Doping to Modulate Photoluminescence Kinetics for Efficient $CsPbBr_3$ Nanocrystals Based Light-Emitting Diodes. *J. Am. Chem. Soc.* **2018**, *140*, 3626−3634.

(156) Begum, R.; Parida, M. R.; Abdelhady, A. L.; Murali, B.; Alyami, N. M.; Ahmed, G. H.; Hedhili, M. N.; Bakr, O. M.; Mohammed, O. F. Engineering Interfacial Charge Transfer in $CsPbBr_3$ Perovskite Nanocrystals by Heterovalent Doping. *J. Am. Chem. Soc.* **2017**, *139*, 731−737.

(157) Milstein, T. J.; Kroupa, D. M.; Gamelin, D. R. Picosecond Quantum Cutting Generates Photoluminescence Quantum Yields Over 100% in Ytterbium-Doped $CsPbCl_3$ Nanocrystals. *Nano Lett.* **2018**, *18*, 3792−3799.

(158) Wang, A. F.; Guo, Y. Y.; Muhammad, F.; Deng, Z. T. Controlled Synthesis of Lead-Free Cesium Tin Halide Perovskite Cubic Nanocages with High Stability. *Chem. Mater.* **2017**, *29*, 6493−6501.

(159) Wu, X.; Song, W.; Li, Q.; Zhao, X.; He, D.; Quan, Z. Synthesis of Lead-free $CsGeI_3$ Perovskite Colloidal Nanocrystals and Electron Beam-induced Transformations. *Chem. - Asian J.* **2018**, *13*, 1654−1659.

(160) Pal, J.; Manna, S.; Mondal, A.; Das, S.; Adarsh, K. V.; Nag, A. Colloidal Synthesis and Photophysics of $M_3Sb_2I_9$ (M = Cs and Rb) Nanocrystals: Lead-Free Perovskites. *Angew. Chem., Int. Ed.* **2017**, *56*, 14187−14191.

(161) Pal, J.; Bhunia, A.; Chakraborty, S.; Manna, S.; Das, S.; Dewan, A.; Datta, S.; Nag, A. Synthesis and Optical Properties of Colloidal $M_3Bi_2I_9$ (M = Cs, Rb) Perovskite Nanocrystals. *J. Phys. Chem. C* **2018**, *122*, 10643−10649.

(162) Pradhan, B.; Kumar, G. S.; Sain, S.; Dalui, A.; Ghorai, U. K.; Pradhan, S. K.; Acharya, S. Size Tunable Cesium Antimony Chloride Perovskite Nanowires and Nanorods. *Chem. Mater.* **2018**, *30*, 2135−2142.

(163) Zhou, L.; Xu, Y. F.; Chen, B. X.; Kuang, D. B.; Su, C. Y. Synthesis and Photocatalytic Application of Stable Lead-Free $Cs_2AgBiBr_6$ Perovskite Nanocrystals. *Small* **2018**, *14*, No. 1703762.

(164) Bekenstein, Y.; Dahl, J. C.; Huang, J.; Osowiecki, W. T.; Swabeck, J. K.; Chan, E. M.; Yang, P.; Alivisatos, A. P. The Making and Breaking of Lead-Free Double Perovskite Nanocrystals of Cesium Silver-Bismuth Halide Compositions. *Nano Lett.* **2018**, *18*, 3502−3508.

(165) Kurlansky, M. *Salt*; Random House, 2011.

(166) Kasai, H.; Nalwa, H. S.; Oikawa, H.; Okada, S.; Matsuda, H.; Minami, N.; Kakuta, A.; Ono, K.; Mukoh, A.; Nakanishi, H. A Novel Preparation Method of Organic Microcrystals. *Jpn. J. Appl. Phys.* **1992**, *31*, L1132.

(167) Zhao, Y. S.; Fu, H.; Peng, A.; Ma, Y.; Xiao, D.; Yao, J. Low-Dimensional Nanomaterials Based on Small Organic Molecules: Preparation and Optoelectronic Properties. *Adv. Mater.* **2008**, *20*, 2859−2876.

(168) Wei, S.; Yang, Y.; Kang, X.; Wang, L.; Huang, L.; Pan, D. Room-temperature and gram-scale synthesis of $CsPbX_3$ (X = Cl, Br, I) perovskite nanocrystals with 50−85% photoluminescence quantum yields. *Chem. Commun.* **2016**, *52*, 7265−7268.

(169) Wang, K.-H.; Wu, L.; Li, L.; Yao, H.-B.; Qian, H.-S.; Yu, S.-H. Large-Scale Synthesis of Highly Luminescent Perovskite-Related $CsPb_2Br_5$ Nanoplatelets and Their Fast Anion Exchange. *Angew. Chem., Int. Ed.* **2016**, *55*, 8328−8332.

(170) Papavassiliou, G. C.; Pagona, G.; Karousis, N.; Mousdis, G. A.; Koutselas, I.; Vassilakopoulou, A. Nanocrystalline/microcrystalline materials based on lead-halide units. *J. Mater. Chem.* **2012**, *22*, 8271−8280.

(171) Zhang, F.; Zhong, H.; Chen, C.; Wu, X. G.; Hu, X.; Huang, H.; Han, J.; Zou, B.; Dong, Y. Brightly Luminescent and Color-Tunable Colloidal CH$_3$NH$_3$PbX$_3$ (X = Br, I, Cl) Quantum Dots: Potential Alternatives for Display Technology. *ACS Nano* **2015**, *9*, 4533−4542.

(172) Huang, H.; Susha, A. S.; Kershaw, S. V.; Hung, T. F.; Rogach, A. L. Control of Emission Color of High Quantum Yield CH$_3$NH$_3$PbBr$_3$ Perovskite Quantum Dots by Precipitation Temperature. *Adv. Sci.* **2015**, *2*, 1500194.

(173) Arunkumar, P.; Gil, K. H.; Won, S.; Unithrattil, S.; Kim, Y. H.; Kim, H. J.; Im, W. B. Colloidal Organolead Halide Perovskite with a High Mn Solubility Limit: A Step Toward Pb-Free Luminescent Quantum Dots. *J. Phys. Chem. Lett.* **2017**, *8*, 4161−4166.

(174) Zhao, Y.; Xu, X.; You, X. Colloidal Organometal Halide Perovskite (MAPbBr$_x$I$_{3-x}$, 0</=x</=3) Quantum Dots: Controllable Synthesis and Tunable Photoluminescence. *Sci. Rep.* **2016**, *6*, 35931.

(175) Luo, B.; Pu, Y.-C.; Lindley, S. A.; Yang, Y.; Lu, L.; Li, Y.; Li, X.; Zhang, J. Z. Organolead Halide Perovskite Nanocrystals: Branched Capping Ligands Control Crystal Size and Stability. *Angew. Chem., Int. Ed.* **2016**, *55*, 8864−8868.

(176) Veldhuis, S. A.; Tay, Y. K. E.; Bruno, A.; Dintakurti, S. S. H.; Bhaumik, S.; Muduli, S.; Li, M.; Mathews, N.; Sum, T. C.; Mhaisalkar, S. G. Benzyl Alcohol-treated CH$_3$NH$_3$PbBr$_3$ Nanocrystals Exhibiting High Luminescence, Stability and Ultralow Amplified Spontaneous Emission Thresholds. *Nano Lett.* **2017**, *17*, 7424−7432.

(177) Luo, B.; Naghadeh, S. B.; Allen, A. L.; Li, X.; Zhang, J. Z. Peptide-Passivated Lead Halide Perovskite Nanocrystals Based on Synergistic Effect between Amino and Carboxylic Functional Groups. *Adv. Funct. Mater.* **2017**, *27*, 1604018.

(178) Shamsi, J.; Abdelhady, A. L.; Accornero, S.; Arciniegas, M.; Goldoni, L.; Kandada, A. R.; Petrozza, A.; Manna, L. N-Methylformamide as a Source of Methylammonium Ions in the Synthesis of Lead Halide Perovskite Nanocrystals and Bulk Crystals. *ACS Energy Lett.* **2016**, *1*, 1042−1048.

(179) Dai, S. W.; Hsu, B. W.; Chen, C. Y.; Lee, C. A.; Liu, H. Y.; Wang, H. F.; Huang, Y. C.; Wu, T. L.; Manikandan, A.; Ho, R. M.; et al. Perovskite Quantum Dots with Near Unity Solution and Neat-Film Photoluminescent Quantum Yield by Novel Spray Synthesis. *Adv. Mater.* **2018**, *30*, 1870048.

(180) Papavassiliou, G. C.; Koutselas, I. B. Structural, optical and related properties of some natural three- and lower-dimensional semiconductor systems. *Synth. Met.* **1995**, *71*, 1713−1714.

(181) Cho, J.; Choi, Y. H.; O'Loughlin, T. E.; De Jesus, L.; Banerjee, S. Ligand-Mediated Modulation of Layer Thicknesses of Perovskite Methylammonium Lead Bromide Nanoplatelets. *Chem. Mater.* **2016**, *28*, 6909−6916.

(182) Levchuk, I.; Herre, P.; Brandl, M.; Osvet, A.; Hock, R.; Peukert, W.; Schweizer, P.; Spiecker, E.; Batentschuk, M.; Brabec, C. J. Ligand-assisted thickness tailoring of highly luminescent colloidal CH$_3$NH$_3$PbX$_3$ (X = Br and I) perovskite nanoplatelets. *Chem. Commun.* **2017**, *53*, 244−247.

(183) Ahmed, G. H.; Yin, J.; Bose, R.; Sinatra, L.; Alarousu, E.; Yengel, E.; AlYami, N. M.; Saidaminov, M. I.; Zhang, Y.; Hedhili, M. N.; et al. Pyridine-Induced Dimensionality Change in Hybrid Perovskite Nanocrystals. *Chem. Mater.* **2017**, *29*, 4393−4400.

(184) Kirakosyan, A.; Kim, J.; Lee, S. W.; Swathi, I.; Yoon, S.-G.; Choi, J. Optical Properties of Colloidal CH$_3$NH$_3$PbBr$_3$ Nanocrystals by Controlled Growth of Lateral Dimension. *Cryst. Growth Des.* **2017**, *17*, 794−799.

(185) Huang, H.; Raith, J.; Kershaw, S. V.; Kalytchuk, S.; Tomanec, O.; Jing, L.; Susha, A. S.; Zboril, R.; Rogach, A. L. Growth mechanism of strongly emitting CH$_3$NH$_3$PbBr$_3$ perovskite nanocrystals with a tunable bandgap. *Nat. Commun.* **2017**, *8*, 996.

(186) Weidman, M. C.; Seitz, M.; Stranks, S. D.; Tisdale, W. A. Highly Tunable Colloidal Perovskite Nanoplatelets through Variable Cation, Metal, and Halide Composition. *ACS Nano* **2016**, *10*, 7830−7839.

(187) Perumal, A.; Shendre, S.; Li, M.; Tay, Y. K.; Sharma, V. K.; Chen, S.; Wei, Z.; Liu, Q.; Gao, Y.; Buenconsejo, P. J.; et al. High

brightness formamidinium lead bromide perovskite nanocrystal light emitting devices. *Sci. Rep.* **2016**, *6*, 36733.

(188) Levchuk, I.; Osvet, A.; Tang, X.; Brandl, M.; Perea, J. D.; Hoegl, F.; Matt, G. J.; Hock, R.; Batentschuk, M.; Brabec, C. J. Brightly Luminescent and Color-Tunable Formamidinium Lead Halide Perovskite FAPbX$_3$ (X = Cl, Br, I) Colloidal Nanocrystals. *Nano Lett.* **2017**, *17*, 2765−2770.

(189) Minh, D. N.; Kim, J.; Hyon, J.; Sim, J. H.; Sowlih, H. H.; Seo, C.; Nam, J.; Eom, S.; Suk, S.; Lee, S.; et al. Room-Temperature Synthesis of Widely Tunable Formamidinium Lead Halide Perovskite Nanocrystals. *Chem. Mater.* **2017**, *29*, 5713−5719.

(190) Kumar, S.; Jagielski, J.; Kallikounis, N.; Kim, Y. H.; Wolf, C.; Jenny, F.; Tian, T.; Hofer, C. J.; Chiu, Y. C.; Stark, W. J.; et al. Ultrapure Green Light-Emitting Diodes Using Two-Dimensional Formamidinium Perovskites: Achieving Recommendation 2020 Color Coordinates. *Nano Lett.* **2017**, *17* (17), 5277−5284.

(191) Li, X.; Wu, Y.; Zhang, S.; Cai, B.; Gu, Y.; Song, J.; Zeng, H. CsPbX$_3$ Quantum Dots for Lighting and Displays: Room-Temperature Synthesis, Photoluminescence Superiorities, Underlying Origins and White Light-Emitting Diodes. *Adv. Funct. Mater.* **2016**, *26*, 2435−2445.

(192) Seth, S.; Samanta, A. A Facile Methodology for Engineering the Morphology of CsPbX$_3$ Perovskite Nanocrystals under Ambient Condition. *Sci. Rep.* **2016**, *6*, 37693.

(193) Kostopoulou, A.; Sygletou, M.; Brintakis, K.; Lappas, A.; Stratakis, E. Low-temperature benchtop-synthesis of all-inorganic perovskite nanowires. *Nanoscale* **2017**, *9*, 18202−18207.

(194) Zhang, X.; Bai, X.; Wu, H.; Zhang, X.; Sun, C.; Zhang, Y.; Zhang, W.; Zheng, W.; Yu, W. W.; Rogach, A. L. Water-Assisted Size and Shape Control of CsPbBr$_3$ Perovskite Nanocrystals. *Angew. Chem., Int. Ed.* **2018**, *57*, 3337−3342.

(195) Eperon, G. E.; Beck, C. E.; Snaith, H. J. Cation exchange for thin film lead iodide perovskite interconversion. *Mater. Horiz.* **2016**, *3*, 63−71.

(196) Mittal, M.; Jana, A.; Sarkar, S.; Mahadevan, P.; Sapra, S. Size of the Organic Cation Tunes the Band Gap of Colloidal Organolead Bromide Perovskite Nanocrystals. *J. Phys. Chem. Lett.* **2016**, *7*, 3270−3277.

(197) Chen, D.; Chen, X.; Wan, Z.; Fang, G. Full-Spectral Fine-Tuning Visible Emissions from Cation Hybrid Cs$_{1-m}$FA$_m$PbX$_3$ (X = Cl, Br, and I, 0 < /= m < /= 1) Quantum Dots. *ACS Appl. Mater. Interfaces* **2017**, *9*, 20671−20678.

(198) Zhang, X.; Liu, H.; Wang, W.; Zhang, J.; Xu, B.; Karen, K. L.; Zheng, Y.; Liu, S.; Chen, S.; Wang, K.; et al. Hybrid Perovskite Light-Emitting Diodes Based on Perovskite Nanocrystals with Organic-Inorganic Mixed Cations. *Adv. Mater.* **2017**, *29*, 1606405.

(199) Xu, B.; Wang, W.; Zhang, X.; Cao, W.; Wu, D.; Liu, S.; Dai, H.; Chen, S.; Wang, K.; Sun, X. Bright and efficient light-emitting diodes based on MA/Cs double cation perovskite nanocrystals. *J. Mater. Chem. C* **2017**, *5*, 6123−6128.

(200) Zhang, Y.-W.; Wu, G.; Dang, H.; Ma, K.; Chen, S. Multicolored Mixed-Organic-Cation Perovskite Quantum Dots (FA$_x$MA$_{1-x}$PbX$_3$, X = Br and I) for White Light-Emitting Diodes. *Ind. Eng. Chem. Res.* **2017**, *56*, 10053−10059.

(201) Ruan, L.; Shen, W.; Wang, A.; Xiang, A.; Deng, Z. Alkyl-Thiol Ligand-Induced Shape- and Crystalline Phase-Controlled Synthesis of Stable Perovskite-Related CsPb$_2$Br$_5$ Nanocrystals at Room Temperature. *J. Phys. Chem. Lett.* **2017**, *8*, 3853−3860.

(202) Ruan, L.; Lin, J.; Shen, W.; Deng, Z. Ligand-mediated synthesis of compositionally related cesium lead halide CsPb$_2$X$_5$ nanowires with improved stability. *Nanoscale* **2018**, *10*, 7658−7665.

(203) Leng, M.; Chen, Z.; Yang, Y.; Li, Z.; Zeng, K.; Li, K.; Niu, G.; He, Y.; Zhou, Q.; Tang, J. Lead-Free, Blue Emitting Bismuth Halide Perovskite Quantum Dots. *Angew. Chem., Int. Ed.* **2016**, *55*, 15012−15016.

(204) Li, X.; Yu, D.; Cao, F.; Gu, Y.; Wei, Y.; Wu, Y.; Song, J.; Zeng, H. Healing All-Inorganic Perovskite Films via Recyclable Dissolution−Recyrstallization for Compact and Smooth Carrier Channels of

Optoelectronic Devices with High Stability. *Adv. Funct. Mater.* **2016**, *26*, 5903−5912.

(205) Zhang, F.; Huang, S.; Wang, P.; Chen, X. M.; Zhao, S. L.; Dong, Y. P.; Zhong, H. Z. Colloidal Synthesis of Air-Stable CH$_3$NH$_3$PbI$_3$ Quantum Dots by Gaining Chemical Insight into the Solvent Effects. *Chem. Mater.* **2017**, *29*, 3793−3799.

(206) Malik, M. A.; Wani, M. Y.; Hashim, M. A. Microemulsion method: A novel route to synthesize organic and inorganic nanomaterials. *Arabian J. Chem.* **2012**, *5*, 397−417.

(207) Lalena, J. N.; Cleary, D. A.; Carpenter, E. E.; Dean, N. F. In *Inorganic Materials Synthesis and Fabrication*; John Wiley & Sons, 2007, DOI: 10.1002/9780470191576.

(208) Zarur, A. J.; Ying, J. Y. Reverse microemulsion synthesis of nanostructured complex oxides for catalytic combustion. *Nature* **2000**, *403*, 65−67.

(209) Huang, H.; Zhao, F.; Liu, L.; Zhang, F.; Wu, X. G.; Shi, L.; Zou, B.; Pei, Q.; Zhong, H. Emulsion Synthesis of Size-Tunable CH$_3$NH$_3$PbBr$_3$ Quantum Dots: An Alternative Route toward Efficient Light-Emitting Diodes. *ACS Appl. Mater. Interfaces* **2015**, *7*, 28128−28133.

(210) Sun, S.; Yuan, D.; Xu, Y.; Wang, A.; Deng, Z. Ligand-Mediated Synthesis of Shape-Controlled Cesium Lead Halide Perovskite Nanocrystals via Reprecipitation Process at Room Temperature. *ACS Nano* **2016**, *10*, 3648−3657.

(211) Amgar, D.; Stern, A.; Rotem, D.; Porath, D.; Etgar, L. Tunable Length and Optical Properties of CsPbX$_3$ (X = Cl, Br, I) Nanowires with a Few Unit Cells. *Nano Lett.* **2017**, *17*, 1007−1013.

(212) Liu, X.-D.; Wang, Q.; Cheng, Z.-Q.; Qiu, Y.-H.; Zhou, L.; Wang, Q.-Q. Solution-phase growth of organolead halide perovskite nanowires and nanoplates assisted by long-chain alkylammonium and solvent polarity. *Mater. Lett.* **2017**, *206*, 75−79.

(213) Kim, Y. H.; Lee, G. H.; Kim, Y. T.; Wolf, C.; Yun, H. J.; Kwon, W.; Park, C. G.; Lee, T. W. High efficiency perovskite light-emitting diodes of ligand-engineered colloidal formamidinium lead bromide nanoparticles. *Nano Energy* **2017**, *38*, 51−58.

(214) Gonzalez-Carrero, S.; Galian, R. E.; Perez-Prieto, J. Max-imizing the emissive properties of CH$_3$NH$_3$PbBr$_3$ perovskite nano-particles. *J. Mater. Chem. A* **2015**, *3*, 9187−9193.

(215) Tyagi, P.; Arveson, S. M.; Tisdale, W. A. Colloidal Organohalide Perovskite Nanoplatelets Exhibiting Quantum Confine-ment. *J. Phys. Chem. Lett.* **2015**, *6*, 1911−1916.

(216) Yuan, Z.; Shu, Y.; Xin, Y.; Ma, B. Highly luminescent nanoscale quasi-2D layered lead bromide perovskites with tunable emissions. *Chem. Commun.* **2016**, *52*, 3887−3890.

(217) Teunis, M. B.; Lawrence, K. N.; Dutta, P.; Siegel, A. P.; Sardar, R. Pure white-light emitting ultrasmall organic-inorganic hybrid perovskite nanoclusters. *Nanoscale* **2016**, *8*, 17433−17439.

(218) Teunis, M. B.; Jana, A.; Dutta, P.; Johnson, M. A.; Mandal, M.; Muhoberac, B. B.; Sardar, R. Mesoscale Growth and Assembly of Bright Luminescent Organolead Halide Perovskite Quantum Wires. *Chem. Mater.* **2016**, *28*, 5043−5054.

(219) Teunis, M. B.; Johnson, M. A.; Muhoberac, B. B.; Seifert, S.; Sardar, R. Programmable Colloidal Approach to Hierarchical Structures of Methylammonium Lead Bromide Perovskite Nanocryst-als with Bright Photoluminescent Properties. *Chem. Mater.* **2017**, *29*, 3526−3537.

(220) Chen, D.; Wan, Z.; Chen, X.; Yuan, Y.; Zhong, J. Large-scale room-temperature synthesis and optical properties of perovskite-related Cs$_4$PbBr$_6$ fluorophores. *J. Mater. Chem. C* **2016**, *4*, 10646−10653.

(221) Zhang, Y.; Saidaminov, M. I.; Dursun, I.; Yang, H.; Murali, B.; Alarousu, E.; Yengel, E.; Alshankiti, B. A.; Bakr, O. M.; Mohammed, O. F. Zero-Dimensional Cs$_4$PbBr$_6$ Perovskite Nanocrystals. *J. Phys. Chem. Lett.* **2017**, *8*, 961−965.

(222) Yang, H. Z.; Zhang, Y. H.; Pan, J.; Yin, J.; Bakr, O. M.; Mohammed, O. F. Room-Temperature Engineering of All-Inorganic Perovskite Nanocrsytals with Different Dimensionalities. *Chem. Mater.* **2017**, *29*, 8978−8982.

(223) Fang, F.; Chen, W.; Li, Y.; Liu, H. C.; Mei, M.; Zhang, R.; Hao, J. J.; Mikita, M.; Cao, W. Q.; Pan, R. K.; et al. Employing Polar Solvent Controlled Ionization in Precursors for Synthesis of High-Quality Inorganic Perovskite Nanocrystals at Room Temperature. *Adv. Funct. Mater.* **2018**, *28*, 1706000.

(224) Hassan, Y.; Song, Y.; Pensack, R. D.; Abdelrahman, A. I.; Kobayashi, Y.; Winnik, M. A.; Scholes, G. D. Structure-Tuned Lead Halide Perovskite Nanocrystals. *Adv. Mater.* **2016**, *28*, 566−573.

(225) Shamsi, J.; Dang, Z.; Ijaz, P.; Abdelhady, A. L.; Bertoni, G.; Moreels, I.; Manna, L. Colloidal CsX (X = Cl, Br, I) Nanocrystals and Their Transformation to CsPbX$_3$ Nanocrystals by Cation Exchange. *Chem. Mater.* **2018**, *30*, 79−83.

(226) Imran, M.; Ijaz, P.; Baranov, D.; Goldoni, L.; Petralanda, U.; Akkerman, Q.; Abdelhady, A. L.; Prato, M.; Bianchini, P.; Infante, I.; et al. Shape-Pure, Nearly Monodispersed CsPbBr3 Nanocubes Prepared Using Secondary Aliphatic Amines. *Nano Lett.* **2018**, *18*, 7822−7831.

(227) Locardi, F.; Cirignano, M.; Baranov, D.; Dang, Z.; Prato, M.; Drago, F.; Ferretti, M.; Pinchetti, V.; Fanciulli, M.; Brovelli, S.; et al. Colloidal Synthesis of Double Perovskite Cs$_2$AgInCl$_6$ and Mn-Doped Cs$_2$AgInCl$_6$ Nanocrystals. *J. Am. Chem. Soc.* **2018**, *140*, 12989−12995.

(228) Song, J.; Li, J.; Li, X.; Xu, L.; Dong, Y.; Zeng, H. Quantum Dot Light-Emitting Diodes Based on Inorganic Perovskite Cesium Lead Halides (CsPbX3). *Adv. Mater.* **2015**, *27*, 7162−7167.

(229) de Mello Donegá, C. Synthesis and properties of colloidal heteronanocrystals. *Chem. Soc. Rev.* **2011**, *40*, 1512−1546.

(230) Owen, J.; Brus, L. Chemical Synthesis and Luminescence Applications of Colloidal Semiconductor Quantum Dots. *J. Am. Chem. Soc.* **2017**, *139*, 10939−10943.

(231) Zhang, H.; Jang, J.; Liu, W.; Talapin, D. V. Colloidal Nanocrystals with Inorganic Halide, Pseudohalide, and Halometallate Ligands. *ACS Nano* **2014**, *8*, 7359−7369.

(232) Dong, A.; Ye, X.; Chen, J.; Kang, Y.; Gordon, T.; Kikkawa, J. M.; Murray, C. B. A Generalized Ligand-Exchange Strategy Enabling Sequential Surface Functionalization of Colloidal Nanocrystals. *J. Am. Chem. Soc.* **2011**, *133*, 998−1006.

(233) Dirin, D. N.; Dreyfuss, S.; Bodnarchuk, M. I.; Nedelcu, G.; Papagiorgis, P.; Itskos, G.; Kovalenko, M. V. Lead halide perovskites and other metal halide complexes as inorganic capping ligands for colloidal nanocrystals. *J. Am. Chem. Soc.* **2014**, *136*, 6550−6553.

(234) Sytnyk, M.; Yakunin, S.; Schofberger, W.; Lechner, R. T.; Burian, M.; Ludescher, L.; Killilea, N. A.; YousefiAmin, A.; Kriegner, D.; Stangl, J.; et al. Quasi-epitaxial Metal-Halide Perovskite Ligand Shells on PbS Nanocrystals. *ACS Nano* **2017**, *11*, 1246−1256.

(235) Yang, Z.; Janmohamed, A.; Lan, X.; Garcia de Arquer, F. P.; Voznyy, O.; Yassitepe, E.; Kim, G. H.; Ning, Z.; Gong, X.; Comin, R.; et al. Colloidal Quantum Dot Photovoltaics Enhanced by Perovskite Shelling. *Nano Lett.* **2015**, *15*, 7539−7543.

(236) Zhang, X.; Zhang, J.; Phuyal, D.; Du, J.; Tian, L.; Öberg, V. A.; Johansson, M. B.; Cappel, U. B.; Karis, O.; Liu, J.; et al. Inorganic CsPbI$_3$ Perovskite Coating on PbS Quantum Dot for Highly Efficient and Stable Infrared Light Converting Solar Cells. *Adv. Energy Mater.* **2018**, *8*, 1702049.

(237) Quintero-Bermudez, R.; Sabatini, R. P.; Lejay, M.; Voznyy, O.; Sargent, E. H. Small-Band-Offset Perovskite Shells Increase Auger Lifetime in Quantum Dot Solids. *ACS Nano* **2017**, *11*, 12378−12384.

(238) Balakrishnan, S. K.; Kamat, P. V. Au−CsPbBr$_3$ Hybrid Architecture: Anchoring Gold Nanoparticles on Cubic Perovskite Nanocrystals. *ACS Energy Lett.* **2017**, *2*, 88−93.

(239) Mokari, T.; Rothenberg, E.; Popov, I.; Costi, R.; Banin, U. Selective Growth of Metal Tips onto Semiconductor Quantum Rods and Tetrapods. *Science* **2004**, *304*, 1787−1790.

(240) Chen, S.; Lyu, D.; Ling, T.; Guo, W. Reversible modulation of CsPbBr$_3$ perovskite nanocrystal/gold nanoparticle heterostructures. *Chem. Commun.* **2018**, *54*, 4605−4608.

(241) Roman, B. J.; Otto, J.; Galik, C.; Downing, R.; Sheldon, M. Au Exchange or Au Deposition: Dual Reaction Pathways in Au-CsPbBr$_3$ Heterostructure Nanoparticles. *Nano Lett.* **2017**, *17*, 5561−5566.

(242) Ye, S.; Yu, M. H.; Yan, W.; Song, J.; Qu, J. L. Enhanced photoluminescence of CsPbBr₃@Ag hybrid perovskite quantum dots. *J. Mater. Chem. C* **2017**, *5*, 8187−8193.

(243) Zhang, X.; Xu, B.; Wang, W.; Liu, S.; Zheng, Y.; Chen, S.; Wang, K.; Sun, X. W. Plasmonic Perovskite Light-Emitting Diodes Based on the Ag-CsPbBr₃ System. *ACS Appl. Mater. Interfaces* **2017**, *9*, 4926−4931.

(244) Chen, W.; Hao, J.; Hu, W.; Zang, Z.; Tang, X.; Fang, L.; Niu, T.; Zhou, M. Optoelectronics: Enhanced Stability and Tunable Photoluminescence in Perovskite CsPbX₃/ZnS Quantum Dot Heterostructure. *Small* **2017**, *13*, DOI: 10.1002/smll.201770114.

(245) Wu, L.; Hu, H.; Xu, Y.; Jiang, S.; Chen, M.; Zhong, Q.; Yang, D.; Liu, Q.; Zhao, Y.; Sun, B.; et al. From Nonluminescent Cs₄PbX₆ (X = Cl, Br, I) Nanocrystals to Highly Luminescent CsPbX₃ Nanocrystals: Water-Triggered Transformation through a CsX-Stripping Mechanism. *Nano Lett.* **2017**, *17*, 5799−5804.

(246) Hu, H.; Wu, L.; Tan, Y.; Zhong, Q.; Chen, M.; Qiu, Y.; Yang, D.; Sun, B.; Zhang, Q.; Yin, Y. Interfacial Synthesis of Highly Stable CsPbX₃/Oxide Janus Nanoparticles. *J. Am. Chem. Soc.* **2018**, *140*, 406−412.

(247) Bhaumik, S.; Veldhuis, S. A.; Ng, Y. F.; Li, M.; Muduli, S. K.; Sum, T. C.; Damodaran, B.; Mhaisalkar, S.; Mathews, N. Highly stable, luminescent core-shell type methylammonium-octylammonium lead bromide layered perovskite nanoparticles. *Chem. Commun.* **2016**, *52*, 7118−7121.

(248) Wang, S.; Bi, C.; Yuan, J.; Zhang, L.; Tian, J. Original Core−Shell Structure of Cubic CsPbBr₃@Amorphous CsPbBr_x Perovskite Quantum Dots with a High Blue Photoluminescence Quantum Yield of over 80%. *ACS Energy Lett.* **2018**, *3*, 245−251.

(249) Li, Z.-J.; Hofman, E.; Li, J.; Davis, A. H.; Tung, C.-H.; Wu, L.-Z.; Zheng, W. Photoelectrochemically Active and Environmentally Stable CsPbBr₃/TiO₂ Core/Shell Nanocrystals. *Adv. Funct. Mater.* **2018**, *28*, 1704288.

(250) Zhong, Q.; Cao, M.; Hu, H.; Yang, D.; Chen, M.; Li, P.; Wu, L.; Zhang, Q. One-Pot Synthesis of Highly Stable CsPbBr₃@SiO₂ Core-Shell Nanoparticles. *ACS Nano* **2018**, *12*, 8579−8587.

(251) Noh, J. H.; Im, S. H.; Heo, J. H.; Mandal, T. N.; Seok, S. I. Chemical management for colorful, efficient, and stable inorganic-organic hybrid nanostructured solar cells. *Nano Lett.* **2013**, *13*, 1764−1769.

(252) Pellet, N.; Teuscher, J.; Maier, J.; Grätzel, M. Transforming Hybrid Organic Inorganic Perovskites by Rapid Halide Exchange. *Chem. Mater.* **2015**, *27*, 2181−2188.

(253) Huang, H.; Bodnarchuk, M.; Kershaw, S. V.; Kovalenko, M. V.; Rogach, A. L. Lead Halide Perovskite Nanocrystals in the Research Spotlight: Stability and Defect-Tolerance. *ACS Energy Lett.* **2017**, *2*, 2071−2083.

(254) De Trizio, L.; Manna, L. Forging Colloidal Nanostructures via Cation Exchange Reactions. *Chem. Rev.* **2016**, *116*, 10852−10887.

(255) Li, G.; Ho, J. Y.-L.; Wong, M.; Kwok, H. S. Reversible Anion Exchange Reaction in Solid Halide Perovskites and Its Implication in Photovoltaics. *J. Phys. Chem. C* **2015**, *119*, 26883−26888.

(256) Mizusaki, J.; Arai, K.; Fueki, K. Ionic conduction of the perovskite-type halides. *Solid State Ionics* **1983**, *11*, 203−211.

(257) Frost, J. M.; Walsh, A. What Is Moving in Hybrid Halide Perovskite Solar Cells? *Acc. Chem. Res.* **2016**, *49*, 528−535.

(258) Haruyama, J.; Sodeyama, K.; Han, L.; Tateyama, Y. First-Principles Study of Ion Diffusion in Perovskite Solar Cell Sensitizers. *J. Am. Chem. Soc.* **2015**, *137*, 10048−10051.

(259) Eames, C.; Frost, J. M.; Barnes, P. R.; O'Regan, B. C.; Walsh, A.; Islam, M. S. Ionic transport in hybrid lead iodide perovskite solar cells. *Nat. Commun.* **2015**, *6*, 7497.

(260) Azpiroz, J. M.; Mosconi, E.; Bisquert, J.; De Angelis, F. Defect migration in methylammonium lead iodide and its role in perovskite solar cell operation. *Energy Environ. Sci.* **2015**, *8*, 2118−2127.

(261) De Bastiani, M.; Dell'Erba, G.; Gandini, M.; D'Innocenzo, V.; Neutzner, S.; Kandada, A. R. S.; Grancini, G.; Binda, M.; Prato, M.; Ball, J. M.et al. Solar Cells: Ion Migration and the Role of Preconditioning Cycles in the Stabilization of the J-V Characteristics

(262) Ball, J. M.; Petrozza, A. Defects in perovskite-halides and their effects in solar cells. *Nat. Energy* **2016**, *1*, 16149.

(263) Mosconi, E.; De Angelis, F. Mobile Ions in Organohalide Perovskites: Interplay of Electronic Structure and Dynamics. *ACS Energy Lett.* **2016**, *1*, 182−188.

(264) Shan, Q.; Song, J.; Zou, Y.; Li, J.; Xu, L.; Xue, J.; Dong, Y.; Han, B.; Chen, J.; Zeng, H. High Performance Metal Halide Perovskite Light-Emitting Diode: From Material Design to Device Optimization. *Small* **2017**, *13*, 1701770.

(265) Ning, C.-Z.; Dou, L.; Yang, P. Bandgap engineering in semiconductor alloy nanomaterials with widely tunable compositions. *Nat. Rev. Mater.* **2017**, *2*, 17070.

(266) Zhang, A.; Dong, C.; Ren, J. Tuning Blinking Behavior of Highly Luminescent Cesium Lead Halide Nanocrystals through Varying Halide Composition. *J. Phys. Chem. C* **2017**, *121*, 13314−13323.

(267) Li, M.; Zhang, X.; Lu, S.; Yang, P. Phase transformation, morphology control, and luminescence evolution of cesium lead halide nanocrystals in the anion exchange process. *RSC Adv.* **2016**, *6*, 103382−103389.

(268) Wang, P.; Dong, B.; Cui, Z.; Gao, R.; Su, G.; Wang, W.; Cao, L. Environmentally-friendly synthesis of highly luminescent cesium lead perovskite nanocrystals using Sn-based halide precursors. *Inorg. Chim. Acta* **2017**, *467*, 251−255.

(269) Parobek, D.; Dong, Y.; Qiao, T.; Rossi, D.; Son, D. H. Photoinduced Anion Exchange in Cesium Lead Halide Perovskite Nanocrystals. *J. Am. Chem. Soc.* **2017**, *139*, 4358−4361.

(270) Ramasamy, P.; Lim, D. H.; Kim, B.; Lee, S. H.; Lee, M. S.; Lee, J. S. All-inorganic cesium lead halide perovskite nanocrystals for photodetector applications. *Chem. Commun.* **2016**, *52*, 2067−2070.

(271) Zhang, T.; Li, G.; Chang, Y.; Wang, X.; Zhang, B.; Mou, H.; Jiang, Y. Full-spectra hyperfluorescence cesium lead halide perovskite nanocrystals obtained by efficient halogen anion exchange using zinc halogenide salts. *CrystEngComm* **2017**, *19*, 1165−1171.

(272) Fang, S.; Li, G.; Lu, Y.; Li, L. Highly Luminescent CsPbX₃ (X = Cl, Br, I) Nanocrystals Achieved by a Novel Rapid Anion Exchange at Room Temperature. *Chem. - Eur. J.* **2018**, *24*, 1898−1904.

(273) Koscher, B. A.; Bronstein, N. D.; Olshansky, J. H.; Bekenstein, Y.; Alivisatos, A. P. Surface- vs Diffusion-Limited Mechanisms of Anion Exchange in CsPbBr₃ Nanocrystal Cubes Revealed through Kinetic Studies. *J. Am. Chem. Soc.* **2016**, *138*, 12065−12068.

(274) Haque, A.; Ravi, V. K.; Shanker, G. S.; Sarkar, I.; Nag, A.; Santra, P. K. Internal Heterostructure of Anion-Exchanged Cesium Lead Halide Nanocubes. *J. Phys. Chem. C* **2018**, *122*, 13399−13406.

(275) Guhrenz, C.; Benad, A.; Ziegler, C.; Haubold, D.; Gaponik, N.; Eychmüller, A. Solid-State Anion Exchange Reactions for Color Tuning of CsPbX₃ Perovskite Nanocrystals. *Chem. Mater.* **2016**, *28*, 9033−9040.

(276) Hoffman, J. B.; Schleper, A. L.; Kamat, P. V. Transformation of Sintered CsPbBr₃ Nanocrystals to Cubic CsPbI₃ and Gradient CsPbBr_xI₃₋ₓ through Halide Exchange. *J. Am. Chem. Soc.* **2016**, *138*, 8603−8611.

(277) Dou, L.; Lai, M.; Kley, C. S.; Yang, Y.; Bischak, C. G.; Zhang, D.; Eaton, S. W.; Ginsberg, N. S.; Yang, P. Spatially resolved multicolor CsPbX₃ nanowire heterojunctions via anion exchange. *Proc. Natl. Acad. Sci. U. S. A.* **2017**, *114*, 7216−7221.

(278) Ravi, V. K.; Scheidt, R. A.; Nag, A.; Kuno, M.; Kamat, P. V. To Exchange or Not to Exchange. Suppressing Anion Exchange in Cesium Lead Halide Perovskites with PbSO₄−Oleate Capping. *ACS Energy Lett.* **2018**, *3*, 1049−1055.

(279) Ravi, V. K.; Markad, G. B.; Nag, A. Band Edge Energies and Excitonic Transition Probabilities of Colloidal CsPbX₃ (X = Cl, Br, I) Perovskite Nanocrystals. *ACS Energy Lett.* **2016**, *1*, 665−671.

(280) Son, D. H.; Hughes, S. M.; Yin, Y.; Paul Alivisatos, A. Cation exchange reactions in ionic nanocrystals. *Science* **2004**, *306*, 1009−1012.

(281) Hills-Kimball, K.; Nagaoka, Y.; Cao, C.; Chaykovsky, E.; Chen, O. Synthesis of formamidinium lead halide perovskite nanocrystals through solid−liquid−solid cation exchange. *J. Mater. Chem. C* 2017, *5*, 5680−5684.

(282) Yu, D.; Cai, B.; Cao, F.; Li, X.; Liu, X.; Zhu, Y.; Ji, J.; Gu, Y.; Zeng, H. Cation Exchange-Induced Dimensionality Construction: From Monolayered to Multilayered 2D Single Crystal Halide Perovskites. *Adv. Mater. Interfaces* 2017, *4*, 1700441.

(283) van der Stam, W.; Geuchies, J. J.; Altantzis, T.; van den Bos, K. H.; Meeldijk, J. D.; Van Aert, S.; Bals, S.; Vanmaekelbergh, D.; de Mello Donega, C. Highly Emissive Divalent-Ion-Doped Colloidal $CsPb_{1-x}M_xBr_3$ Perovskite Nanocrystals through Cation Exchange. *J. Am. Chem. Soc.* 2017, *139*, 4087−4097.

(284) Yu, D.; Yin, C.; Cao, F.; Zhu, Y.; Ji, J.; Cai, B.; Liu, X.; Wang, X.; Zeng, H. Enhancing Optoelectronic Properties of Low-Dimensional Halide Perovskite via Ultrasonic-Assisted Template Refinement. *ACS Appl. Mater. Interfaces* 2017, *9*, 39602−39609.

(285) Yu, D.; Cao, F.; Gao, Y.; Xiong, Y.; Zeng, H. Room-Temperature Ion-Exchange-Mediated Self-Assembly toward Formamidinium Perovskite Nanoplates with Finely Tunable, Ultrapure Green Emissions for Achieving Rec. 2020 Displays. *Adv. Funct. Mater.* 2018, *28*, 1800248.

(286) Castelli, I. E.; García-Lastra, J. M.; Thygesen, K. S.; Jacobsen, K. W. Bandgap calculations and trends of organometal halide perovskites. *APL Mater.* 2014, *2*, No. 081514.

(287) Gao, D.; Qiao, B.; Xu, Z.; Song, D.; Song, P.; Liang, Z.; Shen, Z.; Cao, J.; Zhang, J.; Zhao, S. Postsynthetic, Reversible Cation Exchange between Pb^{2+} and Mn^{2+} in Cesium Lead Chloride Perovskite Nanocrystals. *J. Phys. Chem. C* 2017, *121*, 20387−20395.

(288) Xu, W.; Li, F. M.; Lin, F. Y.; Chen, Y.; Cai, Z. X.; Wang, Y. R.; Chen, X. Synthesis of CsPbCl₃-Mn Nanocrystals via Cation Exchange. *Adv. Opt. Mater.* 2017, *5*, 1700520.

(289) Huang, G.; Wang, C.; Xu, S.; Zong, S.; Lu, J.; Wang, Z.; Lu, C.; Cui, Y. Postsynthetic Doping of MnCl₂ Molecules into Preformed CsPbBr₃ Perovskite Nanocrystals via a Halide Exchange-Driven Cation Exchange. *Adv. Mater.* 2017, *29*, 1700095.

(290) Li, F.; Xia, Z.; Gong, Y.; Gu, L.; Liu, Q. Optical properties of Mn^{2+} doped cesium lead halide perovskite nanocrystals via a cation−anion co-substitution exchange reaction. *J. Mater. Chem. C* 2017, *5*, 9281−9287.

(291) Li, F.; Xia, Z.; Pan, C.; Gong, Y.; Gu, L.; Liu, Q.; Zhang, J. Z. High Br- content $CsPb(Cl_yBr_{1-y})_3$ perovskite nanocrystals with strong Mn^{2+} emission through diverse cation/anion exchange engineering. *ACS Appl. Mater. Interfaces* 2018, *10*, 11739−11746.

(292) Li, Q.-L.; Lu, W.-X.; Wan, N.; Ding, S.-N. Tuning optical properties of perovskite nanocrystals by supermolecular mercapto-[small beta]-cyclodextrin. *Chem. Commun.* 2016, *52*, 12342−12345.

(293) Zhang, X.; Sun, C.; Zhang, Y.; Wu, H.; Ji, C.; Chuai, Y.; Wang, P.; Wen, S.; Zhang, C.; Yu, W. W. Bright Perovskite Nanocrystal Films for Efficient Light-Emitting Devices. *J. Phys. Chem. Lett.* 2016, *7*, 4602−4610.

(294) Pan, J.; Quan, L. N.; Zhao, Y.; Peng, W.; Murali, B.; Sarmah, S. P.; Yuan, M.; Sinatra, L.; Alyami, N. M.; Liu, J.; et al. Highly Efficient Perovskite-Quantum-Dot Light-Emitting Diodes by Surface Engineering. *Adv. Mater.* 2016, *28*, 8718−8725.

(295) Koscher, B. A.; Swabeck, J. K.; Bronstein, N. D.; Alivisatos, A. P. Essentially Trap-Free CsPbBr₃ Colloidal Nanocrystals by Postsynthetic Thiocyanate Surface Treatment. *J. Am. Chem. Soc.* 2017, *139*, 6566−6569.

(296) Yarita, N.; Tahara, H.; Saruyama, M.; Kawawaki, T.; Sato, R.; Teranishi, T.; Kanemitsu, Y. Impact of Postsynthetic Surface Modification on Photoluminescence Intermittency in Formamidinium Lead Bromide Perovskite Nanocrystals. *J. Phys. Chem. Lett.* 2017, *8*, 6041−6047.

(297) Suh, Y.-H.; Kim, T.; Choi, J. W.; Lee, C.-L.; Park, J. High-performance CsPbX₃ perovskite quantum dot light emitting devices via solid-state ligand exchange. *ACS Appl. Nano Mater.* 2018, *1*, 488−496.

(298) Giansante, C.; Infante, I. Surface Traps in Colloidal Quantum Dots: A Combined Experimental and Theoretical Perspective. *J. Phys. Chem. Lett.* 2017, *8*, 5209−5215.

(299) ten Brinck, S.; Infante, I. Surface Termination, Morphology, and Bright Photoluminescence of Cesium Lead Halide Perovskite Nanocrystals. *ACS Energy Lett.* 2016, *1*, 1266−1272.

(300) Yu, Z.-L.; Ma, Q.-R.; Zhao, Y.-Q.; Liu, B.; Cai, M.-Q. The Surface Termination -A Key Factor to Influence Electronic and Optical Properties of CsSnI₃. *J. Phys. Chem. C* 2018, *122*, 9275−9282.

(301) De Roo, J.; Ibanez, M.; Geiregat, P.; Nedelcu, G.; Walravens, W.; Maes, J.; Martins, J. C.; Van Driessche, I.; Kovalenko, M. V.; Hens, Z. Highly Dynamic Ligand Binding and Light Absorption Coefficient of Cesium Lead Bromide Perovskite Nanocrystals. *ACS Nano* 2016, *10*, 2071−2081.

(302) Maes, J.; Balcaen, L.; Drijvers, E.; Zhao, Q.; De Roo, J.; Vantomme, A.; Vanhaecke, F.; Geiregat, P.; Hens, Z. On the Light Absorption Coefficient of CsPbBr₃ Perovskite Nanocrystals. *J. Phys. Chem. Lett.* 2018, *9*, 3093−3097.

(303) Ravi, V. K.; Santra, P. K.; Joshi, N.; Chugh, J.; Singh, S. K.; Rensmo, H.; Ghosh, P.; Nag, A. Origin of the Substitution Mechanism for the Binding of Organic Ligands on the Surface of CsPbBr₃ Perovskite Nanocubes. *J. Phys. Chem. Lett.* 2017, *8*, 4988−4994.

(304) Green, M. L. H. A new approach to the formal classification of covalent compounds of the elements. *J. Organomet. Chem.* 1995, *500*, 127−148.

(305) Huang, S.; Wang, B.; Zhang, Q.; Li, Z.; Shan, A.; Li, L. Postsynthesis Potassium-Modification Method to Improve Stability of CsPbBr₃ Perovskite Nanocrystals. *Adv. Opt. Mater.* 2018, *6*, 1701106.

(306) Wang, R.; Shang, Y.; Kanjanaboos, P.; Zhou, W.; Ning, Z.; Sargent, E. H. Colloidal quantum dot ligand engineering for high performance solar cells. *Energy Environ. Sci.* 2016, *9*, 1130−1143.

(307) Palazon, F.; Almeida, G.; Akkerman, Q. A.; De Trizio, L.; Dang, Z.; Prato, M.; Manna, L. Changing the Dimensionality of Cesium Lead Bromide Nanocrystals by Reversible Postsynthesis Transformations with Amines. *Chem. Mater.* 2017, *29*, 4167−4171.

(308) Udayabhaskararao, T.; Houben, L.; Cohen, H.; Menahem, M.; Pinkas, I.; Avram, L.; Wolf, T.; Teitelboim, A.; Leskes, M.; Yaffe, O.; et al. A Mechanistic Study of Phase Transformation in Perovskite Nanocrystals Driven by Ligand Passivation. *Chem. Mater.* 2018, *30*, 84−93.

(309) Chen, X.; Chen, D.; Li, J.; Fang, G.; Sheng, H.; Zhong, J. Tunable CsPbBr₃/Cs₄PbBr₆ Phase Transformation and Their Optical Spectroscopy. *Dalton Trans.* 2018, *47*, 5670−5678.

(310) Liu, Z.; Bekenstein, Y.; Ye, X.; Nguyen, S. C.; Swabeck, J.; Zhang, D.; Lee, S. T.; Yang, P.; Ma, W.; Alivisatos, A. P. Ligand Mediated Transformation of Cesium Lead Bromide Perovskite Nanocrystals to Lead Depleted Cs₄PbBr₆ Nanocrystals. *J. Am. Chem. Soc.* 2017, *139*, 5309−5312.

(311) Li, J.; Zhang, H.; Wang, S.; Long, D.; Li, M.; Wang, D.; Zhang, T. Inter-Conversion between Different Compounds of Ternary Cs-Pb-Br System. *Materials* 2018, *11*, 717.

(312) Palazon, F.; Urso, C.; De Trizio, L.; Akkerman, Q.; Marras, S.; Locardi, F.; Nelli, I.; Ferretti, M.; Prato, M.; Manna, L. Postsynthesis Transformation of Insulating Cs₄PbBr₆ Nanocrystals into Bright Perovskite CsPbBr₃ through Physical and Chemical Extraction of CsBr. *ACS Energy Lett.* 2017, *2*, 2445−2448.

(313) Li, G.; Wang, H.; Zhu, Z.; Chang, Y.; Zhang, T.; Song, Z.; Jiang, Y. Shape and phase evolution from CsPbBr₃ perovskite nanocubes to tetragonal CsPb₂Br₅ nanosheets with an indirect bandgap. *Chem. Commun.* 2016, *52*, 11296−11299.

(314) Balakrishnan, S. K.; Kamat, P. V. Ligand Assisted Transformation of Cubic CsPbBr₃ Nanocrystals into Two-Dimensional CsPb₂Br₅ Nanosheets. *Chem. Mater.* 2018, *30*, 74−78.

(315) Palazon, F.; Dogan, S.; Marras, S.; Locardi, F.; Nelli, I.; Rastogi, P.; Ferretti, M.; Prato, M.; Krahne, R.; Manna, L. From CsPbBr₃ Nano-Inks to Sintered CsPbBr₃−CsPb₂Br₅ Films via Thermal Annealing: Implications on Optoelectronic Properties. *J. Phys. Chem. C* 2017, *121*, 11956−11961.

(316) Shen, W.; Ruan, L.; Shen, Z.; Deng, Z. Reversible Light-Mediated Compositional and Structural Transitions between CsPbBr$_3$ and CsPb$_2$Br$_5$ Nanosheets. *Chem. Commun.* **2018**, *54*, 2804−2807.

(317) Turedi, B.; Lee, K.; Dursun, I.; Alamer, B.; Wu, Z.; Alarousu, E.; Mohammed, O. F.; Cho, N.; Bakr, O. M. Water-Induced Dimensionality Reduction in Metal-Halide Perovskites. *J. Phys. Chem. C* **2018**, *122*, 14128−14134.

(318) Wang, Y.; Li, X.; Sreejith, S.; Cao, F.; Wang, Z.; Stuparu, M. C.; Zeng, H.; Sun, H. Photon Driven Transformation of Cesium Lead Halide Perovskites from Few-Monolayer Nanoplatelets to Bulk Phase. *Adv. Mater.* **2016**, *28*, 10637−10643.

(319) Yin, T.; Fang, Y.; Chong, W. K.; Ming, K. T.; Jiang, S.; Li, X.; Kuo, J. L.; Fang, J.; Sum, T. C.; White, T. J.; et al. High-Pressure-Induced Comminution and Recrystallization of CH$_3$NH$_3$PbBr$_3$ Nanocrystals as Large Thin Nanoplates. *Adv. Mater.* **2018**, *30*, 1705017.

(320) Palazon, F.; Prato, M.; Manna, L. Writing on Nanocrystals: Patterning Colloidal Inorganic Nanocrystal Films through Irradiation-Induced Chemical Transformations of Surface Ligands. *J. Am. Chem. Soc.* **2017**, *139*, 13250−13259.

(321) Xiao, G.; Cao, Y.; Qi, G.; Wang, L.; Liu, C.; Ma, Z.; Yang, X.; Sui, Y.; Zheng, W.; Zou, B. Pressure Effects on Structure and Optical Properties in Cesium Lead Bromide Perovskite Nanocrystals. *J. Am. Chem. Soc.* **2017**, *139*, 10087−10094.

(322) Boles, M. A.; Engel, M.; Talapin, D. V. Self-Assembly of Colloidal Nanocrystals: From Intricate Structures to Functional Materials. *Chem. Rev.* **2016**, *116*, 11220−11289.

(323) Soetan, N.; Erwin, W. R.; Tonigan, A. M.; Walker, D. G.; Bardhan, R. Solvent-Assisted Self-Assembly of CsPbBr$_3$ Perovskite Nanocrystals into One-Dimensional Superlattice. *J. Phys. Chem. C* **2017**, *121*, 18186−18194.

(324) Wang, K. H.; Yang, J. N.; Ni, Q. K.; Yao, H. B.; Yu, S. H. Metal Halide Perovskite Supercrystals: Gold-Bromide Complex Triggered Assembly of CsPbBr$_3$ Nanocubes. *Langmuir* **2018**, *34*, 595−602.

(325) Pan, A.; Jurow, M.; Zhao, Y.; Qiu, F.; Liu, Y.; Yang, J.; Urban, J. J.; He, L.; Liu, Y. Templated self-assembly of one-dimensional CsPbX$_3$ perovskite nanocrystal superlattices. *Nanoscale* **2017**, *9*, 17688−17693.

(326) Rainò, G.; Becker, M. A.; Bodnarchuk, M. I.; Mahrt, R. F.; Kovalenko, M. V.; Stöferle, T. Superfluorescence from lead halide perovskite quantum dot superlattices. *Nature* **2018**, *563*, 671−675.

(327) Leijtens, T.; Eperon, G. E.; Noel, N. K.; Habisreutinger, S. N.; Petrozza, A.; Snaith, H. J. Stability of Metal Halide Perovskite Solar Cells. *Adv. Energy Mater.* **2015**, *5*, 1500963.

(328) Berhe, T. A.; Su, W. N.; Chen, C. H.; Pan, C. J.; Cheng, J. H.; Chen, H. M.; Tsai, M. C.; Chen, L. Y.; Dubale, A. A.; Hwang, B. J. Organometal halide perovskite solar cells: degradation and stability. *Energy Environ. Sci.* **2016**, *9*, 323−356.

(329) Meyns, M.; Peralvarez, M.; Heuer-Jungemann, A.; Hertog, W.; Ibanez, M.; Nafria, R.; Genc, A.; Arbiol, J.; Kovalenko, M. V.; Carreras, J.; et al. Polymer-Enhanced Stability of Inorganic Perovskite Nanocrystals and Their Application in Color Conversion LEDs. *ACS Appl. Mater. Interfaces* **2016**, *8*, 19579−19586.

(330) Raja, S. N.; Bekenstein, Y.; Koc, M. A.; Fischer, S.; Zhang, D.; Lin, L.; Ritchie, R. O.; Yang, P.; Alivisatos, A. P. Encapsulation of Perovskite Nanocrystals into Macroscale Polymer Matrices: Enhanced Stability and Polarization. *ACS Appl. Mater. Interfaces* **2016**, *8*, 35523−35533.

(331) Aleshin, A. N.; Shcherbakov, I. P.; Gushchina, E. V.; Matyushkin, L. B.; Moshnikov, V. A. Solution-processed field-effect transistors based on polyfluorene − cesium lead halide nanocrystals composite films with small hysteresis of output and transfer characteristics. *Org. Electron.* **2017**, *50*, 213−219.

(332) He, J.; Chen, H.; Chen, H.; Wang, Y.; Wu, S. T.; Dong, Y. Hybrid downconverters with green perovskite-polymer composite films for wide color gamut displays. *Opt. Express* **2017**, *25*, 12915−12925.

(333) Hou, S.; Guo, Y.; Tang, Y.; Quan, Q. Synthesis and Stabilization of Colloidal Perovskite Nanocrystals by Multidentate Polymer Micelles. *ACS Appl. Mater. Interfaces* **2017**, *9*, 18417−18422.

(334) Ma, K.; Du, X.-Y.; Zhang, Y.-W.; Chen, S. In situ fabrication of halide perovskite nanocrystals embedded in polymer composites via microfluidic spinning microreactors. *J. Mater. Chem. C* **2017**, *5*, 9398−9404.

(335) Xi, L.; Boothroyd, C. B.; Salim, T.; Borghardt, S.; Lam, Y. M.; Kardynał, B. E. Facile in situ synthesis of stable luminescent organic−inorganic lead halide perovskite nanoparticles in a polymer matrix. *J. Mater. Chem. C* **2017**, *5*, 7207−7214.

(336) An, H.; Kim, W. K.; Wu, C.; Kim, T. W. Highly-stable memristive devices based on poly(methylmethacrylate): CsPbCl$_3$ perovskite quantum dot hybrid nanocomposites. *Org. Electron.* **2018**, *56*, 41−45.

(337) Li, X.; Xue, Z. J.; Luo, D.; Huang, C. H.; Liu, L. Z.; Qiao, X. Z.; Liu, C.; Song, Q.; Yan, C.; Li, Y. C.; et al. A stable lead halide perovskite nanocrystals protected by PMMA. *Sci. China Mater.* **2018**, *61*, 363−370.

(338) Xin, Y.; Zhao, H.; Zhang, J. Highly Stable and Luminescent Perovskite-Polymer Composites from a Convenient and Universal Strategy. *ACS Appl. Mater. Interfaces* **2018**, *10*, 4971−4980.

(339) Yang, S.; Zhang, F.; Tai, J.; Li, Y.; Yang, Y.; Wang, H.; Zhang, J.; Xie, Z.; Xu, B.; Zhong, H.; et al. A Detour Strategy for Colloidal-Stable Block-Copolymer Grafted MAPbBr$_3$ Quantum Dots in Water with Long Photoluminescence Lifetime. *Nanoscale* **2018**, *10*, 5820−5826.

(340) Zhang, M.; Wang, M.; Yang, Z.; Li, J.; Qiu, H. Preparation of all-inorganic perovskite quantum dots-polymer composite for white LEDs application. *J. Alloys Compd.* **2018**, *748*, 537−545.

(341) Wei, Y.; Deng, X.; Xie, Z.; Cai, X.; Liang, S.; Ma, P. a.; Hou, Z.; Cheng, Z.; Lin, J. Enhancing the Stability of Perovskite Quantum Dots by Encapsulation in Crosslinked Polystyrene Beads via a Swelling−Shrinking Strategy toward Superior Water Resistance. *Adv. Funct. Mater.* **2017**, *27*, 1703535.

(342) Zhang, H.; Wang, X.; Liao, Q.; Xu, Z.; Li, H.; Zheng, L.; Fu, H. Embedding Perovskite Nanocrystals into a Polymer Matrix for Tunable Luminescence Probes in Cell Imaging. *Adv. Funct. Mater.* **2017**, *27*, 1604382.

(343) Pan, A.; Wang, J.; Jurow, M. J.; Jia, M.; Liu, Y.; Wu, Y.; Zhang, Y.; He, L.; Liu, Y. General Strategy for the Preparation of Stable Luminous Nanocomposite Inks Using Chemically Addressable CsPbX$_3$ Peroskite Nanocrystals. *Chem. Mater.* **2018**, *30*, 2771−2780.

(344) Demchyshyn, S.; Roemer, J. M.; Groiß, H.; Heilbrunner, H.; Ulbricht, C.; Apaydin, D.; Böhm, A.; Rütt, U.; Bertram, F.; Hesser, G.; et al. Confining metal-halide perovskites in nanoporous thin films. *Sci. Adv.* **2017**, *3*, No. e1700738.

(345) Di, X.; Jiang, J.; Hu, Z.; Zhou, L.; Li, P.; Liu, S.; Xiang, W.; Liang, X. Stable and brightly luminescent all-inorganic cesium lead halide perovskite quantum dots coated with mesoporous silica for warm WLED. *Dyes Pigm.* **2017**, *146*, 361−367.

(346) Li, Z.; Kong, L.; Huang, S.; Li, L. Highly Luminescent and Ultrastable CsPbBr$_3$ Perovskite Quantum Dots Incorporated into a Silica/Alumina Monolith. *Angew. Chem., Int. Ed.* **2017**, *56*, 8134−8138.

(347) Chen, Y.; Yu, M.; Ye, S.; Song, J.; Qu, J. All-inorganic CsPbBr$_3$ perovskite quantum dots embedded in dual-mesoporous silica with moisture resistance for two-photon-pumped plasmonic nanoLasers. *Nanoscale* **2018**, *10*, 6704−6711.

(348) He, M.; Cheng, Y.; Yuan, R.; Zhou, L.; Jiang, J.; Xu, T.; Chen, W.; Liu, Z.; Xiang, W.; Liang, X. Mn-Doped cesium lead halide perovskite nanocrystals with dual-color emission for WLED. *Dyes Pigm.* **2018**, *152*, 146−154.

(349) Yoon, H. C.; Lee, S.; Song, J. K.; Yang, H.; Do, Y. R. Efficient and Stable CsPbBr$_3$ Quantum-Dot Powders Passivated and Encapsulated with a Mixed Silicon Nitride and Silicon Oxide Inorganic Polymer Matrix. *ACS Appl. Mater. Interfaces* **2018**, *10*, 11756−11767.

(350) Hu, Z. P.; Liu, Z. Z.; Bian, Y.; Li, S. Q.; Tang, X. S.; Du, J.; Zang, Z. G.; Zhou, M.; Hu, W.; Tian, Y. X.; et al. Enhanced Two-Photon-Pumped Emission from In Situ Synthesized Nonblinking CsPbBr$_3$/SiO$_2$ Nanocrystals with Excellent Stability. *Adv. Opt. Mater.* **2018**, *6*, 1700997.

(351) Loiudice, A.; Saris, S.; Oveisi, E.; Alexander, D. T. L.; Buonsanti, R. CsPbBr$_3$ QD/AlO$_x$ Inorganic Nanocomposites with Exceptional Stability in Water, Light, and Heat. *Angew. Chem., Int. Ed.* **2017**, *56*, 10696−10701.

(352) Sun, C.; Shen, X.; Zhang, Y.; Wang, Y.; Chen, X.; Ji, C.; Shen, H.; Shi, H.; Wang, Y.; Yu, W. W. Highly luminescent, stable, transparent and flexible perovskite quantum dot gels towards light-emitting diodes. *Nanotechnology* **2017**, *28*, 365601.

(353) Xu, L.; Chen, J.; Song, J.; Li, J.; Xue, J.; Dong, Y.; Cai, B.; Shan, Q.; Han, B.; Zeng, H. Double-Protected All-Inorganic Perovskite Nanocrystals by Crystalline Matrix and Silica for Triple-Modal Anti-Counterfeiting Codes. *ACS Appl. Mater. Interfaces* **2017**, *9*, 26556−26564.

(354) He, M.; Cheng, Y.; Shen, L.; Shen, C.; Zhang, H.; Xiang, W.; Liang, X. Mn-doped CsPbCl$_3$ perovskite quantum dots (PQDs) incorporated into silica/alumina particles used for WLEDs. *Appl. Surf. Sci.* **2018**, *448*, 400−406.

(355) Quan, L. N.; Quintero-Bermudez, R.; Voznyy, O.; Walters, G.; Jain, A.; Fan, J. Z.; Zheng, X.; Yang, Z.; Sargent, E. H. Highly Emissive Green Perovskite Nanocrystals in a Solid State Crystalline Matrix. *Adv. Mater.* **2017**, *29*, 1605945.

(356) Wang, Y.; Yu, D.; Wang, Z.; Li, X.; Chen, X.; Nalla, V.; Zeng, H.; Sun, H. Solution-Grown CsPbBr$_3$/Cs$_4$PbBr$_6$ Perovskite Nanocomposites: Toward Temperature-Insensitive Optical Gain. *Small* **2017**, *13*, 1701587.

(357) Chen, X.; Zhang, F.; Ge, Y.; Shi, L.; Huang, S.; Tang, J.; Lv, Z.; Zhang, L.; Zou, B.; Zhong, H. Centimeter-Sized Cs$_4$PbBr$_6$ Crystals with Embedded CsPbBr$_3$ Nanocrystals Showing Superior Photoluminescence: Nonstoichiometry Induced Transformation and Light-Emitting Applications. *Adv. Funct. Mater.* **2018**, *28*, 1706567.

(358) Chen, Y.; Zhou, Y.; Zhao, Q.; Zhang, J.; Ma, J.-P.; Xuan, T.-T.; Guo, S.-Q.; Yong, Z.-J.; Wang, J.; Kuroiwa, Y.; et al. Cs$_4$PbBr$_6$/CsPbBr$_3$ Perovskite Composites with Near-Unity Luminescence Quantum Yield: Large-Scale Synthesis, Luminescence and Formation Mechanism, and White Light-Emitting Diode Application. *ACS Appl. Mater. Interfaces* **2018**, *10*, 15905−15912.

(359) Chen, J.-S.; Doane, T. L.; Li, M.; Zang, H.; Maye, M. M.; Cotlet, M. 0D-2D and 1D-2D Semiconductor Hybrids Composed of All Inorganic Perovskite Nanocrystals and Single-Layer Graphene with Improved Light Harvesting. *Part. Part. Syst. Charact.* **2018**, *35*, 1700310.

(360) Huang, H.; Li, J.; Yi, Y.; Wang, J.; Kang, Y.; Chu, P. K.; Ong, H. C.; Yu, X. F. In situ growth of all-inorganic perovskite nanocrystals on black phosphorus nanosheets. *Chem. Commun.* **2018**, *54*, 2365−2368.

(361) Li, H.; Zheng, X.; Liu, Y.; Zhang, Z.; Jiang, T. Ultrafast interfacial energy transfer and interlayer excitons in the monolayer WS$_2$/CsPbBr$_3$ quantum dot heterostructure. *Nanoscale* **2018**, *10*, 1650−1659.

(362) Muduli, S.; Pandey, P.; Devatha, G.; Babar, R.; M, T.; Kothari, D. C.; Kabir, M.; Pillai, P.; Ogale, S. B. Photoluminescence quenching in self-assembled CsPbBr$_3$ quantum dots on few layer black phosphorous sheets. *Angew. Chem., Int. Ed.* **2018**, *57*, 7682−7686.

(363) Lou, S.; Xuan, T.; Yu, C.; Cao, M.; Xia, C.; Wang, J.; Li, H. Nanocomposites of CsPbBr$_3$ perovskite nanocrystals in an ammonium bromide framework with enhanced stability. *J. Mater. Chem. C* **2017**, *5*, 7431−7435.

(364) Sun, J.-Y.; Rabouw, F. T.; Yang, X.-F.; Huang, X.-Y.; Jing, X.-P.; Ye, S.; Zhang, Q.-Y. Facile Two-Step Synthesis of All-Inorganic Perovskite CsPbX$_3$ (X = Cl, Br, and I) Zeolite-Y Composite Phosphors for Potential Backlight Display Application. *Adv. Funct. Mater.* **2017**, *27*, 1704371.

(365) Xu, W.; Cai, Z.; Li, F.; Dong, J.; Wang, Y.; Jiang, Y.; Chen, X. Embedding lead halide perovskite quantum dots in carboxybenzene microcrystals improves stability. *Nano Res.* **2017**, *10*, 2692−2698.

(366) Zheng, Z.; Zhuge, F.; Wang, Y.; Zhang, J.; Gan, L.; Zhou, X.; Li, H.; Zhai, T. Decorating Perovskite Quantum Dots in TiO$_2$ Nanotubes Array for Broadband Response Photodetector. *Adv. Funct. Mater.* **2017**, *27*, 1703115.

(367) Liu, S.; He, M.; Di, X.; Li, P.; Xiang, W.; Liang, X. Precipitation and tunable emission of cesium lead halide perovskites (CsPbX$_3$, X = Br, I) QDs in borosilicate glass. *Ceram. Int.* **2018**, *44*, 4496−4499.

(368) Yuan, R.; Shen, L.; Shen, C.; Liu, J.; Zhou, L.; Xiang, W.; Liang, X. CsPbBr$_3$:xEu^{3+} perovskite QD borosilicate glass: a new member of the luminescent material family. *Chem. Commun.* **2018**, *54*, 3395−3398.

(369) Yang, G. L.; Fan, Q. S.; Chen, B. K.; Zhou, Q. C.; Zhong, H. Z. Reprecipitation synthesis of luminescent CH$_3$NH$_3$PbBr$_3$/NaNO$_3$ nanocomposites with enhanced stability. *J. Mater. Chem. C* **2016**, *4*, 11387−11391.

(370) Shen, X.; Sun, C.; Bai, X.; Zhang, X.; Wang, Y.; Wang, Y.; Song, H.; Yu, W. W. Efficient and Stable CsPb(Br/I)$_3$@Anthracene Composites for White Light Emitting Devices. *ACS Appl. Mater. Interfaces* **2018**, *10*, 16768−16775.

(371) Li, P.; Hu, C.; Zhou, L.; Jiang, J.; Cheng, Y.; He, M.; Liang, X.; Xiang, W. Novel synthesis and optical characterization of CsPb$_2$Br$_5$ quantum dots in borosilicate glasses. *Mater. Lett.* **2017**, *209*, 483−485.

(372) Pan, A.; Jurow, M. J.; Qiu, F.; Yang, J.; Ren, B.; Urban, J. J.; He, L.; Liu, Y. Nanorod Suprastructures from a Ternary Graphene Oxide-Polymer-CsPbX$_3$ Perovskite Nanocrystal Composite That Display High Environmental Stability. *Nano Lett.* **2017**, *17*, 6759−6765.

(373) Li, Y.; Lv, Y.; Guo, Z.; Dong, L.; Zheng, J.; Chai, C.; Chen, N.; Lu, Y.; Chen, C. One-step preparation of long-term stable and flexible CsPbBr$_3$ perovskite quantum dots/ethylene vinyl acetate copolymer composite films for white LEDs. *ACS Appl. Mater. Interfaces* **2018**, *10*, 15888−15894.

(374) Erman, B.; Flory, P. J. Critical Phenomena and Transitions in Swollen Polymer Networks and in Linear Macromolecules. *Macromolecules* **1986**, *19*, 2342−2353.

(375) Dirin, D. N.; Protesescu, L.; Trummer, D.; Kochetygov, I. V.; Yakunin, S.; Krumeich, F.; Stadie, N. P.; Kovalenko, M. V. Harnessing Defect-Tolerance at the Nanoscale: Highly Luminescent Lead Halide Perovskite Nanocrystals in Mesoporous Silica Matrixes. *Nano Lett.* **2016**, *16*, 5866−5874.

(376) Park, D. H.; Han, J. S.; Kim, W.; Jang, H. S. Facile synthesis of thermally stable CsPbBr$_3$ perovskite quantum dot-inorganic SiO$_2$ composites and their application to white light-emitting diodes with wide color gamut. *Dyes Pigm.* **2018**, *149*, 246−252.

(377) Liu, Z.; Zhang, Y.; Fan, Y.; Chen, Z.; Tang, Z.; Zhao, J.; Lv, Y.; Lin, J.; Guo, X.; Zhang, J.; et al. Toward Highly Luminescent and Stabilized Silica-Coated Perovskite Quantum Dots through Simply Mixing and Stirring under Room Temperature in Air. *ACS Appl. Mater. Interfaces* **2018**, *10*, 13053−13061.

(378) Li, X.; Wang, Y.; Sun, H.; Zeng, H. Amino-Mediated Anchoring Perovskite Quantum Dots for Stable and Low-Threshold Random Lasing. *Adv. Mater.* **2017**, *29*, 1701185.

(379) Zhang, C.; Wang, B.; Li, W.; Huang, S.; Kong, L.; Li, Z.; Li, L. Conversion of invisible metal-organic frameworks to luminescent perovskite nanocrystals for confidential information encryption and decryption. *Nat. Commun.* **2017**, *8*, 1138.

(380) Zhou, H. C.; Long, J. R.; Yaghi, O. M. Introduction to metal-organic frameworks. *Chem. Rev.* **2012**, *112*, 673−674.

(381) Huang, H.; Polavarapu, L.; Sichert, J. A.; Susha, A. S.; Urban, A. S.; Rogach, A. L. Colloidal lead halide perovskite nanocrystals: synthesis, optical properties and applications. *NPG Asia Mater.* **2016**, *8*, e328.

(382) Tanaka, K.; Takahashi, T.; Ban, T.; Kondo, T.; Uchida, K.; Miura, N. Comparative study on the excitons in lead-halide-based

perovskite-type crystals CH₃NH₃PbBr₃ CH₃NH₃PbI₃. *Solid State Commun.* **2003**, *127*, 619−623.

(383) Umebayashi, T.; Asai, K.; Kondo, T.; Nakao, A. Electronic structures of lead iodide based low-dimensional crystals. *Phys. Rev. B: Condens. Matter Mater. Phys.* **2003**, *67*, 155405.

(384) Schulz, P.; Edri, E.; Kirmayer, S.; Hodes, G.; Cahen, D.; Kahn, A. Interface energetics in organo-metal halide perovskite-based photovoltaic cells. *Energy Environ. Sci.* **2014**, *7*, 1377−1381.

(385) Eperon, G. E.; Stranks, S. D.; Menelaou, C.; Johnston, M. B.; Herz, L. M.; Snaith, H. J. Formamidinium lead trihalide: a broadly tunable perovskite for efficient planar heterojunction solar cells. *Energy Environ. Sci.* **2014**, *7*, 982.

(386) Meloni, S.; Palermo, G.; Ashari-Astani, N.; Gratzel, M.; Rothlisberger, U. Valence and conduction band tuning in halide perovskites for solar cell applications. *J. Mater. Chem. A* **2016**, *4*, 15997−16002.

(387) Hao, F.; Stoumpos, C. C.; Cao, D. H.; Chang, R. P. H.; Kanatzidis, M. G. Lead-free solid-state organic-inorganic halide perovskite solar cells. *Nat. Photonics* **2014**, *8*, 489−494.

(388) Chen, Q.; De Marco, N.; Yang, Y.; Song, T. B.; Chen, C. C.; Zhao, H. X.; Hong, Z. R.; Zhou, H. P.; Yang, Y. Under the spotlight: The organic-inorganic hybrid halide perovskite for optoelectronic applications. *Nano Today* **2015**, *10*, 355−396.

(389) Brennan, M. C.; Herr, J. E.; Nguyen-Beck, T. S.; Zinna, J.; Draguta, S.; Rouvimov, S.; Parkhill, J.; Kuno, M. Origin of the Size-Dependent Stokes Shift in CsPbBr₃ Perovskite Nanocrystals. *J. Am. Chem. Soc.* **2017**, *139*, 12201−12208.

(390) Brennan, M. C.; Zinna, J.; Kuno, M. Existence of a Size-Dependent Stokes Shift in CsPbBr₃ Perovskite Nanocrystals. *ACS Energy Lett.* **2017**, *2*, 1487−1488.

(391) Bohn, B. J.; Simon, T.; Gramlich, M.; Richter, A. F.; Polavarapu, L.; Urban, A. S.; Feldmann, J. Dephasing and Quantum Beating of Excitons in Methylammonium Lead Iodide Perovskite Nanoplatelets. *ACS Photonics* **2018**, *5*, 648−654.

(392) Utzat, H.; Shulenberger, K. E.; Achorn, O. B.; Nasilowski, M.; Sinclair, T. S.; Bawendi, M. G. Probing Linewidths and Biexciton Quantum Yields of Single Cesium Lead Halide Nanocrystals in Solution. *Nano Lett.* **2017**, *17*, 6838−6846.

(393) Kang, J.; Wang, L. W. High Defect Tolerance in Lead Halide Perovskite CsPbBr3. *J. Phys. Chem. Lett.* **2017**, *8*, 489−493.

(394) Liu, M.; Zhong, G.; Yin, Y.; Miao, J.; Li, K.; Wang, C.; Xu, X.; Shen, C.; Meng, H. Aluminum-Doped Cesium Lead Bromide Perovskite Nanocrystals with Stable Blue Photoluminescence Used for Display Backlight. *Adv. Sci.* **2017**, *4*, 1700335.

(395) Talapin, D. V.; Lee, J. S.; Kovalenko, M. V.; Shevchenko, E. V. Prospects of colloidal nanocrystals for electronic and optoelectronic applications. *Chem. Rev.* **2010**, *110*, 389−458.

(396) Ha, S. T.; Liu, X.; Zhang, Q.; Giovanni, D.; Sum, T. C.; Xiong, Q. Synthesis of Organic-Inorganic Lead Halide Perovskite Nanoplatelets: Towards High-Performance Perovskite Solar Cells and Optoelectronic Devices. *Adv. Opt. Mater.* **2014**, *2*, 838−844.

(397) Wang, Y.; Li, X.; Song, J.; Xiao, L.; Zeng, H.; Sun, H. All-Inorganic Colloidal Perovskite Quantum Dots: A New Class of Lasing Materials with Favorable Characteristics. *Adv. Mater.* **2015**, *27*, 7101−7108.

(398) Bohn, B. J.; Tong, Y.; Gramlich, M.; Lai, M. L.; Doblinger, M.; Wang, K.; Hoye, R. L. Z.; Muller-Buschbaum, P.; Stranks, S. D.; Urban, A. S.; et al. Boosting tunable blue luminescence of halide perovskite nanoplatelets through post-synthetic surface trap repair. *Nano Lett.* **2018**, *18*, 5231−5238.

(399) Jagielski, J.; Kumar, S.; Wang, M.; Scullion, D.; Lawrence, R.; Li, Y.-T.; Yakunin, S.; Tian, T.; Kovalenko, M. V.; Chiu, Y.-C.; et al. Aggregation-induced emission in lamellar solids of colloidal perovskite quantum wells. *Sci. Adv.* **2017**, *3*, No. eaaq0208.

(400) Sapori, D.; Kepenekian, M.; Pedesseau, L.; Katan, C.; Even, J. Quantum confinement and dielectric profiles of colloidal nanoplatelets of halide inorganic and hybrid organic-inorganic perovskites. *Nanoscale* **2016**, *8*, 6369−6378.

(401) Stoumpos, C. C.; Cao, D. H.; Clark, D. J.; Young, J.; Rondinelli, J. M.; Jang, J. I.; Hupp, J. T.; Kanatzidis, M. G. Ruddlesden−Popper Hybrid Lead Iodide Perovskite 2D Homologous Semiconductors. *Chem. Mater.* **2016**, *28*, 2852−2867.

(402) Huang, H.; Liu, M.; Li, J.; Luo, L.; Zhao, J.; Luo, Z.; Wang, X.; Ye, Z.; He, H.; Zeng, J. Atomically thin cesium lead bromide perovskite quantum wires with high luminescence. *Nanoscale* **2017**, *9*, 104−108.

(403) Zhao, J.; Liu, M.; Fang, L.; Jiang, S.; Zhou, J.; Ding, H.; Huang, H.; Wen, W.; Luo, Z.; Zhang, Q.; et al. Great Disparity in Photoluminesence Quantum Yields of Colloidal CsPbBr₃ Nanocrystals with Varied Shape: The Effect of Crystal Lattice Strain. *J. Phys. Chem. Lett.* **2017**, *8*, 3115−3121.

(404) Di Stasio, F.; Imran, M.; Akkerman, Q. A.; Prato, M.; Manna, L.; Krahne, R. Reversible Concentration-Dependent Photoluminescence Quenching and Change of Emission Color in CsPbBr₃ Nanowires and Nanoplatelets. *J. Phys. Chem. Lett.* **2017**, *8*, 2725−2729.

(405) Peng, L.; Tang, A.; Yang, C.; Teng, F. Size-controlled synthesis of highly luminescent organometal halide perovskite quantum dots. *J. Alloys Compd.* **2016**, *687*, 506−513.

(406) Ling, Y.; Tan, L.; Wang, X.; Zhou, Y.; Xin, Y.; Ma, B.; Hanson, K.; Gao, H. Composite Perovskites of Cesium Lead Bromide for Optimized Photoluminescence. *J. Phys. Chem. Lett.* **2017**, *8*, 3266−3271.

(407) Yin, J.; Yang, H.; Song, K.; El-Zohry, A. M.; Han, Y.; Bakr, O. M.; Brédas, J.-L.; Mohammed, O. F. Point Defects and Green Emission in Zero-Dimensional Perovskites. *J. Phys. Chem. Lett.* **2018**, *9*, 5490−5495.

(408) Almutlaq, J.; Yin, J.; Mohammed, O. F.; Bakr, O. M. The Benefit and Challenges of Zero-Dimensional Perovskites. *J. Phys. Chem. Lett.* **2018**, *9*, 4131−4138.

(409) Dohner, E. R.; Jaffe, A.; Bradshaw, L. R.; Karunadasa, H. I. Intrinsic white-light emission from layered hybrid perovskites. *J. Am. Chem. Soc.* **2014**, *136*, 13154−13157.

(410) Yuan, Z.; Zhou, C.; Tian, Y.; Shu, Y.; Messier, J.; Wang, J. C.; van de Burgt, L. J.; Kountouriotis, K.; Xin, Y.; Holt, E.; et al. One-dimensional organic lead halide perovskites with efficient bluish white-light emission. *Nat. Commun.* **2017**, *8*, 14051.

(411) Zhou, C.; Lin, H.; Tian, Y.; Yuan, Z.; Clark, R.; Chen, B.; van de Burgt, L. J.; Wang, J. C.; Zhou, Y.; Hanson, K.; et al. Luminescent zero-dimensional organic metal halide hybrids with near-unity quantum efficiency. *Chem. Sci.* **2018**, *9*, 586−593.

(412) Fu, M.; Ehrat, F.; Wang, Y.; Milowska, K. Z.; Reckmeier, C.; Rogach, A. L.; Stolarczyk, J. K.; Urban, A. S.; Feldmann, J. Carbon Dots: A Unique Fluorescent Cocktail of Polycyclic Aromatic Hydrocarbons. *Nano Lett.* **2015**, *15*, 6030−6035.

(413) Lin, H.; Zhou, C.; Tian, Y.; Siegrist, T.; Ma, B. Low-Dimensional Organometal Halide Perovskites. *ACS Energy Lett.* **2018**, *3*, 54−62.

(414) Herz, L. M. Charge-Carrier Dynamics in Organic-Inorganic Metal Halide Perovskites. *Annu. Rev. Phys. Chem.* **2016**, *67*, 65−89.

(415) Amgar, D.; Wierzbowska, M.; Uvarov, V.; Gutkin, V.; Etgar, L. Novel rubidium lead chloride nanocrystals: synthesis and characterization. *Nano Futures* **2017**, *1*, No. 021002.

(416) Yang, Y.; Ostrowski, D. P.; France, R. M.; Zhu, K.; van de Lagemaat, J.; Luther, J. M.; Beard, M. C. Observation of a hot-phonon bottleneck in lead-iodide perovskites. *Nat. Photonics* **2016**, *10*, 53−59.

(417) Li, J.; Luo, L.; Huang, H.; Ma, C.; Ye, Z.; Zeng, J.; He, H. 2D Behaviors of Excitons in Cesium Lead Halide Perovskite Nanoplatelets. *J. Phys. Chem. Lett.* **2017**, *8*, 1161−1168.

(418) Tanaka, K.; Kondo, T. Bandgap and exciton binding energies in lead-iodide-based natural quantum-well crystals. *Sci. Technol. Adv. Mater.* **2003**, *4*, 599−604.

(419) Wang, Q.; Liu, X.-D.; Qiu, Y.-H.; Chen, K.; Zhou, L.; Wang, Q.-Q. Quantum Confinement Effect and Exciton Binding Energy of Layered Perovskite Nanoplatelets. *AIP Adv.* **2018**, *8*, No. 025108.

(420) Chernikov, A.; Berkelbach, T. C.; Hill, H. M.; Rigosi, A.; Li, Y.; Aslan, O. B.; Reichman, D. R.; Hybertsen, M. S.; Heinz, T. F.

Exciton binding energy and nonhydrogenic Rydberg series in monolayer WS$_2$. *Phys. Rev. Lett.* **2014**, *113*, No. 076802.

(421) Makarov, N. S.; Guo, S.; Isaienko, O.; Liu, W.; Robel, I.; Klimov, V. I. Spectral and Dynamical Properties of Single Excitons, Biexcitons, and Trions in Cesium–Lead-Halide Perovskite Quantum Dots. *Nano Lett.* **2016**, *16*, 2349–2362.

(422) Aneesh, J.; Swarnkar, A.; Kumar Ravi, V.; Sharma, R.; Nag, A.; Adarsh, K. V. Ultrafast Exciton Dynamics in Colloidal CsPbBr$_3$ Perovskite Nanocrystals: Biexciton Effect and Auger Recombination. *J. Phys. Chem. C* **2017**, *121*, 4734–4739.

(423) Castañeda, J. A.; Nagamine, G.; Yassitepe, E.; Bonato, L. G.; Voznyy, O.; Hoogland, S.; Nogueira, A. F.; Sargent, E. H.; Cruz, C. H. B.; Padilha, L. A. Efficient Biexciton Interaction in Perovskite Quantum Dots Under Weak and Strong Confinement. *ACS Nano* **2016**, *10*, 8603–8609.

(424) Yarita, N.; Tahara, H.; Ihara, T.; Kawawaki, T.; Sato, R.; Saruyama, M.; Teranishi, T.; Kanemitsu, Y. Dynamics of Charged Excitons and Biexcitons in CsPbBr$_3$ Perovskite Nanocrystals Revealed by Femtosecond Transient-Absorption and Single-Dot Luminescence Spectroscopy. *J. Phys. Chem. Lett.* **2017**, *8*, 1413–1418.

(425) Elkins, M. H.; Pensack, R.; Proppe, A. H.; Voznyy, O.; Quan, L. N.; Kelley, S. O.; Sargent, E. H.; Scholes, G. D. Biexciton Resonances Reveal Exciton Localization in Stacked Perovskite Quantum Wells. *J. Phys. Chem. Lett.* **2017**, *8*, 3895–3901.

(426) Thouin, F.; Neutzner, S.; Cortecchia, D.; Dragomir, V. A.; Soci, C.; Salim, T.; Lam, Y. M.; Leonelli, R.; Petrozza, A.; Kandada, A. R. S.; et al. Stable biexcitons in two-dimensional metal-halide perovskites with strong dynamic lattice disorder. *Physi. Rev. Mater.* **2018**, *2*, No. 034001.

(427) de Jong, E. M. L. D.; Yamashita, G.; Gomez, L.; Ashida, M.; Fujiwara, Y.; Gregorkiewicz, T. Multiexciton Lifetime in All-Inorganic CsPbBr$_3$ Perovskite Nanocrystals. *J. Phys. Chem. C* **2017**, *121*, 1941–1947.

(428) Becker, M. A.; Vaxenburg, R.; Nedelcu, G.; Sercel, P. C.; Shabaev, A.; Mehl, M. J.; Michopoulos, J. G.; Lambrakos, S. G.; Bernstein, N.; Lyons, J. L.; et al. Bright triplet excitons in caesium lead halide perovskites. *Nature* **2018**, *553*, 189–193.

(429) Fu, M.; Tamarat, P.; Huang, H.; Even, J.; Rogach, A. L.; Lounis, B. Neutral and Charged Exciton Fine Structure in Single Lead Halide Perovskite Nanocrystals Revealed by Magneto-optical Spectroscopy. *Nano Lett.* **2017**, *17*, 2895–2901.

(430) Yin, C.; Chen, L.; Song, N.; Lv, Y.; Hu, F.; Sun, C.; Yu, W. W.; Zhang, C.; Wang, X.; Zhang, Y.; et al. Bright-Exciton Fine-Structure Splittings in Single Perovskite Nanocrystals. *Phys. Rev. Lett.* **2017**, *119*, No. 026401.

(431) Bychkov, Y. A.; Rashba, E. I. Properties of a 2d Electron-Gas with Lifted Spectral Degeneracy. *Journal of Experimental and Theoretical Physics Letters* **1984**, *39*, 78–81.

(432) Nirmal, M.; Norris, D. J.; Kuno, M.; Bawendi, M. G.; Efros, A. L.; Rosen, M. Observation of the "Dark Exciton" in CdSe Quantum Dots. *Phys. Rev. Lett.* **1995**, *75*, 3728–3731.

(433) Wang, Y.; Li, X.; Zhao, X.; Xiao, L.; Zeng, H.; Sun, H. Nonlinear Absorption and Low-Threshold Multiphoton Pumped Stimulated Emission from All-Inorganic Perovskite Nanocrystals. *Nano Lett.* **2016**, *16*, 448–453.

(434) Lu, W.-G.; Chen, C.; Han, D.; Yao, L.; Han, J.; Zhong, H.; Wang, Y. Nonlinear Optical Properties of Colloidal CH$_3$NH$_3$PbBr$_3$ and CsPbBr$_3$ Quantum Dots: A Comparison Study Using Z-Scan Technique. *Adv. Opt. Mater.* **2016**, *4*, 1732–1737.

(435) Chen, W.; Bhaumik, S.; Veldhuis, S. A.; Xing, G.; Xu, Q.; Grätzel, M.; Mhaisalkar, S.; Mathews, N.; Sum, T. C. Giant five-photon absorption from multidimensional core-shell halide perovskite colloidal nanocrystals. *Nat. Commun.* **2017**, *8*, 15198.

(436) Schaller, R. D.; Petruska, M. A.; Klimov, V. I. Effect of electronic structure on carrier multiplication efficiency: Comparative study of PbSe and CdSe nanocrystals. *Appl. Phys. Lett.* **2005**, *87*, 253102.

(437) Manzi, A.; Tong, Y.; Feucht, J.; Yao, E.-P.; Polavarapu, L.; Urban, A. S.; Feldmann, J. Resonantly enhanced multiple exciton generation through below-band-gap multi-photon absorption in perovskite nanocrystals. *Nat. Commun.* **2018**, *9*, 1518.

(438) Sommerdijk, J. L.; Bril, A.; de Jager, A. W. Two photon luminescence with ultraviolet excitation of trivalent praseodymium. *J. Lumin.* **1974**, *8*, 341–343.

(439) Piper, W. W.; DeLuca, J. A.; Ham, F. S. Cascade fluorescent decay in Pr^{3+}-doped fluorides: Achievement of a quantum yield greater than unity for emission of visible light. *J. Lumin.* **1974**, *8*, 344–348.

(440) Wegh, R. T.; Donker, H.; Oskam, K. D.; Meijerink, A. Visible Quantum Cutting in LiGdF$_4$:Eu^{3+} Through Downconversion. *Science* **1999**, *283*, 663–666.

(441) Dexter, D. L. Possibility of Luminescent Quantum Yields Greater than Unity. *Phys. Rev.* **1957**, *108*, 630–633.

(442) Dieke, G. H.; Crosswhite, H. M. The Spectra of the Doubly and Triply Ionized Rare Earths. *Appl. Opt.* **1963**, *2*, 675–686.

(443) Timmerman, D.; Izeddin, I.; Stallinga, P.; Yassievich, I. N.; Gregorkiewicz, T. Space-separated quantum cutting with silicon nanocrystals for photovoltaic applications. *Nat. Photonics* **2008**, *2*, 105.

(444) Wright, A. D.; Verdi, C.; Milot, R. L.; Eperon, G. E.; Pérez-Osorio, M. A.; Snaith, H. J.; Giustino, F.; Johnston, M. B.; Herz, L. M. Electron–phonon coupling in hybrid lead halide perovskites. *Nat. Commun.* **2016**, *7*, 11755.

(445) Almeida, G.; Ashton, O. J.; Goldoni, L.; Maggioni, D.; Petralanda, U.; Mishra, N.; Akkerman, Q. A.; Infante, I.; Snaith, H. J.; Manna, L. The Phosphine Oxide Route toward Lead Halide Perovskite Nanocrystals. *J. Am. Chem. Soc.* **2018**, *140*, 14878–14886.

(446) Tan, Y.; Zou, Y.; Wu, L.; Huang, Q.; Yang, D.; Chen, M.; Ban, M.; Wu, C.; Wu, T.; Bai, S.; et al. Highly Luminescent and Stable Perovskite Nanocrystals with Octylphosphonic Acid as a Ligand for Efficient Light-Emitting Diodes. *ACS Appl. Mater. Interfaces* **2018**, *10*, 3784–3792.

(447) Nowack, B. Environmental chemistry of phosphonates. *Water Res.* **2003**, *37*, 2533–2546.

(448) Knepper, T. Synthetic chelating agents and compounds exhibiting complexing properties in the aquatic environment. *TrAC, Trends Anal. Chem.* **2003**, *22*, 708–724.

(449) Nenon, D. P.; Pressler, K.; Kang, J.; Koscher, B. A.; Olshansky, J. H.; Osowiecki, W. T.; Koc, M. A.; Wang, L.-W.; Alivisatos, A. P. Design Principles for Trap-Free CsPbX$_3$ Nanocrystals: Enumerating and Eliminating Surface Halide Vacancies with Softer Lewis Bases. *J. Am. Chem. Soc.* **2018**, *140*, 17760.

(450) Bodnarchuk, M. I.; Boehme, S. C.; ten Brinck, S.; Bernasconi, C.; Shynkarenko, Y.; Krieg, F.; Widmer, R.; Aeschlimann, B.; Günther, D.; Kovalenko, M. V.; et al. Rationalizing and Controlling the Surface Structure and Electronic Passivation of Cesium Lead Halide Nanocrystals. *ACS Energy Lett.* **2018**, *4*, 63–74.

(451) Luo, Z.; Marson, D.; Ong, Q. K.; Loiudice, A.; Kohlbrecher, J.; Radulescu, A.; Krause-Heuer, A.; Darwish, T.; Balog, S.; Buonsanti, R.; et al. Quantitative 3D determination of self-assembled structures on nanoparticles using small angle neutron scattering. *Nat. Commun.* **2018**, *9*, 1343.

(452) Yu, Y.; Zhang, D.; Yang, P. Ruddlesden-Popper Phase in Two-Dimensional Inorganic Halide Perovskites: A Plausible Model and the Supporting Observations. *Nano Lett.* **2017**, *17*, 5489–5494.

(453) Morrell, M. V.; He, X.; Luo, G.; Thind, A. S.; White, T. A.; Hachtel, J. A.; Borisevich, A. Y.; Idrobo, J.-C.; Mishra, R.; Xing, Y. Significantly Enhanced Emission Stability of CsPbBr$_3$ Nanocrystals via Chemically Induced Fusion Growth for Optoelectronic Devices. *ACS Appl. Nano Mater.* **2018**, *1*, 6091.

(454) Zhu, R.; Luo, Z.; Chen, H.; Dong, Y.; Wu, S. T. Realizing Rec. 2020 color gamut with quantum dot displays. *Opt. Express* **2015**, *23*, 23680–23693.

(455) Wu, Y.; Wei, C.; Li, X.; Li, Y.; Qiu, S.; Shen, W.; Cai, B.; Sun, Z.; Yang, D.; Deng, Z.; et al. In-situ Passivation of PbBr$_6^{4-}$-Octahedrons towards Blue Luminescent CsPbBr$_3$ Nanoplatelets with Near 100% Absolute Quantum Yield. *ACS Energy Lett.* **2018**, *3*, 2030–2037.

(456) Swarnkar, A.; Mir, W. J.; Nag, A. Can B-Site Doping or Alloying Improve Thermal- and Phase-Stability of All-Inorganic CsPbX$_3$ (X = Cl, Br, I) Perovskites? *ACS Energy Lett.* **2018**, *3*, 286−289.

(457) Liu, F.; Ding, C.; Zhang, Y.; Ripolles, T. S.; Kamisaka, T.; Toyoda, T.; Hayase, S.; Minemoto, T.; Yoshino, K.; Dai, S.; et al. Colloidal Synthesis of Air-Stable Alloyed CsSn$_{1-x}$Pb$_x$I$_3$ Perovskite Nanocrystals for Use in Solar Cells. *J. Am. Chem. Soc.* **2017**, *139*, 16708−16719.

(458) Lu, M.; Zhang, X.; Zhang, Y.; Guo, J.; Shen, X.; Yu, W. W.; Rogach, A. L. Simultaneous Strontium Doping and Chlorine Surface Passivation Improve Luminescence Intensity and Stability of CsPbI$_3$ Nanocrystals Enabling Efficient Light-Emitting Devices. *Adv. Mater.* **2018**, *30*, 1804691.

(459) Zhang, X.; Lu, M.; Zhang, Y.; Wu, H.; Shen, X.; Zhang, W.; Zheng, W.; Colvin, V. L.; Yu, W. W. PbS Capped CsPbI$_3$ Nanocrystals for Efficient and Stable Light-Emitting Devices Using p−i−n Structures. *ACS Cent. Sci.* **2018**, *4*, 1352−1359.

(460) Xuan, T.; Lou, S.; Huang, J.; Cao, L.; Yang, X.; Li, H.; Wang, J. Monodisperse and brightly luminescent CsPbBr3/Cs4PbBr6 perovskite composite nanocrystals. *Nanoscale* **2018**, *10*, 9840−9844.

(461) Giustino, F.; Snaith, H. J. Toward Lead-Free Perovskite Solar Cells. *ACS Energy Lett.* **2016**, *1*, 1233−1240.

(462) Luo, J.; Wang, X.; Li, S.; Liu, J.; Guo, Y.; Niu, G.; Yao, L.; Fu, Y.; Gao, L.; Dong, Q.; et al. Efficient and stable emission of warm-white light from lead-free halide double perovskites. *Nature* **2018**, *563*, 541−545.

(463) Yang, B.; Mao, X.; Hong, F.; Meng, W.; Tang, Y.; Xia, X.; Yang, S.; Deng, W.; Han, K. Lead-Free Direct Band Gap Double-Perovskite Nanocrystals with Bright Dual-Color Emission. *J. Am. Chem. Soc.* **2018**, *140*, 17001−17006.